Investigating the biomarker potential of extracellular vesicle nucleic acids in cancer, and the role of extracellular vesicle DNA in cell-to-cell communication

Inaugural-Dissertation
Zur
Erlangung des Doktorgrades
Dr. rer. nat.

der Fakultät für
Biologie
an der

Universität Duisburg-Essen

vorgelegt von
Sarah Strachan

aus Schottland

10/2020

Angaben zur Prüfung

Die der vorliegenden Arbeit zugrunde liegenden Experimente wurden in der Klinik für Kinderheilkunde III in der Arbeitsgruppe Pädiatrische Hämatologie und Onkologie des Universitätsklinikum Essen durchgeführt.

1. Gutachter: Prof. Dr. Dirk Reinhardt
2. Gutachter: Prof. Dr. Ralf Küppers

Vorsitzender des Prüfungsausschusses: Prof. Dr. Bernd Giebel

Tag der mündlichen Prüfung: 12.01.2021

DOI: 10.17185/duepublico/73984
URN: urn:nbn:de:hbz:464-20210215-101706-2

Contents

List of Figures

List of Tables

Abbreviations

°C	Degrees Celsius
µg	Microgram
µL	Microliter
µm	Micrometer
µM	Micromole
A.t.	*Arabidopsis thaliana*
AF488	Alexa Fluor 488
AF647	Alexa Fluor 647
AML	Acute Myeloid Leukaemia
AT/RT	Atypical Teratoid/Rhabdoid Tumour
BCA	Bicinchoninic Acid Assay
cfDNA	Cell-free DNA
cfRNA	Cell-free RNA
CO_2	Carbon Dioxide
CSF	Cerebral Spinal Fluid
DAPI	4', 6-diamidin-2-phenylindol
dH_20	Distilled Water
DMEM	Dulbecco's Modified Eagle Medium
DMSO	Dimethyl sulfoxide
DNA	Deoxyribonucleic Acid
DPBS	Dulbecco's Phosphate-buffered Saline
dsDNA	Double-stranded DNA
EDTA	Ethylenediaminetetraacetic Acid
EdU	5-ethylene-2'-deoxyuridin
EP	Extracellular Particles
ESCRT	Endosomal Sorting Complex Required for Transport
ES	Ewing Sarcoma
EV	Extracellular Vesicle
EV-DNA	Extracellular Vesicle DNA
EV-RNA	Extracellular Vesicle RNA
FACS	Fluorescence-activated Cell Scanning

FBS	Foetal Bovine Serum
FITC	Fluorescein Isothiocyanate
FLT3-ITD	FMS-like tyrosine kinase 3 internal tandem repeats
g	G Force
gDNA	Genomic DNA
GFP	Green Fluorescent Protein
Hsp	Heat Shock Protein
ILV	Intralumenal Vesicles
IMCES	Imaging Center Essen
ISEV	International Society of Extracellular Vesicles
kb	Kilobase Pairs
LAMP1	Lysosome-associated Membrane Protein 1
LEVs	Large Extracellular Vesicles
mg	Milligram
min	Minutes
mL	Milliliter
mM	Millimolar
mtDNA	Mitochondrial DNA
MVB	Multivesicular Body
nm	Nanometer
NPC	Nuclear Pore Complex
NPM1	Nucleophosmin1
NTA	Nanoparticle Tracking Analysis
PBS	Phosphate Buffered Saline
PBS-T	Phosphate Buffered Saline Solution with 0,01% Tween20
PEG	Polyethylene Glycol
Pen/Strep	Penicillin/Streptomycin
PFA	Paraformaldehyde
PI	Propidium Iodide
pmol	Picomole
RNA	Ribonucleic Acid
RT	Room Temperature
SEC	Size Exclusion Chromatography
sEV	Small Extracellular Vesicles
s	Seconds

SMARCB1	SWI/SNF-related Matrix-associated, Actin-dependent, Regulator of Chromatin, subfamily B, member 1
ssDNA	Single Stranded DNA
TAE	Tris-acetate-EDTA
TEM	Transmission Electron Microscopy
TFF	Tangential Flow Filtration
UC	Ultracentrifugation
WLL	White Light Laser

1. Introduction

1.1 An Overview of Extracellular Vesicles

Extracellular vesicles (EVs) are a heterogeneous population of membrane-bordered vesicles secreted by almost all cell types (Abels & Breakefield, 2016; Gould & Raposo, 2013; Raposo & Stoorvogel, 2013; Simons & Raposo, 2009). Several distinct groups of vesicles have been identified, with the three main categories being exosomes, microvesicles (ectosomes) and apoptotic bodies which can be categorised based on their size and origin (N. García-Romero et al., 2019). Exosomes (~30-150nm), the most popular vesicle sub-group in terms of research, are believed to have an endosomal origin (Muller, 2020). While exosomes are released from the cell after the fusion of the exosome-containing multivesicular bodies (MVB) with the plasma membrane, microvesicles (~100-1000nm) are shed directly from the cell surface (Abels & Breakefield, 2016). The final group, apoptotic bodies (~500-3000nm), are a product of the end stages of apoptosis due to the destruction of the cell (Dilsiz, 2020); however, most research focuses on the two previously described sub-groups with common EV isolation methods removing these larger vesicles. Due to the overlap in certain vesicle properties, such as density and size, it has been challenging to separate these sub-groups of vesicles with current EV isolation methods. This has led to disputes about what is the correct terminology to be applied when working in this field. Subsequently, different nomenclature is present in the current literature depending on the working group of origin. More recently there has been speculation of there being further subgroups of EVs including oncosomes, exomeres and chromatimeres which are broadly grouped in to small EVs (sEVs) that include all EVs under 150nm in size and large EVs (LEVs)(Brennan et al., 2020; Malkin & Bratman, 2020). Due to this inconsistency, in this project we simply refer to extracellular vesicles.

The first acknowledgment of EVs came in the 1980s, however, the term exosome came many years later (Abels & Breakefield, 2016; Muller, 2020). Originally, these vesicles were dismissed as no more than a cell waste disposal mechanism, whereas now it is known that EVs have a particular phospholipid-bilayer which encloses several biological molecules including various RNAs, proteins, lipids, single-stranded DNA and double-stranded DNA (dsDNA) (Abels & Breakefield, 2016; Becker et al., 2016; Raeven et al., 2018; Raposo & Stoorvogel, 2013; Thakur et al., 2014; G.

Zhang et al., 2015) (Fig. 1.1). Due to their method of biogenesis, there are several proteins, lipids and surface markers that are associated with EVs and their various sub-groups, all of which have been shown to vary depending on cell of origin and the intended function of the EV (Raeven et al., 2018).

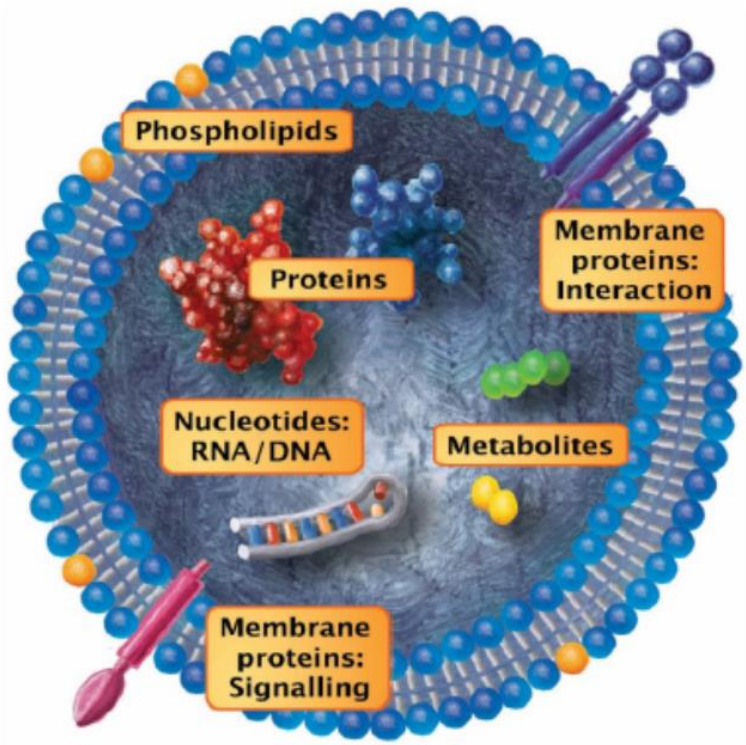

Figure 1.1: Extracellular Vesicle Composition. The composition and contents of an extracellular vesicle. Graphic taken from Raeven et al. 2018.

It has also been established that EVs are biologically functional and play important roles in intercellular communication and modulation of the immune system (Becker et al., 2016; Théry, 2011). This method of communication is thought to be evolutionarily conserved from Gram-positive and Gram-negative bacteria as well as archea (Choi, Kim, et al., 2013). This communication involves the release of EVs in to the extracellular matrix where they can enter in to the circulation and be internalised by recipient cells at near and distant sites in the body via various uptake methods (Kalluri & LeBleu, 2020). Besides intercellular communication, it has been suggested that EVs can be potentially utilised in clinical settings as diagnostic and prognostic markers for several cancers and diseases, due to their new found roles in pathogenesis (Becker et al., 2016; Keller et al., 2011; Taverna et al., 2016; Théry, 2011; J. Zhang et al., 2015). They have been suspected of playing crucial parts in tumour development, metastasis and the development of diseases such as neurodegenerative disorders (Kalluri & LeBleu, 2020). Their accessibility is another

advantage for their use in a clinical or research setting, having previously been isolated from several body fluids including plasma, serum, urine, amniotic fluid, cerebrospinal fluid and breast milk (Becker et al., 2016; Keller et al., 2011; Street et al., 2012). Despite the recent increase in popularity, there are still several aspects of EVs that are still to be fully understood.

1.2 EV Biogenesis

As previously mentioned, EVs are highly heterogeneous which is also reflected in their methods of biogenesis and source of origin. Ectosomes or microvesicles are produced directly from the plasma membrane via outward budding, which is thought to be orchestrated by several mechanisms, including some that overlap with the production of exosomes (Bebelman et al., 2018; Kalluri & LeBleu, 2020). These mechanisms include involvement of ESCRT (the Endosomal Sorting Complex Required for Transport), acid sphingomyelinases or membrane blebbing (Bebelman et al., 2018). In comparison to microvesicles/ectosomes, the biogenesis of exosomes is more complex. The first step requires the invagination of the plasma membrane creating an early-sorting endosome containing cell-surface and extracellular proteins, as well as contents contributed by the trans-Golgi-network and the endoplasmic reticulum. These early-sorting endosomes can progress in to late-sorting endosomes, from which multivesicular bodies (MVBs) are formed due to the invagination of the endosomal membrane, creating intraluminal vesicles (ILV). When these MVBs fuse with the plasma membrane, the ILVs are released as exosomes into the extracellular space; however, it is also known that these MVBs can have another fate in which they fuse with lysosomes and are destroyed (Fig. 1.2) (Bruno et al., 2020; Hessvik & Llorente, 2018; Kahlert, 2014; Kalluri & LeBleu, 2020; Kalra et al., 2016; Mathieu et al., 2019; McAndrews & Kalluri, 2019; Willms et al., 2018). The fact that exosomes are created via a cellular process that appears to be deliberate and highly regulated is what makes them a more popular sub-group in terms of research in comparison to their fellow EVs. As time goes by, more and more is being understood about the origin of EVs, with identification of several key players in biogenesis already having been achieved - even if their roles are not yet fully understood. These key players include phospholipids, ceramides, tetraspanins (specifically CD9, CD63, CD81), TSG101, Syntenin-1, Rab proteins, ESCRT proteins, ALIX, Snare proteins and sphingomyelinases, and many more (Bebelman et al., 2018; Ciardiello et al., 2016; Kalluri & LeBleu, 2020; Mathieu et al., 2019). Some of these molecules are regularly used to prove the presence of EVs or specific

subtypes in EV fractions or preparations. It is also known that EVs are heterogeneous in terms of their cargo which is incorporated during their biogenesis. As stated previously, it is known they contain proteins of various origins, lipids and nucleic acids, however, it is also clear that these are not evenly distributed, even within sub-groups (Abels & Breakefield, 2016; Becker et al., 2016; Keerthikumar et al., 2016; Pathan et al., 2019; Raposo & Stoorvogel, 2013; Thakur et al., 2014; J. Zhang et al., 2015). Their size is also not uniform, with a range of sizes being identified within each vesicle category, which could also contribute to the uneven distribution of cargo (Kalluri & LeBleu, 2020). With evidence that the type of parental cells, the microenvironment and the physiological state can affect all aspects of EVs including cargo and markers (Van Niel et al., 2018), it is understandable that there is some struggle in defining explicit EV sub-groups and appropriate nomenclature.

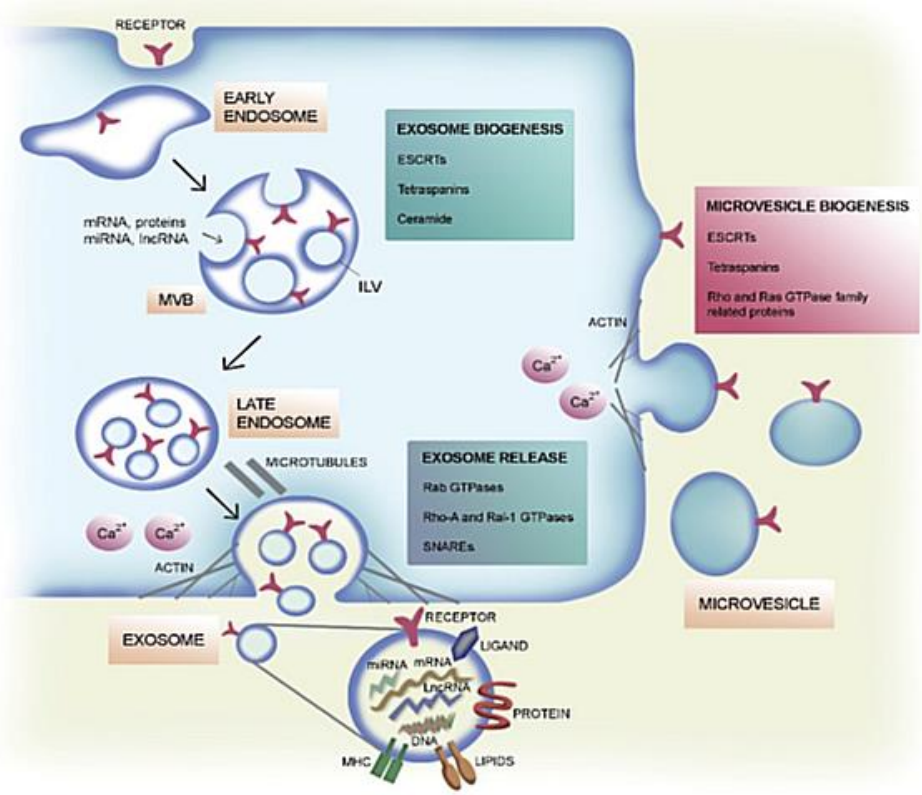

Figure 1.2: Extracellular Vesicle Biogenesis. Image depicting the routes of EV biogenesis and some of the key players involved in the biogenesis and release processes. Image taken from Bruno et al.2020.

1.3 EV Interaction with Recipient Cells

It is understood that once released the EVs can be uptaken by neighbouring cells or can enter the circulation and be internalised by target cells elsewhere in the body (Kalluri & LeBleu, 2020; McKelvey et al., 2015). It has now been identified that there is not just one generic method of EV uptake but several, including endocytosis, receptor-mediated endocytosis, micropinocytosis, direct fusion, lipid rafts and

clathrin-coated pits (Kalluri & LeBleu, 2020) (Fig. 1.3). What causes the recipient cells to favour one mechanism over the other is not completely clear. It's thought that factors such as the parental cell type as well as environmental factors such as pH can affect EV uptake rate and method (Kalluri & LeBleu, 2020; Parolini et al., 2009), A study suggested that donor cell origin does not play role in recipient cell EV uptake mechanism, but rather the recipient cell type is the deciding influence (Horibe et al., 2018). For example, one study showed that EVs fused with the plasma membrane of melanoma cells, while another showed pancreatic cells uptaking EVs via macropinocytosis, with a third showing neurosecretory PC12 cells uptaking EVs mainly using a clathrin-dependent endocytosis mechanism (Kalluri & LeBleu, 2020; Kamerkar et al., 2017; Parolini et al., 2009; Tian et al., 2014). In addition, it's thought that therapeutic agents can also impact the EV internalisation which could have good connotations for cancer treatments (Kalluri & LeBleu, 2020).

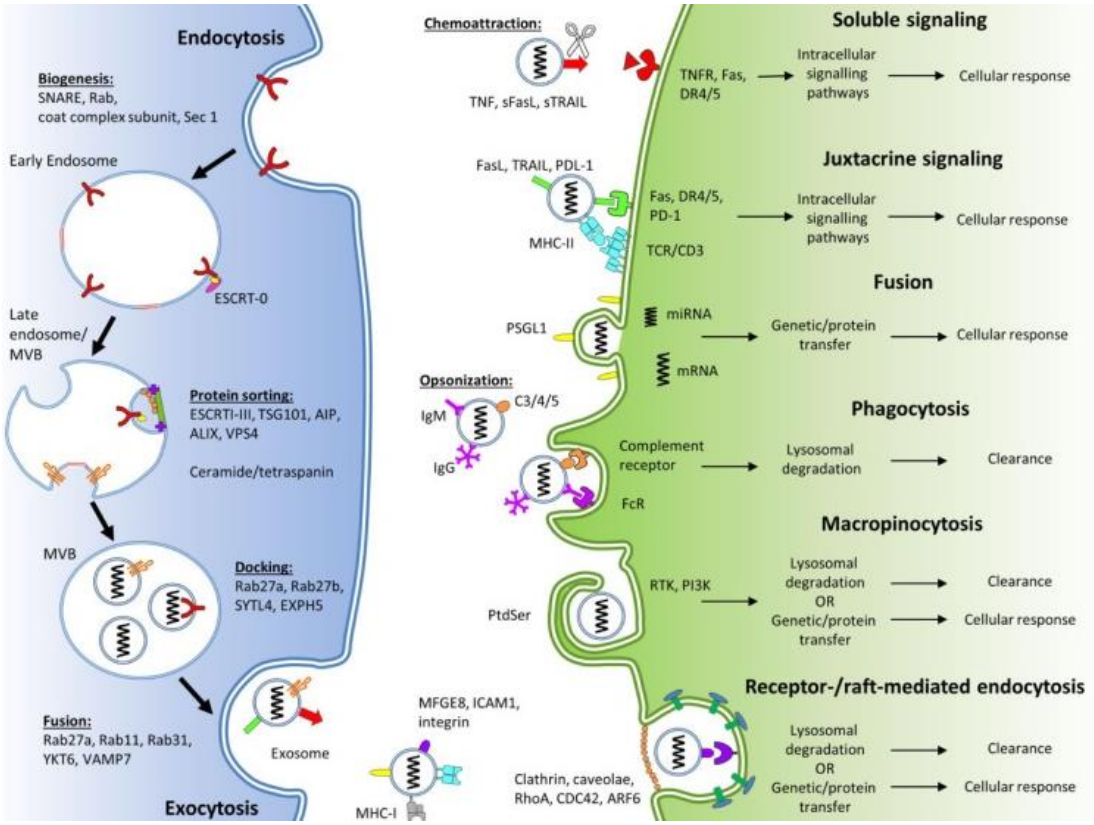

Figure 1.3: EV Internalisation Methods. An example of the various EV internalisation methods and their downstream cellular responses. Image taken from McKelvey 2015

Once the EVs or EV cargo have been internalised, they illicit different cellular responses or are directed to be cleared by the cell (McKelvey et al., 2015). It is thought that the method of internalisation or the way in which the EV interacts with the recipient cell can determine the downstream cellular response. Some outcomes

due to these cellular responses that have been documented thus far include apoptosis, cytokine production, modulation of the immune system and metastasis (McKelvey et al., 2015). EVs internalised by phagocytosis or macropinocytosis are more likely to be degraded and cleared by the cell due to activation of the endosomal-lysosomal degradation pathway. Any EVs uptaken by a form of endocytosis will end up in endosomes which will result in either lysosomal degradation, recycling of components back to the cell membrane, or escape in the trans-Golgi network (McKelvey et al., 2015). Intracellular microtubules and actin filaments have been shown to play a role in transport of vesicles containing internalised EVs within the cell (Caspi et al., 2001; McKelvey et al., 2015; Murray et al., 2000). However, a lot of open questions associated with EV uptake and trafficking remain.

1.4 EV Isolation techniques

Due to being released into the circulation, EVs are present in several body fluids, from which they can be isolated and further analysed. One problem that still exists in the field of EVs is the inability to agree upon a suitable universal EV isolation technique. The most traditional EV isolation method is ultracentrifugation (UC) in which dead cells, larger vesicles, apoptotic bodies and cell debris are separated from EVs through a series of differential centrifugation/ultracentrifugation steps with increasing length and centrifugal force (Li et al., 2017). Although it is still one of the most popular isolation techniques (Fig 1.4), several disadvantages exist (Gardiner et al., 2016; Pathan et al., 2019). Some literature suggests the presence of a relatively high amount of contaminating proteins and lipoproteins (Gardiner et al., 2016; Li et al., 2017). Moreover, it has been suggested that the harsh method of ultracentrifugation at 100,000 x g can affect the integrity of the isolated EVs, which can in turn affect the evaluation of EV nucleic acids and proteins and potentially hinder functional research assays that require biologically active EVs (Hong et al., 2016; Lobb et al., 2015). Additionally, ultracentrifugation-based EV isolation is considered to be a time-consuming and laborious technique during which many EVs can be lost with previous findings showing that only 5 % of total EVs are recovered using the UC technique (Baranyai et al., 2015; N. García-Romero et al., 2019; Li et al., 2017). Furthermore, the similarity in density and size of EV subpopulations makes it difficult to distinguish between EVs and other contaminating vesicles and non-EV associated free biomolecules like protein (Li et al., 2017; Rider et al., 2016). Another downside to this traditional method is that it requires access to an

ultracentrifuge – an expensive piece of equipment - which for many working groups is not a viable option.

Due to these findings, there are now several alternative EV isolation techniques that have been described in the literature. These include methods such as sucrose cushion density gradient centrifugation, immunoaffinity capture, precipitation, ultrafiltration and size exclusion chromatography (SEC) (Gámez-Valero et al., 2016; Helwa et al., 2017; Karimi et al., 2018; Li et al., 2017; Taylor & Shah, 2015), as well as several commercially available kits and new emerging microfluidic-based methods (Li et al., 2017; Macías et al., 2019) - all with their own advantages and disadvantages. For example, many of these methods would suffice for isolation of EVs from samples with low volume but would not be suitable or cost-effective for high-throughput analyses or processing of large volumes of starting material. Some may be suitable for downstream diagnostic purposes but not functional assays, and vice versa. As a result, this is an area of EV research that is still drawing a lot of attention.

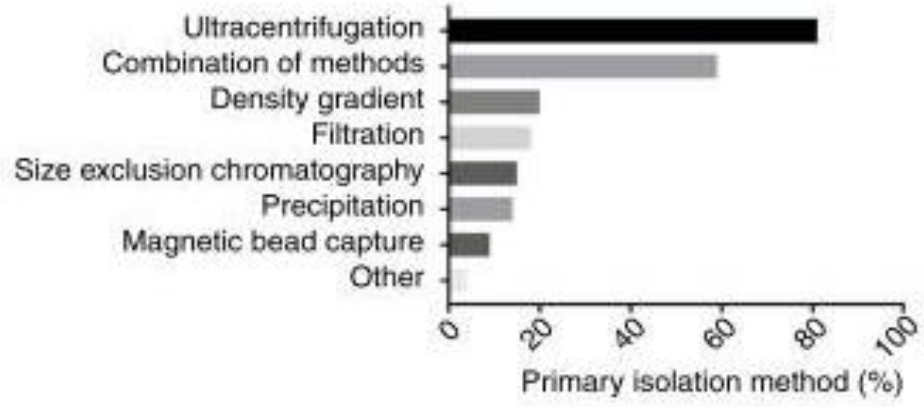

Figure 1.4: The Most Popular EV Isolation Techniques. Results of a survey from 2016 showed which EV isolation techniques were the most used by participants. Image taken from Gardiner et al.2016.

1.5 Role of EVs in Cancer

As well as having roles in every day bodily processes, EVs have been implicated in being major players in the development and progression of cancer. It has emerged that EVs can support tumorigenesis, tumour progression, preparation of the pre-metastatic niche and metastasis itself. It is thought they support these processes by facilitating functions such as immune suppression, coagulation, neovascularisation, angiogenesis, vascular leakiness and drug resistance (Alderton, 2012; Becker et al., 2016; Dilsiz, 2020; Peinado et al., 2012). EVs are used as a way of communicating

between tumour cells and other tumour cells; tumour cells and stroma cells; and, oppositely, from stroma cells to tumour cells (Bebelman et al., 2018; Kalluri & LeBleu, 2020; McAndrews & Kalluri, 2019). It is known that cancerous cells produce higher numbers of EVs than healthy cells, an act thought to either rid the cell of unwanted molecules that could inhibit the cancer cell growth, or is a deliberate attempt to communicate with and influence surrounding cells as well as distant metastatic sites (Becker et al., 2016; Dilsiz, 2020). The mere act of producing EVs has also been shown to have a role in cancer, as the extensive production of microvesicles through membrane blebbing having been shown to enable cell motility and migration in tumour cells (Bebelman et al., 2018). One clear way in which EVs contribute to cancer progression is through the transfer of their cargo molecules into recipient cells, which are suspected of being capable of having transformational effects (Dilsiz, 2020). With such clear involvement in cancer progression, it is only logical that these EVs and their cargo should be studied and utilised in order to develop early diagnostic systems, and identification of potential molecular components which could be targeted to inhibit cancer progression.

1.6 An Overview of EV Nucleic Acid Cargo

Along with proteins, RNA is one of the most studied elements of EV cargo. It is now common knowledge that EVs contain RNA with the identification of mRNA, miRNA, circular RNA and many other small non-coding RNA species (Bebelman et al., 2018; Chevillet et al., 2014; Lasda & Parker, 2016; Pathan et al., 2019; Van Balkom et al., 2015). The fact that EV-RNA can be transferred into recipient cells and that they are functional has been proven (Ratajczak et al., 2006; Skog et al., 2008; Valadi et al., 2007). It was shown by Valadi et al. (2007) and Skog et al. (2008) that mRNA could be horizontally transferred via EVs, and that the mRNA could be translated into protein. Later, Pegtel et al. (2010) also provided evidence that small non-coding RNA molecules that were transferred into recipient dendritic cells via EVs could regulate gene expression. It has also been demonstrated that some miRNA types can potentially play a role in progression of cancer (Hongyun Zhao et al., 2016). How RNA is packaged in to the EVs is thought to be a regulated process, still not fully understood. It has been suggested that different levels of mRNA and miRNAs in the cell cytoplasm can affect their sorting in to EVs (Squadrito et al., 2014), and one study in breast cancer even proposed that EVs themselves contain protein machinery capable of producing mature miRNA from packaged pre-miRNA (Melo et al., 2014). Several RNA binding proteins have been implicated in the sorting of RNA

species in to extracellular vesicles, however, it is suspected that there are several sorting mechanisms at play rather one definitive pathway (Bebelman et al., 2018).

While it was accepted quite early on in EV research that EVs contain several subtypes of RNA (Choi, Kim, et al., 2013; Choi, Lee, et al., 2013), more recently, it came to light that some EVs also contain DNA. In 2011, Balaj *et al*. showed evidence of the presence of single stranded DNA (ssDNA) in the EV (Balaj et al., 2011). This was followed by the discovery of double stranded DNA (dsDNA) in 2014 by Thakur et al. who subsequently presented evidence that the majority of the DNA in the EV is fragmented (100 bp-2.5 kb) and is double-stranded in nature. In addition to the internal DNA, it has been shown that EVs also possess external DNA that is bound to the EV surface, which is considered to play a potential role in EV binding and extracellular matrix communication (Bebelman et al., 2018; Németh et al., 2017). The literature is also conflicted on whether the majority of EV-DNA is inside or outside of the EV (Fischer et al., 2016; Lázaro-Ibáñez et al., 2019; Thakur et al., 2014). Many important questions still remain with concern to EV-DNA, including what the origin of the EV-DNA is and how it ends up inside the EV. It has already been identified that EVs can contain fragmented genomic DNA (gDNA), mitochondrial DNA (mtDNA) and parasitic DNA, and that some cancer EVs even contain gDNA that is resistant to DNase degradation (Cai et al., 2013; Guescini et al., 2010; Lázaro-Ibáñez et al., 2019; Sansone et al., 2017; Sisquella et al., 2017; Thakur et al., 2014).The method and reasons for the packaging of the DNA inside the EVs are still elusive, with one group hinting towards it being to rid the cell of damaged DNA that would otherwise accumulate in the cytoplasm of the cell (Takahashi et al., 2017). The fact that DNA spanning all chromosomes can be found in EVs could be a signal that the DNA is not packaged with purpose, which highlights that there is still a lot unknown about how the DNA comes to be packaged within the EV (Kahlert et al., 2014).

1.7 EV Nucleic Acids as Biomarkers in Cancer

Certain properties of EVs make them prime candidates for use as cancer biomarkers. One such property is that they can be recovered from many body fluids such as blood, saliva, semen, cerebrospinal fluid, amniotic fluid, breast milk and urine meaning they can be easily collected and used for liquid biopsies (Choi, Kim, et al., 2013; Dear et al., 2013; Lässer et al., 2011; Street et al., 2012). Another property is that almost all cells release EVs, including diseased cells, and these EVs contain signatures reflective of the parental cell from which they were released (Choi, Lee, et

al., 2013; Kontopoulou et al., 2020; Kunz et al., 2019; Thakur et al., 2014). These signatures are also well protected from potential degradation by nucleases and proteases due to being packaged inside the EV (Choi, Lee, et al., 2013). EV nucleic acids can be considered as one of these signatures, making them potentially useful diagnostic tools. It has been previously shown that EV-DNA derived from EVs released by tumour cells mirrored the mutational status of the parental tumour cells, and it was possible to detect cancer-related mutations in the EVs from patient plasma samples (Kontopoulou et al., 2020; Thakur et al., 2014). Recently, Kontopoulou et al.(2020) showed that AML-related mutations were detectable in paediatric patient plasma EVs, while other studies have demonstrated that EV-DNA isolated from urine could be a biomarker for bladder cancer and kidney disease (Malkin & Bratman, 2020). Interestingly, it has also been suggested that the amount of DNA inside EVs could potential reflect the severity of the cancer, with higher amounts of dsDNA being found in EVs of patients with metastatic melanoma in comparison to those with less aggressive melanoma types (Thakur et al., 2014). Additionally, several studies have been able to use EV-RNA to detect disease related mutations in EVs isolated from cell-line supernatants or patient plasma. Kunz et al.(2019) showed it was possible to identify cancer-specific mutations from mRNA of EVs derived from AML cell line supernatants and paediatric AML patient plasma Additionally, it was demonstrated that microvesicles from glioblastoma patient serum and tissue contained mRNA that mirrored the EGFRvIII mutational status (Becker et al., 2016; Skog et al., 2008). The presence and expression level of certain miRNA species within EVs have also been shown to have prognostic implications in many cancers, including prostate, melanoma, esophageal and colorectoral cancers (Becker et al., 2016). All of these findings highlight that evaluation of EV nucleic acids could have positive connotations for cancer diagnostics and prognostics.

1.8 Functional Aspects of EV-DNA

As well as having biomarker potential, research in recent years has revealed that EVs play functional roles in everyday processes within the body including intercellular communication, immune modulation, development, and reproduction. They have also been implicated in pathological processes including tumour progression and metastasis, as well as conditions such as metabolic- cardiovascular- and neurodegenerative diseases (Kalluri & LeBleu, 2020). Although less is known about EV-DNA than its fellow packaged biomolecules, a handful of research groups have communicated findings hinting towards its functional capabilities. So far it has been

shown that EV-DNA can be transferred to- and up-taken by recipient cells along with other EV cargo (Cai et al., 2013; Fischer et al., 2016; Waldenström et al., 2012). The fact that EV-DNA can be detected in the cytoplasm and nucleus of recipient cells was first shown by Waldenstrom et al. (2012) using EVs from cardiomyocytes, but was later additionally modelled by other groups using different cell types (Cai et al., 2013; Fischer et al., 2016; Lee et al., 2014; Waldenström et al., 2012). Additionally, it has been demonstrated that the transferred EV-DNA is capable of recruiting nuclear factor κB (NF-κB) and can be transcribed (Cai et al., 2013).In the same study, it was shown that it was possible to transfer a unique BCR/ABL hybrid gene from a K562 cell line to recipient neutrophils via the EVs. Horizontal gene transfer from EVs to recipient cells was also demonstrated by Fischer et al. (2016) who could detect *Arabidopsis thaliana*-DNA (*A.t*.-DNA) from lentivirally transduced BM-hMSC EVs in recipient hMSCs, with a suggestion of stable integration in to the recipient cell genome. Furthermore, another group showed the transient expression of H-ras DNA in recipient RAT-1 cells for 30 days after it was transferred from EVs of RAS-3 cells (Lee et al., 2014).There is still a lot unknown about the transfer of EV-DNA and whether it has functional use once uptaken by recipient cells. So far no clear function of EV-DNA in the healthy situation has been found, however, in some disease models it been claimed that transfer of this DNA can cause pro-inflammatory and pro-oncogenic physiological changes in the recipient cell (Malkin & Bratman, 2020). Despite these findings, the exact function of the EV-DNA, how it is loaded in to EVs, and how it is trafficked inside the recipient cell is currently unclear.

1.9 Therapeutic Aspects of EVs

EVs have also gained a lot of attention as potential therapeutic agents (Fig 1.5). One property which makes them interesting therapeutic candidates is that they appear to be well accepted by the body and do not cause adverse effects such as toxicity or large immune responses. This is thought to perhaps be due to their pharmacokinetic properties which could be affected by their protein and lipid composition (Kalluri & LeBleu, 2020). Other therapeutic advantages offered by EVs is they can target specific tissues, they can penetrate barriers such as the blood brain barrier, and the cargo they carry is protected during its journey in the circulation (Zhu et al., 2018). One patient was reportedly already successfully treated by EVs from MSCs for graft versus host disease (Kordelas et al., 2014). In addition to EVs themselves having therapeutic properties, several groups have tried to engineer EVs to contain therapeutic agents such as short interfering RNAs (siRNAs), immune modulators,

chemotherapeutic agents, and antisense oligonucleotides, with hope the EVs will deliver these agents to a desired cell target (Kalluri & LeBleu, 2020). Clinical trials using such EV constructs containing therapeutic agents have already begun. Due to previously mentioned issues such as EV isolation and purification methods, the development of synthetic and chimeric EVs to be used in therapeutics has been approached (Villata et al., 2020). Whether EV-DNA could also be used in a therapeutic manner remains to be seen. If the DNA integrates in to the recipient cell genome as previously suggested (Fischer et al., 2016), engineered EV-DNA could potentially be utilised for gene therapies. If more can be uncovered about how and why EV-DNA is packaged in to the EVs and how exactly it is transferred to recipient cells and its localisation within the recipient cell, then this would open the door to the potential utilisation of EV-DNA in a therapeutic manner.

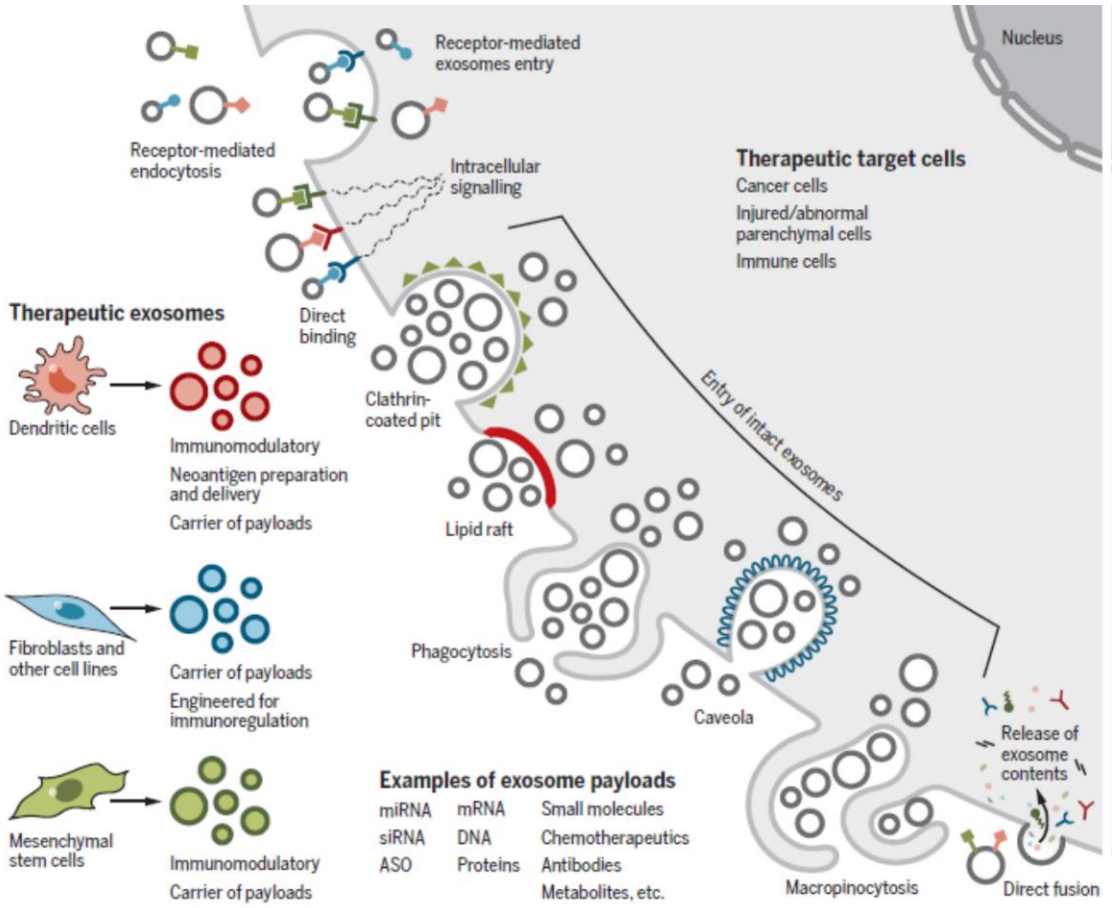

Figure 1.5: Extracellular Vesicle Therapeutic Applications. An image depicting the possible therapeutic roles of EVs and the possible methods of EV uptake by recipient cells. Image taken from Kalluri 2020.

1.10 Aim of the Project

This project considers three different aspects of EVs, namely their diagnostic potential, the transfer and uptake of EV-DNA as a cellular communication tool, and the development of an effective EV isolation technique.

1.10.1 Investigating the diagnostic potential of EV nucleic acids

In this project, we utilised the liquid biopsy idea to assess the validity of using EV nucleic acids as diagnostic markers in cancer. This project started with assessing the possibility of using EV-DNA to detect *SMARCB1* mutations in Atypical teratoid/rhabdoid tumours (AT/RT), starting in cell lines with the idea of moving forward into mice models and patient plasma samples. AT/RT is an aggressive type of brain tumour which is commonly found in infants under the age of three, with an average overall survival rate of just 17 months (Johann et al., 2016). SMARCB1 is a part of the ATP-dependent chromatin remodeling SWI/SNF complex which plays roles in gene regulation (Wilson & Roberts, 2011). Mutations in the *SMARCB1* gene are the only known consistent genetic abnormalities associated with AT/RT, therefore this would be an ideal biomarker for its detection (Johann et al., 2016). Additionally, the opportunity arose to also investigate the diagnostic potential of EV-RNA in Ewing sarcoma (ES). Ewing sarcoma is a rare but aggressive malignancy most commonly identified in the bones of young adults and children (Cidre-Aranaz & Alonso, 2015). Due to a high relapse rate, survival rates of ES patients are low (Potratz et al., 2012) *EWS-FLI1* has been identified as a driving mutation in ES, which is brought about by a chromosomal translocation where the *EWSR1* gene fuses with transcription factors of the ETS family such as FLI1 (Johann et al., 2016). As this is the most common translocation in ES, it makes it a prime candidate for biomarker development. These projects were established with the collective future aim of being able to replace invasive tissue biopsy diagnostic methods with a simpler EV-based liquid biopsy assay.

1.10.2 Investigating the transfer and uptake of EV-DNA into recipient cells

Understanding the mechanism behind EV-DNA uptake and its trafficking within the recipient cells will help to identify the functional significance of EV-DNA and its potential role in intercellular communication. Here, we aimed to investigate the transfer, uptake and localisation of EV-DNA in recipient cells by (i) establishing and optimising an EV-DNA labelling and visualisation method using EdU (5-ethynyl-2'-deoxyuridine) - a nucleoside analogue of thymidine which is incorporated into DNA during active DNA synthesis, (ii) time kinetics experiments to identify localisation and trafficking of EV-DNA in the recipient cell, (iii) co-localisation and knockdown experiments to identify uptake and trafficking methods, (iv) inhibitor treatments to highlight uptake mechanisms, and (vi) detection of exogenous DNA in recipient cells

to confirm transfer and localisation. By optimising an EV-DNA labelling method, this project aimed to further the knowledge surrounding the purpose of EV-DNA cargo.

1.10.3 Development of an EV isolation technique for large starting materials

With the disadvantages of the traditional ultracentrifugation isolation method becoming ever clearer, and the absence of a universally supported alternative technique, here, we endeavoured to optimise an EV isolation technique that circumvents the need for an ultracentrifuge. This was carried out in parallel to the two previously mentioned projects (1.10.1;1.10.2). We attempted to develop a protocol that combines the EV precipitating effect of polyethylene glycol (PEG) with the previously described “mini-SEC” technique (Hong et al., 2016) for isolation of EVs from large volumes of conditioned media. For reference, this technique would be compared with that of UC, with consideration of EV yield, reproducibility, protein content and EV integrity. Additionally, to our knowledge, this is the first project to characterise DNA from the EV preparations isolated by the PEG/SEC-based method, with the intent to utilise the EV-DNA for cancer-related mutational analysis.

1.10.4 Collective aim

Considering these three aforementioned aspects together, the collective aim of this doctoral thesis was to contribute to the ever-expanding information base surrounding these nanosized vesicles, with hope that it could be of use to future EV studies that are based on one of these directions.

2. Materials

2.1 Consumable Materials

All standard consumable materials used in this doctoral thesis and their manufacturers are listed in the table below.

Table 2.1 Consumable materials

Material	Company
Cellstar® Standard Cell Culture Flasks 50ml-650mL	Greiner Bio-one International GmbH, Germany
Accuvettes	Beckman Coulter GmbH, Germany
Cryogen Tubes	ClearLine®Biosigma Italy
Sterile Filter 250 mL	TPP®
Ultracentrifuge tubes Polycarbonate	Beckman Coulter GmbH, Germany
1mL BD Plastipak Syringes	Becton, Dickinson and Company, Germany
10mL BD Discardit II ™ Syringes	Becton, Dickinson and Company, Germany
96-Well PCR Plate	Biocentrix, Steinbrenner Labor Systeme Gmb
FACS Tubes 5mL	Greiner bio-one
TFF-EASY Tangential Flow Filter for Extracellular Vesicle Concentration	HansBioMed Life Sciences
Plastic Syringe 20 mL	Fisherbrand, Fisherscientific, China
Syringe Filter 0.45 µm	Sartorius Stedim Biotech GmbH, Germany
Size Exclusion Chromatography Columns qEV10 35 nm	IZON Science, Germany
Amnicon Ultra -15 centrifugal filters	Merck Millipore Ltd., Ireland
Econo-Pac chromatography columns 1.5cm x 12cm	Bio-Rad, Hercules, USA
Mini- Trans-blot filter paper	Bio-Rad Laboratories, Inc., USA
PVDF Blotting Membrane	GE Healthcare Life Science
Nitrocellulose Blotting Membrane	GE Healthcare Life Science
4-12% NuPAGE Gels	Invitrogen, Thermo Fisher Scientific, Germany
Cover Slips 12mm	Paul Marienfeld GmbH, Germany
Microscopy Slides 76x26mm	Medizin- & Labortechnik GmbH, Germany
FalconTubes 15mL/50mL	Greiner Bio-one International GmbH, Germany
Eppendorf MicrocentrifugeTubes	Eppendorf AG, Germany
Low Retention 1.7 Microcentrifuge Tubes	Kisker, Germany
Pipette Tips	Greiner Bio-one International GmbH, Germany
CytoOne12-/24-/96-Well Plates	USA Scientific, Inc., USA
Parafilm	Bemis Company, Inc,USA
Cellstar® Pipettes for the Pipette boy	Greiner Bio-one International GmbH, Germany

Glass Pasteurpipettes 150mm	Brand GmbH, Germany

2.2 Technical Equipment

All technical equipment and devices used in this doctoral project are summarised in the table below.

Table 2.2 Technical Equipment

Technical Equipment	Company
Laminar airflow cabinet TC 48	Gelaire Flow Laboratories ^{LTD}, Australia
Incubator HERA cell 150 Heraeus	ThermoFisherScientific GmbH, German
Z1 Coulter Particle Counter	Beckman Coulter GmbH, Germany
Optima XPN-80 Ultracentrifuge	Beckman Coulter GmbH, Germany
Waage Kern 572, GöntgenWägetechnik	Kern &Sohn GmbH, Germany
Ultracentrifuge Rotor Ti 14U4968	Beckman Coulter GmbH, Germany
Zeta View® Particle tracking analyzer	Particle Metrix GmbH, Germany
Gel Running machine	PeQ Lab Biotechnologie GmbH, Germany
Multipipette® Stream	Eppendorf AG, Germany
SureLock Electrophoresis Chamber	ThermoFisherScientific GmbH, German
Transfer Chamber	Bio-Rad Laboratories, Inc., USA
Biometra Fastblot Device	Analytik Jena AG, Germany
Pipettes	Eppendorf AG, Germany
Pipette Boy,Pipettus ®	Hirschmann Laborgeräte GmbH & Co. KG, Germany
BioDocAnalyze, Biometra	Analytik Jena AG, Germany
Microscope Axiovert 25	Carl Zeiss Microscopy LLC, USA
Allegra™ x-22R Centrifuge	Beckman Coulter GmbH, Germany
Centrifuge 5415D	Eppendorf AG, Germany
Rotixa 50 RS, centrifuge	Hettich
Water Bath GFL	Peter Oehmenlabortechnik GmbH, Germany
StepOnePlusReal-time PCR system	Applied Biosystems
FC500 Flow Cytometer	Beckman Coulter GmbH, Germany
EL800 microplate reader	Bio-TEK Instruments INC.
Modulus™ Microplate Luminometer	Turner Biosystems, Inc., USA
Fusion FX Machine	Vilmer Lourmat
MACSQuant Flow Cytometer	MACSQuant
Thermomixer comfort	Eppendorf AG, Germany
JEM-1400+ transmission electron microscope	JEOL GmbH
Vortex MS2 Minishaker	IKA Werke, Germany
ND-1000 Spectrophotometer	Nanodrop
C1000 Thermal Cycler	Biorad, Germany
Agilent 4200 TapeStation instrument	Agilent Technologies

2.3 Media, Reagents, Chemicals and Commercial Buffers

All chemicals, reagents, media and commercially bought buffers used in this doctoral project are summarised in the table below.

Table 2.3 Media, Reagaents, Chemicals and Commercial Buffers

Media, Reagents Chemicals and Commercial Buffers	Company
PBS	Gibco® Life Technologies Corp., USA
DMEM (1x) + GlutaMax™ I	Gibco® Life Technologies Corp., USA
Penicillin-Streptomycin	Gibco® Life Technologies Corp., USA
FBS (Fetal Bovine Serum)	Gibco® Life Technologies Corp., USA
0.05 % Trypsin – EDTA (1x)	Gibco® Life Technologies Corp., USA
RPMI	Gibco® Life Technologies Corp., USA
PhosSTOP Phosphatase Inhibitor	Roche, Sigma Aldrich, Germany
cOmplete Protease Inhibitor	Roche, Sigma Aldrich, Germany
My-Budget Universal Agarose	Bio Budget Technologies GmbH
TAE	Thermo Fisher Scientific GmbH, Germany
6x Orange DNA Loading Dye	Thermo Fisher Scientific GmbH, Germany
Gene Ruler 1 kb DNA ladder	Thermo Fisher Scientific GmbH, Germany
Gene Ruler 100 bp DNA ladder	Invitrogen, Life Technologies
SYBR Green Master Mix	Roche Deutschland Holding GmbH
Dest.H_2O	Ampuwa®
Propidium Iodide	BD Pharmingen, BD Biosciences
Lipofectamine RNAiMAX reagent	Invitrogen, Thermo Fisher Scientific, Germany
Opti-MEM	Gibco® Life Technologies Corp., USA
Dimethylsulphoxide (DMSO)	Carl Roth GmbH + Co,Germany
Isotone	Beckman Coulter GmbH, Germany
Ethidium Bromide	Carl Roth GmbH + Co. KG, Germany
Poly(ethylene glycol) 6000	Sigma Aldrich, Germany
Sepharose CL-2B	GE Healthcare Life Science
Milk Powder	Carl Roth GmbH + Co.KG
Tween20	Carl Roth GmbH + Co.KG
Ponceau Rot	Cell Signaling Technology
ECL Prime Western Blotting Detection Reagents	GE Healthcare Life Science
Precision Plus Protein Dual Color Standards	Thermo Fisher Scientific GmbH, Germany
Coomassie Brilliant Blue R-250	Bio-Rad Laboratories, Inc., USA
Albumin Fraction V (BSA)	Carl Roth GmbH + Co.KG
Tween20	Carl Roth GmbH + Co.KG
Triton-X100	E.Merck, Germany
DAPI	Carl Roth GmbH + Co.KG
Paraformaldehyde 4%	Thermo Fisher Scientific GmbH, Germany
Flouromount-G medium	SouthernBiotech, USA
Aqua	B. Brown Biotech International GmbH,

	Germany
Terralin Liquid	Schülke&Mayr GmbH, Germany
siRNA Rab5A	Santa Cruz, Biotechnology
siRNA Rab7	Santa Cruz, Biotechnology
siRNA control with GFP	Santa Cruz, Biotechnology
siRNA control	Santa Cruz, Biotechnology
Ivermectin I8898-1G	Sigma Aldrich, Germany
Hydroxyurea H8627-5G	Sigma Aldrich, Germany
Aphidicolin from Nigrospora spherical A0781-1MG	Sigma Aldrich, Germany
Methanol	J.T. Baker, USA
2x MyTaq reaction mixture	Bioline
Hot Start Taq 2x mastermix	HighQU
Phusion PCR Master Mix	Thermo Fisher Scientific GmbH, Germany
Aldehyde/Sulfate latex beads	Thermo Fisher Scientific GmbH, Germany

2.4 Buffers and Solutions

All buffers and solutions that were prepared in the laboratory and used in this doctoral project are summarised in the table below.

Table 2.4 Buffers and Solutions

Buffers and Solutions	Volume	Company
RIPA Buffer:		
Tris HCL pH 7.4	50 mM	Carl Roth GmbH + Co.KG
NaCl	150 mM	Carl Roth GmbH + Co.KG
NP-40	1%	Carl Roth GmbH + Co.KG
Sodium Deoxycholate	0.5%	Carl Roth GmbH + Co.KG
SDS	0.1%	Carl Roth GmbH + Co.KG
10X Running Buffer:		
MES	97.6 g	Carl Roth GmbH + Co.KG
Tris Base	60.6 g	Carl Roth GmbH + Co.KG
SDS	10 g	Carl Roth GmbH + Co.KG
EDTA	3 g	Carl Roth GmbH + Co.KG
dH_20	1 L	-
1X Running buffer:		
10X Running buffer	100 mL	-
dH_20	900 mL	-
10X Transfer Buffer (wet WB):		
Tris Base	15 g	Carl Roth GmbH + Co.KG
SDS	5 g	Carl Roth GmbH + Co.KG
Glycine	72 g	Sigma Aldrich, Germany
dH_20	500 mL	
1X Transfer Buffer:		
10X Running buffer	100 mL	-

dH_20	800 mL	-
Methanol	100 mL	J.T. Baker, Poland
10X TBS:		
Tris Base	12.12 g	Carl Roth GmbH + Co.KG
NaCl	43.88 g	Sigma Aldrich, Germany
dH_20	450 mL	-
TBS-T:		
10X TBS	50 mL	-
dH_20	450 mL	-
Tween20	250 µL	Carl Roth GmbH + Co.KG
Transfer Buffer (semi-dry WB):		
Tris Base	5.82g	Carl Roth GmbH + Co.KG
SDS	0.38g	Carl Roth GmbH + Co.KG
Glycine	2.93g	Sigma Aldrich, Germany
Methanol	175 mL	J.T. Baker, Poland
dH_20	825mL	-
5% Blocking Milk:		
Milk powder	2.5 g	Carl Roth GmbH + Co.KG
PBS	50 mL	Gibco® Life Technologies Corp., USA
Tween 20 (optional)	25 µL	Carl Roth GmbH + Co.KG
Destaining Solution:		
Methanol	5%	J.T. Baker, Poland
Acetic Acid	7.5%	Carl Roth GmbH + Co.KG
dH_20	87.5%	-

2.5 Kits

All commercially bought kits that were used in this doctoral project are summarised in the table below.

Table 2.5 Kits

Kit	Company
QIAamp DNA Micro Kit	Qiagen Sample & Assay Technologies, GmbH, Germany
QIAamp DNA Mini Kit	Qiagen Sample & Assay Technologies, GmbH, Germany
Quantifluor® dsDNA System Kit	Promega GmbH, Germany
NucleoSpin RNA XS	Machery-Nagel, Germany
Quantifluor RNA System	Promega GmbH, Germany
Pierce™ BCA Protein Assay Kit	Thermo Fisher Scientific GmbH, Germany
BD Annexin V: FITC Apoptosis detection Kit I	BD Biosciences, Germany
Click-iT™ EdU Alexa Fluor™ 647 Imaging Kit	Thermo Fisher Scientific GmbH, Germany
PKH67 Green Fluorescent Cell Linker Midi Kit	Sigma Aldrich, Germany

REPLI-g Single Cell Kit	Qiagen
Nuclear Extract Kit	Active Motif
Agilent High Sensitivity D1000 ScreenTape Assay Kit	Agilent Technologies
Transcriptor First Strand DNA Synthesis Kit	Roche

2.6 Antibodies

All antibodies that were used in this doctoral project are listed in the table below along with their manufacturers and catalogue numbers.

Table 2.6 Antibodies

Antibody	Company	Catalogue Number
Goat Anti-Rabbit IgG H&L (Alexa Fluor 488)	Abcam	ab150077
Anti-mouse IgG HRP linked	Cell Signalling technology	7076S
Anti-Rabbit IgG HRP linked	Cell Signalling technology	7074s
Anti-LaminB1	Abcam	ab16048
Anti-ß-tubulin	Abcam	ab6046
Anti-Nup153	Abcam	ab84872
Anti-Lamp1	Abcam	ab24170
Anti-Rab5	Abcam	ab18211
Anti-Rab7	Abcam	ab126712
Anti-ß-Actin	Abcam	ab8226
Anti-TSG101	Sigma	HPA006161
Anti-Syntenin	Abcam	Ab133267
Anti-H2A	Cell Signalling technology	25278S
Anti-Hsp70	System Biosciences	EXOAB-KIT-1
Anti-CD63	System Biosciences	EXOAB-KIT-1
Anti-CD81	System Biosciences	EXOAB-KIT-1
Anti-CD9	System Biosciences	EXOAB-KIT-1
Anti-Rabbit HRP	System Biosciences	EXOAB-KIT-1
Apolipoprotein-B (FITC)	Abcam	ab27637
CD63 (PE)	BD Bioscience	564222
CD9 (APC)	EXBIO antibodies	1A-567-C100

2.7 Primers

All primers used in PCR-based methods in the doctoral project are listed in the table below along with their manufacturers or the collaborators who provided them.

Table 2.7 Primers

Primers	Sequence	Source
Mycoplasma Fwd	5’-GGGAGCAAACAGGATTAGATACCCT-3’	Provided by Anja Rieb, University

		hospital Essen
Mycoplasma Rev	5'-TGCACCATCTGTCACTCTGTTAACCTC-3'	Provided by Anja Rieb, University hospital Essen
Mycoplasma Rev	5'-TGCACCATCTGTCACTCCGTTAACCTC-3'	Provided by Anja Rieb, University hospital Essen
FLI-1 Fwd	5'-TCCTACAGCCAAGCTCCAAGTC-3'	Provided by AG Dirksen, University hospital Essen
FLI-1 Rev	5'-GTTGGCGCTGTCGGAGAGC-3'	Provided by AG Dirksen, University hospital Essen
FLI-1 Fwd nested	5'-CAGAGCAGCAGCTACGGGCA-3'	Provided by AG Dirksen, University hospital Essen
FLI-1 Rev nested	5'-GAGGAATTGCCACAGCTGG-3'	Provided by AG Dirksen,University hospital Essen
FLT3-ITD Fwd	5'-GTAAAACGACGGCCAGGCAATTTAGGTA TGAAAGCCAGC-3'	Eurofins
FLT3-ITD Rev	5'–FAM-CTTTCAGCATTT TGACGGCAACC-3'	Eurofins
NPM1 Fwd	5'-GTAAAACGACGGCCAGGATGTCTATGAA GTGTTGTGGTTCC-3'	Eurofins
NPM1 Rev	5'–VIC-ATCAAACACGGTAGGGAAAGTTC-3'	Eurofins
Braf WT fwd	5'-AGGTGATTTTGGTCTAGCTACAGT-'3	Eurofins
Braf V600E fwd	5'-AGGTGATTTTGGTCTAGCTACAGA-'3	Eurofins
Braf rev	5'-TAGTAACTCAGCAGCATCTCAGGGC-'3	Eurofins

2.8 Cell Lines

All cell lines that were used in this doctoral project are listed in the table below along with their manufacturers or the collaborators that provided them.

Table 2.8 Cell Lines

Cell Lines	Cell Type	Source
B16-F10(CRL-6475)	Mouse Melanoma	Provided by AG Jablonska, University hospital Essen
MDA-MB-231	Human Breast Cancer adenocarcinoma	Provided by Dr. Vera Rebmann, University Hospital Essen
HeLa	Human Cervical Cancer adenocarcinoma	ATCC (CCL-2)
SK-MEL-28	Human Melanoma	Provided by Dr.Alexander Rösch, University hospital Essen
HEK-CD63-GFP	Human Embryonic Kidney with GFP-tag	Provided by AG Giebel University hospital Essen

G401	Human AT/RT	Provided by Kornelius Kerl, University hospital of Münster
BT16	Human AT/RT	Provided by Dr. Kornelius Kerl, University hospital of Münster
A204	Human AT/RT	Provided by Dr. Kornelius Kerl, University hospital of Münster
MV4-11	Human Acute Monocytic Leukaemia	Provided by AML diagnostic laboratory, University hospital Essen
OCI-AML3	Human Acute Myeloid Leukaemia	Provided by AML diagnostic laboratory, University hospital Essen
NB4	Human Acute Promyelocytic Leukaemia	Provided by Prof. Dr. Alex Carpinteiro University hospital Essen
ATRT-SHH-311	Human AT/RT	Provided by Kornelius Kerl University hospital of Münster
HT-29	Human Colorectal Adenocarcinoma	ATCC HTB-38
TC-71	Human Ewing Sarcoma	Provided by AG Dirksen, University hospital Essen
HEK-293	Human Embryonic Kidney	Provided by AG Dirksen University hospital Essen

2.9 Software

All software programmes that were used in this doctoral project are summarised in the table below.

Table 2.9 Software

Software	Company
StepOne® Software V2.2.1	Applied Biosystems
CXP Software	Beckman Coulter GmbH, Germany
FlowJo® Analysis Software	FlowJo®, LLC
Software BioDocAnalyze, Biometra	Analytik Jena AG, Germany
MACSquant software	MACSquant
ImageJ	National Institue of Health, USA
FusionFX software	Vilber
Leica LAS AF3	Leica Microsystems, Germany
Microsoft Excel	Microsoft, USA
Microsoft Word	Microsoft, USA
EM-Menu 4 software	TVIPS, Gauting, Germany
ZetaView Software 2.3	Particle Metrix GmbH
Agilent Tapestation Analysis Software.	Agilent Technologies

3. Methods

3.1 Cell Culture Methods

In this section, all methods used in the culturing and propagation of cell lines are described.

3.1.1 Cell culture conditions

Cell lines HT 29 (colorectal adenocarcinoma), B16-F10 (murine melanoma), MDA-MB-231 (breast adenocarcinoma), HEK-CD63-GFP (human embryonic kidney with a GFP tag on CD63), HEK-293 (human embryonic kidney) and NIH-3T3 (murine fibroblast), were cultivated and maintained in Dulbecco's minimal essential media (DMEM; Gibco® Life Technologies Corp., USA) with 10% foetal bovine serum (Biowest, France) and 1% penicillin/streptomycin (Gibco® Life Technologies Corp., USA). Cell lines HeLa (cervical cancer adenocarcinoma), MV4-11 (acute monocytic leukaemia), NB4 (acute promyelocytic leukaemia), TC-71 (Ewing sarcoma) and SK-MEL-28 (melanoma) were maintained in Roswell Park Memorial Institute 1640 (RPMI1640; Gibco® Life Technologies Corp., USA) with 10% foetal bovine serum and 1% penicillin/streptomycin. Cell line OCI-AML3 (acute myeloid leukaemia) was maintained in Alpha-MEM (Gibco® Life Technologies Corp., USA), 20% foetal bovine serum and 1% penicillin/streptomycin. Cells were cultivated at 37 °C with 5% CO_2

3.1.2 Passaging of cells

Medium was removed from the culture flasks using a pump and the cells were washed in 1X PBS. After the PBS was removed,1.5-3 mL (depending on flask size) of 0.5 % Trypsin/EDTA were added to the cells and flasks were placed at 37 °C until cells were detached. Growth medium was added in order to deactivate the trypsin, and the cell suspension was collected in a falcon tube. If the number of cells were required, the cells were counted by adding 100 µL of cell suspension to 9.9 mL of Isotone and placing the suspension in a Z1 Coulter Particle Counter (Beckmann Coulter). The cells were then briefly spun down and resuspended in fresh medium. Finally, the cells were then seeded into new flasks containing fresh medium and maintained at 37 °C, 5% CO_2.

3.1.3 Freezing of cell lines

A freezing medium consisting of 10% DMSO and 90% growth medium was prepared. Before freezing, the cells were washed with PBS, trypsinised, collected and counted,

as previously described in section *3.1.2.* Cells were then centrifuged at 300 x g for 5 min, after which the cell pellet was resuspended in the desired volume of freezing medium and aliquoted into cryogen tubes, 1 mL per tube. Cells were placed at –80°C, after which they were moved into the liquid nitrogen container for long term storage.

3.1.4 Mycoplasma testing

All cell lines used in the laboratory were tested for mycoplasma contamination. Supernatants were collected and stored at -20°C until analysis. First, 10-20 µL of supernatant were denatured by heating at 95°C for 10 minutes. A mastermix containing 5 µL 2x MyTaq Reactions mix (Bioline, Cat. No. 25048), 0.5 µL forward primers 5'-GGGAGCAAACAGGATTAGATACCCT-3' (20 µM), 0.5 µL reverse primer 5'-TGCACCATCTGTCACTCTGTTAACCTC-3' (10 µM) and 0.5 µL reverse primer 5'-TGCACCATCTGTCACTCCGTTAACCTC-3' (10 µM) and 2.5 µL dH_20 per sample was prepared. Next, 2µL of the denatured supernatants were added to 9µL of mastermix. For amplification, samples were heated at 94°C for 5mins followed by 30 cycles of 94°C for 1 min, 60°C for 1 min and 72°C for 1min, followed by a final step of 72°C for 10 min in a C100 Thermal Cycler (Biorad).The PCR products were then run on a 2 % agarose gel at 120V for 40 minutes with a 100 bp marker. Positive controls and a negative control (H_20) were also used.

3.1.4.1 **Preparation of 2% agarose gel**

To prepare a 2% agarose gel, 2 g of agarose powder was added to 100 mL of 1X tris-acetate-EDTA (TAE) buffer in a conical flask. This was then placed in a microwave until the powder had completely dissolved. Next, 3 µL of ethidium bromide was added and the mixture was poured into a mould for the gels containing a comb with enough teeth for 20 wells. The gel was then left to polymerise for 45 min.

3.2 EV Isolation Methods

In this section, all methods used for isolation of EVs from plasma or cell line-conditioned media are described.

3.2.1 Depletion of EVs from FBS

To remove bovine EVs from FBS, FBS was aliquoted into 94 mL ultracentrifugation tubes and centrifuged at 100,000 x g for 3 hours in a Beckman Coulter Optima XPN-80 ultracentrifuge. Later, this length of time was increased to overnight (~18 hours)

as new literature and recommendations became available. The supernatants were then filtered (0.2 µm), aliquoted in to 50 mL falcons and stored at -20°C until used.

3.2.2 Preparation of cell lines for EV extraction

AT/RT cell lines were seeded in 12 T175 flasks (Cell star, Cat No. 660175) with 25 mL of media supplemented with 10 % EV-depleted FBS and 1 % P/S. All other cell lines were seeded in 4 petri dishes PS, 145/20 mm, (Greiner bio-one, Germany) with 30 mL of media supplemented with 10 % EV-depleted FBS and 1 % P/S. In experiments using the TFF/SEC isolation method, 8 petri dishes were used instead of 4. Normally, between 3-5 million cells per flask/petri dish were seeded, depending on the growth rate of the cell line. Cells were cultured for 72 hours at 37 °C, 5 % CO_2, after which the supernatants were collected in 50 mL falcon tubes.

3.2.3 Preparation of plasma samples for EV extraction

All human plasma used in this study was obtained from five venous blood samples (7.5 mL) that were collected in EDTA-coated tubes from consenting healthy volunteers, all under 35 years of age. All blood samples were centrifuged at 500 x g for 10 min at 10℃ to separate out the plasma fraction. Plasma was then centrifuged at 3000 x g for 20 min at 10℃, before being aliquoted and frozen at-80℃ until further analysis. The mouse plasma used in this study was supplied to us from a collaboration partner, Dr. Kornelius Kerl, University of Münster. NODSCID mice were transplanted with G401 or A204 AT/RT cells causing tumour growth, after which blood was drawn, the plasma separated and 250 µL aliquots were received for EV extraction. The plasma was then centrifuged at 3000 x g for 20 min at 10℃, before being aliquoted and frozen at-80℃ until further analysis.

3.2.4 EV isolation with ultracentrifugation (UC)

EVs from plasma were isolated using several steps of differential centrifugation followed by ultracentrifugation (Fig 3.1). First, 2 mL of human plasma or 250 µL mouse plasma were centrifuged at 12,000 x g for 20 min at 10℃, the supernatant was transferred to ultracentrifugal polycarbonate 4mL tubes (Beckmann Coulter, Germany) and ultracentrifuged (Optima XPN-80 Ultracentrifuge Beckman Coulter GmbH, Germany) using a fixed angle rotor (Beckman Coulter Ti 50,4) at 100,000 x g for 70 min at 10℃. The pellet containing EVs was washed by resuspending in 2 mL of PBS, and then ultracentrifuged at 100,000 x g for 70 min at 10℃. After discarding the supernatant, the final EV pellet was resuspended in 1 mL of PBS and stored at -

80℃ until further analysis. For the isolation of EVs from cell line-conditioned media, the supernatant was centrifuged at 500 x g for 10 min, then 3000 x g for 20 minutes, followed by 12,000 x g for 20 min at 10℃. The supernatant was transferred to ultracentrifugal polycarbonate 94 mL tubes (Beckmann Coulter GmbH, Germany) and ultracentrifuged using a fixed angle rotor (Beckman Coulter Ti 45) at 100,000 x g for 70 min at 10℃. The pellets containing EVs from the same cell line were washed by resuspending in 30 mL of PBS, pooled together and ultracentrifuged at 100,000 x g for 70 min at 10℃. After discarding the supernatant, the final EV pellet was resuspended in 1 mL of PBS. Samples were stored at -80°C until further analysis. Ultracentrifugation steps were performed at the Institute of Transfusion Medicine, University Hospital Essen

3.2.5 EV precipitation using polyethylene Glycol (PEG) 6000

The previously collected cell line conditioned media (section 3.2.2) was centrifuged at 500 x g for 10 minutes, followed by another centrifugation step at 3000 x g for 20 minutes after which it was filtered through a 0.2 µm 250 mL rapid filtermax vacuum filter (TPP, Cat. No.99250). Supernatants were then mixed with PEG6000 (Sigma, Cat.No.81260) and PBS at a ratio of 1:0.256:0.025, respectfully, and placed at 4°C overnight. After the PEG precipitation step, conditioned media was centrifuged at 1500 x g for 30 min at 4°C. Supernatant and any residual medium were removed, pellets were resuspended and pooled together in 1 mL PBS in preparation for size exclusion chromatography.

3.2.6 EV isolation using size exclusion chromatography (SEC) with sepharose beads

EVs from healthy donor plasma were isolated using several steps of differential centrifugation followed by SEC (Fig. 3.1). Firstly, 2 mL of healthy donor plasma were centrifuged at 14,000 x g for 30 min at 4°C. Next, 1 mL of plasma was added to 1.5 cm x 12 cm Econo-Pac® chromatography columns (Biorad, Hercules, CA, USA) filled with 10 mL of Sepharose® 2B 60-200 µm (Sigma-Aldrich, USA). Six 1 mL PBS fractions containing EVs were collected per plasma sample. For the isolation of EVs from PEG precipitated cell line-conditioned media samples (section 3.2.5), 1 mL was added to the SEC columns as previously described for healthy donor plasma samples above. Six 1 mL PBS fractions containing EVs were collected per cell line sample, until an optimum fraction was established.

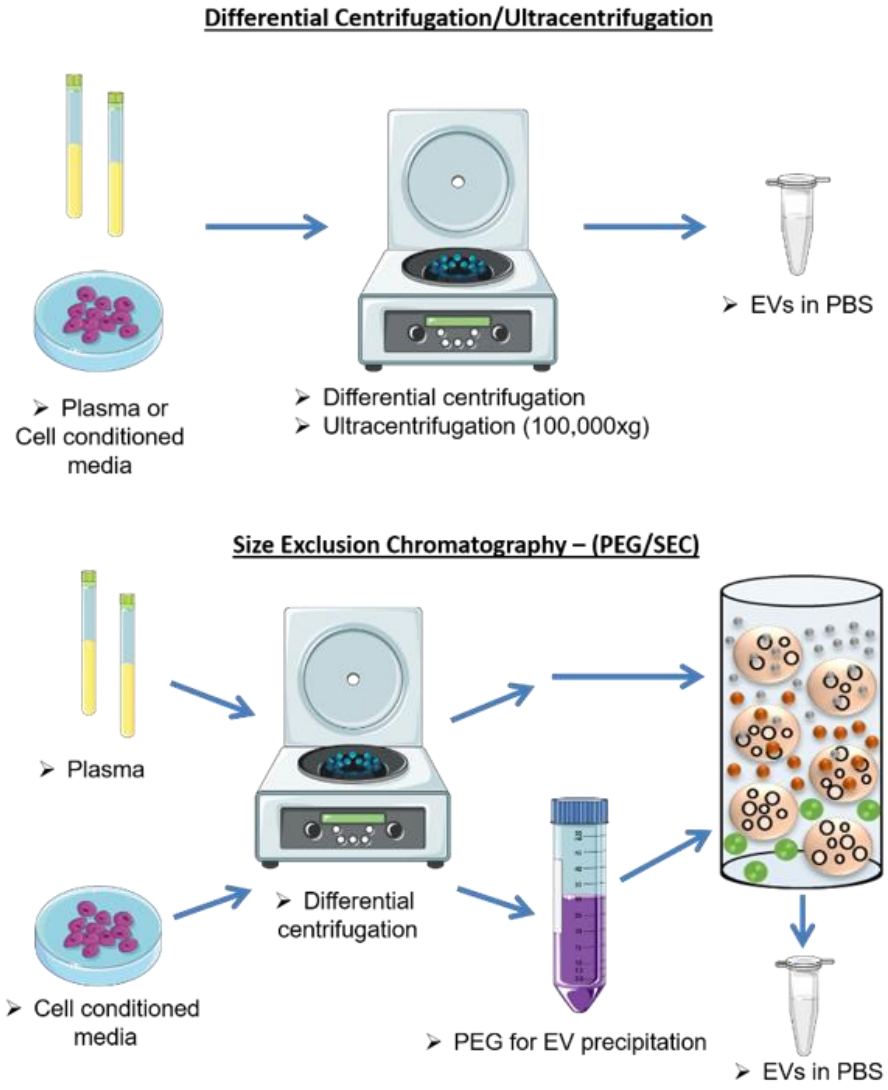

Figure 3.1: EV Isolation workflow. Workflow of the two main EV Isolation methods used in this project: ultracentrifugation (UC) and PEG/SEC. These isolation methods will be compared in section 4.3. Image made using smartservier.com and PowerPoint software.

3.2.5 Tangential flow filtration (TFF)

The previously collected cell line conditioned media (section 3.2.2) was centrifuged at 500 x g for 10 min, followed by another centrifugation step at 3000 x g for 20 min, after which it was filtered using a 0.45 µm filter (Satorius, Cat. No. 17829). The supernatant was added to two 20 mL syringes (FisherScientific, Cat. No. 14955460) and was then passed several times through a tangential flow filtration filter cartridge containing polysulfone hollow fibers with 5 nm pores (HansaBioMed Sciences, Cat.No.HBM-TFF). The cell medium and small molecules (<100 kDa) passed through the cartridge and were discarded as waste. This was repeated until 10 mL of concentrated supernatant remained, containing the EVs.

3.2.8 EV isolation using size exclusion chromatography with IZON columns

The qEV10 IZON column (Izon, Cat. No. 10283) was prepared by running 5 mL of filtered PBS through the reservoir. The reservoir was then attached to the column and filled with filtered (0.1 µm) PBS. The PBS was allowed to run though the column until the reservoir was empty. The 10 mL of concentrated supernantant from TFF (section 3.2.7) was added to the column, followed by 10 mL of filtered PBS. Once the 20 mL void volume had flowed through the column, 5 mL of filtered PBS was added and 5 mL flow through was collected. This was repeated until the desired number of fractions were collected.

3.2.9 EV concentration using amnicon columns

Collected SEC fractions (section 3.2.8) were added to Amnicon-Ultra 15 columns (Merkmillipore, Cat. No. UFC901024) and centrifuged at 4000 x g for 10 min at 4°C. If the volume of the fractions was still above 1 mL, the fractions were centrifuged again, until ≤1 mL of the fraction remained. The flow through was discarded and the concentrated fractions were then aliquoted into low retention 1.7 mL microcentrifuge tubes (Kisker, Cat. No. G017) and stored at -80 °C until desired date of use.

3.3 EV Fraction Characterisation Methods

In this section, all methods used for the characterisation of EV fractions isolated from plasma or cell line-conditioned media are described.

3.3.1 Transmission electron microscopy (TEM)

To confirm the presence of EVs in our preparations, TEM was performed at the Electron Microscopy Unit (EMU) of the Imaging Center Essen (IMCES). Briefly, 3 µL of the EV fractions were added on to a Formvar-coated 200 mesh copper grid (PLANO GmbH, Cat. No. SF162) which had a hydrophilic surface due to being exposed to glow discharging for 1.5 minutes (easiGlow™, PELCO). Samples were then negatively stained with 10 µL of 1.5% v/v Phosphotungstic acid (PTA) for 2 min or 3 µL of v/v Uranyl-acetate for 1 min. Excess liquid was removed and the grids were allowed to dry for at least 15 minutes. Samples were observed using a JEOL JEM-1400 Plus TEM (JEOL) at 120 kV. Images were processed using ImageJ or EM-Menu 4 software (TVIPS, Gauting, Germany). TEM was always performed with assistance from an IMCES associate.

3.3.2 Nanoparticle tracking analysis (NTA)

The size range and concentration of particles in the EV preparations were analysed by Nanoparticle Tracking Analysis using a ZetaView device (Particle Metrix GmbH). The system was calibrated using 100 nm polystyrene latex beads (Particle Metrix GmbH) and the following settings were applied for all samples: 11 positions, 5 cycles, medium quality, minimal brightness of 20, minimal size of 5 nm, maximal size of 200 nm, tracelength of 15 seconds, sensitivity of 75%, shutter speed of 75 ms and a frame rate of 30. Samples were diluted as required and made up to a final volume of 1 mL using DPBS. Size and concentration of particles were determined using Zetaview software (version 2.3), (Particle Metrix GmbH).

3.3.3 Protein concentration analysis

The protein content of EV fractions were determined by performing a bicinchoninic acid assay (BCA) using a BCA protein assay kit (Thermo Scientific, Rockford, IL, USA, Prod. Cat. No. 23225) according to the manufacturer's instructions. Protein concentrations were determined using the modulus microplate reader (Turner Biosystems) at a wavelength of 562 nm.

3.3.4 Bead-based FACS for EV fraction analysis

To analyse the percentage of EVs and contaminating apolipoproteins in EV fractions, a latex bead-based FACS assay was utilized. Firstly, 5 µL of latex beads (ThermoFisher, Cat. No. A37304) were mixed with 20 µL of the EV fraction of interest and incubated for 30 min on a shaker. Next, 200 µL of PBS were added to the sample and they were again incubated for 30 min on a shaker to remove unbound beads. After the incubation, 300 µL of PBS were added to the sample, followed by a 5 min centrifugation step at 2000 x g at room temperature (RT). The supernatant was removed leaving a residual volume of around 20 µL. Blocking of the beads was then performed by adding 20 µL of 5% BSA to the samples and incubating them for 30 min on a shaker, RT. PBS was added to the samples which were then centrifuged at 2000 x g for 5 min. The supernatant was discarded leaving a residual volume of around 50 µL. Next, 5 µL antibody anti-CD9-APC (EXBIO antibodies, Cat. No. 1A-567-C100), 10 µL anti-CD63-PE (BD Biosciences, Cat. No. 564222) or 5 µL anti-ApoB-FITC (Abcam, Cat. No. ab27637) were added to the samples and incubate for 30-40 min, RT, on a shaker. Then, 700 µL of PBS were added to the samples and centrifuged as previously described. The pellet containing the bead-bound EVs was

resuspended in 1 mL of PBS and analysed using a MACSQuant10 FACS instrument (MACSQuant). The results were analysed using FlowJo software.

3.4 Nucleic Acids- and Protein-related Assays

In this section, methods generally related to extraction and analysis of nucleic acids and proteins are described.

3.4.1 DNA extraction and quantification

QIAamp DNA Micro Kit (Qiagen, Cat. No. 56304) was used to extract EV-DNA from healthy donor and cell line EV fractions, according to the manufacturer's instructions. From each EV fraction, 100 µL were used, and DNA was eluted in 30-50 µL ddH_2O. QIAamp DNA Mini Kit (Qiagen, Cat. No. 51304) was used to extract DNA from cells, according to the manufacturer's instructions. From each sample, 200 µL of resuspended cells were used, and DNA was eluted in 50 µL ddH_2O.The DNA was quantified using Nanodrop or the QuantiFluor® dsDNA System (promega, Cat. No. E2670) according to the manufacturer's instructions. The dsDNA concentrations were determined using fluorescence with the modulus microplate reader (Turner biosystems) at a wavelength of 504 nm (excitation)/ 531 nm (emission).

3.4.2 Amplification of EV-DNA

When a higher concentration of DNA was required for the mutational detection of *SMARCB1* in mouse plasma EV DNA, protocol 2 of a REPLI-g Single Cell Kit (Qiagen, Cat. No, 150343) was used according to the manufacturer's instructions.

3.4.3 DNA bioanalysis

The sizes of the EV-DNA fragments that were extracted from the EV fractions were determined using an Agilent High Sensitivity D1000 ScreenTape Assay. Briefly, 2 µL High Sensitivity D1000 sample buffer and 2 µL High Sensitivity D1000 ladder (Agilent Technologies, Cat. No. 0006371807) were added to one tube of a tube strip (Agilent Technologies, Cat. No. 0200794-260). Next, 2 µL High Sensitivity D1000 sample buffer and 2 µL of each sample were added to the remaining tubes of the tube strip. The tube strip was then mixed by vortexing for 1 min and then briefly spun down. The tube strip was then loaded into the Agilent 4200 TapeStation instrument (4200 TapeStation, Agilent Technologies). Results were generated using the Agilent Tapestation Analysis Software.

3.4.4 DNase treatment

For specific experiments, the EV fractions were treated with DNase in order to degrade any non-EV-DNA or DNA on the EV outer surface. The DNase used was the rDNase provided with a Machery Nagel RNA extraction kit (Macherey-Nagel, Cat. No. 740902.50). To prepare the DNase, 1 µL of rDNase was added to 10 µL of the provided buffer. Next, the DNase solution was added to the EV fraction at a ratio of 1:10, respectively. Samples were heated at 37°C for 10 minutes. Samples were then used for recipient cell education experiments or the EVs were lysed and the DNA extracted for bioanalyser analysis.

3.4.5 RNA extraction and quantification

NucleoSpin® RNA XS kit (Macherey-Nagel, Cat. No. 740902.50) was used to extract EV-RNA from healthy donor and cell line EV fractions, according to the manufacturer's instructions. From each EV fraction, 100 µL were used, and RNA was eluted in 50 µL ddH_2O. The RNA was quantified using the QuantiFluor® RNA System (promega, Cat. No. E3310) according to the manufacturer's instructions. RNA concentrations were determined using fluorescence with the modulus microplate reader (Turner biosystems) at a wavelength of 562 nm.

3.4.6 Preparation of cDNA

The TC-71 and HEK-293 RNA that was previously isolated was transcribed into cDNA using a Transcriptor First Strand DNA Synthesis Kit (Roche, Cat. No. 04379012001). Briefly, 11 µl of RNA and 2 µl of the provided random hexamer primer were transferred to a 0.5 mL Eppendorf tube and heated for 10 min at 65 °C, after which they were cooled on ice. Then, 7 µl of a master mix consisting of the provided, protector RNase inhibitor, deoxynucleotide mix, reverse transcriptase reaction buffer and reverse transcriptase were added to the RNA samples, to a final volume of 20 µl. Samples were heated at 25°C for 10 min, followed by 55°C for 30 min and 85°C for 5 min in a C1000 Thermal Cycler (Biorad,Germany) for the cDNA synthesis.

3.4.7 Nested PCR

A two-step PCR procedure was performed for the detection of the FLI-1 translocation in an Ewing Sarcoma cell line, TC-71. For the specific amplification of the FLI1 gene region in the cDNA, PCR was performed in collaboration with AG Dirksen, University Hospital Essen. Briefly, 10µl of the synthesized cDNA was added to 15 µl Phusion PCR Master Mix (Thermo Fisher, Cat. No. F531S), 0.5 µl of each primer (forward 5'-

TCCTACAGCCAAGCTCCAAGTC-3' and reverse 5'-GTTGGCGCTGTCGGAGAGC-3'), 1 µl dimethylsulfoxide (DMSO) and 3 µl PCR H_20. For amplification, samples were heated at 95°C for 4 min, followed by 30 cycles of 95°C for 30 secs, 65°C for 30 secs and 72°C for 45 secs in a C1000 Thermal Cycler (Biorad). To increase the specificity of the PCR, a second nested PCR was subsequently performed using the products of the previous PCR, using a pair of primers that specifically bind to regions within the first template (forward 5'-CAGAGCAGCAGCTACGGGCA-3' and reverse 5'-GAGGAATTGCCACAGCTGG-3'). The PCR reagents were prepared according to the previous PCR. For amplification, samples were heated at 95°C for 4 min, followed by 30 cycles of 95°C for 30 secs, 60°C for 30 secs and 72°C for 45 secs in a C1000 Thermal Cycler (Biorad). After amplification, products were visualised in a 2% agarose gel using a BioDocAnalyzer (Biometra).

3.4.8 Real-time allele-specific PCR

To see if donor cell mutations, *BRAF*V600E, could be detected in EV-educated recipient HeLa cells, DNA was extracted for an allele-specific RT-PCR. Three primers were used in this assay which were previously described (Jarry et al., 2004). The Forward primer 'V' sequence was 'AGGTGATTTTGGTCTAGCTACAGT', the forward primer 'E' sequence was 'AGGTGATTTTGGTCTAGCTACAGA' and the reverse primer sequence was 'TAGTAACTCAGCAGCATCTCAGGGC' (Eurofins). The forward primer 'V' was for detection of the WT *BRAF* gene and the forward primer 'E' was used to detect the mutant *BRAF* V600E gene. The primers were prepared at a concentration of 100 µM µl-1, according to the manufacturer's instructions. Two mixes of the primers were then prepared, 'mix E' contained forward primer E and the reverse primer, and 'mix V' contained forward primer 'V' and the same reverse primer. Each primer mix had a concentration of 5 µM µl-1. Each gDNA sample was prepared in a 96-well PCR plate as shown in table 3.1.

Table 3.1: Preparation of samples for real-time allele-specific PCR.

Reagents	**Volume (µl)**
SYBR Green	10
Primer Mix V or E	1.6
gDNA	2
PCR H20	6.4
Final Volume	**20 µl**

The samples were analsyed using a OneStepPlus Real-Time PCR System (Applied Biosciences). For amplification, samples were heated at 95°C for 10 min, followed by 40 cycles of 95°C for 15 secs, 60°C for 1 min followed by a melting curve analysis temperature ramp from 60°C to 95°C.

3.4.9 GeneScan-based fragment-length analysis

To see if donor cell mutations, FLT3-ITD or NPM1, could be detected in EV-educated recipient cells, or donor cell EV-DNA, DNA was extracted for PCR. For PCR, the following primers were used: FLT3-ITD Primers - forward 5'-GTAAAACGACGGCCAGGCAATTTAGGTATGAAAGCCAGC-3' and reverse 5'–FAM-CTTTCAGCATTTTGACGGCAACC-3'; NPM1 primers - forward 5'-GTAAAACGACGGCCAGGATGTCTATGAAGTGTTGTGGTTCC-3' and reverse 5'–VIC-ATCAAACACGGTAGGGAAAGTTC-3' (Eurofins). From each primer, 1 µL (10 pmol/µL) were added to 12.5 µL of a Hot Start Taq 2x mastermix, along with 10 µL of the DNA sample. The amplification protocol was as follows: 95°C for 15 min; 35 cycles of 94°C for 30 seconds, 59°C for 30 seconds and 72°C for 60 seconds; a final step of 72°C for 10 min. PCR products were diluted (1:80) in H_2O, from which 1 µL was mixed with 0.3 µL GeneScan 600 LIZ Size Standard v 2.0 (Thermo Fisher) and 10 µL HiDi Formamid (Applied Biosystems). PCR products were heated for 5 min at 95°C for denaturation. Samples were then loaded on to the 3500 genetic analyser and GeneScan-based fragment-length analysis was performed.

3.4.10 Cell or EV lysis and protein extraction

For preparation of cell lysates for western blotting analysis, the growth medium of the cells of interest were removed and cells were washed in PBS. After washing, 1 mL of PBS was added to each well and a scraper was used to scrape cells from the surface of the well plate. The PBS containing the scraped cells was placed into corresponding Eppendorf tubes which were then centrifuged for 5 minutes at 1200 x g at 4°C. The supernatant was then discarded. A mastermix containing RIPA buffer, phosphatase- and protease inhibitors was prepared, and 100 µl was added to the cell pellet and vortexed. The cells were then incubated in the mastermix for 10 minutes on ice, after which they were centrifuged for 10 min at 16,000 x g at 4°C. The supernatants were then transferred into new Eppendorf tubes and the pellets were discarded. The protein concentration was determined by BCA (section 3.3.3), after which samples were then stored at -80 °C until desired date of use**.** For EV lysis,

equal volumes of EV fraction and RIPA buffer mastermix were mixed together and incubated for 10 minutes on ice, after which they were centrifuged for 10 min at 16,000 x g at 4°C samples were then stored at -80 °C until desired date of use**.**

3.4.11 Western blotting – Wet

For analysis of EV fractions, 25 µL of the lysed EV fractions were added to a master mix of β-mercaptoethanol (Sigma-Aldrich, Cat. No. M-7522) and 6x SDS Protein Loading Buffer pH 6.8 (Morganville Scientific, Cat. No. LB0100). For analysis of cell protein, 20-25ug of protein, according to BCA, were added to a master mix of β-mercaptoethanol and 6x SDS Protein Loading Buffer. Samples were heated at 95°C for 10 min before being loaded on to NuPAGE 4-12% Gels (Invitrogen, ThermoFischer Scientific, Cat. No. NPO321Box) with the PageRuler Prestained protein ladder (ThermoFischer Scientific, Cat No. 26616) for separation. Samples were then transferred on to a nitrocellulose blotting membrane (GE Healthcare, Amersham, Cat. No. 10600001) in a chamber submerged with 1x Transfer buffer. After transfer, membranes were stained with Ponceau Staining Solution (Cell Signaling Technology, Cat. No. 59803S) after which membranes were washed with TBS-T and blocked in 5 % milk blocking solution with 0.05% Tween-20 for 30 min. The membranes were incubated at 4°C overnight with primary antibodies in 5% milk blocking solution (1:1000): Anti-HSP70, Anti-CD63, Anti-CD81 (System Biosciences; Cat. No. EXOAB-KIT-1), Anti-TSG101 (Sigma; Cat.No. HPA006161), Anti-Beta-Tubulin (Abcam, Cat. No. ab6046), Anti-LaminB1(Abcam; Cat. No. ab16048), Anti-Rab5 (Abcam; Cat. No. ab18211) Anti-Rab7 (1:500) (Abcam; Cat. No. ab126712), Anti-Beta-Actin (Abcam; Cat. No. ab8226), Anti-Syntenin (Abcam; Cat: No. ab133267), Anti-H2A (Cell Signalling; Cat. No. 25278S). Membranes were washed with TBS-T and incubated at RT for 90 minutes with the secondary antibody (1:20,000 for the Goat Anti-rabbit HRP, Cat. No. EXOAB-KIT-1, System Biosciences) or (1:10,000 for the Anti-Rabbit IgG, HRP-linked Antibody, Cat.No.7074S, Cell Signalling). Blots were washed with TBST and developed with ECL Prime Western Blotting Detection reagents (GE Healthcare, Amersham Biosciences, Cat. No. 2232) and detected with Fusion FX Machine (Vilmer Lourmat).

3.4.12 Western blotting- Semi-dry

The same method was used as stated above for the ‘wet’ western blotting (section 3.4.11, however the transfer method was altered. The gel was washed with dH_20, equilibrated in transfer buffer for 15 min before the proteins were transferred on to a

PVDF membrane (GE Healthcare, Cat. No.10600058) using a Biometra Fastblot Device (Analytik Jena AG, Germany). After transfer, the membrane was washed in methanol after which is was left to completely dry. The membrane was then reactivated using methanol and rinsed in dH_2O, before proceeding with the rest of the method as stated above.

3.4.13 Coomassie blue staining

Equal volumes of EV fractions were treated 1:1 with RIPA buffer containing protease and phosphatase inhibitors. Next, 24 µL of the EV fractions were added to a master mix of β-mercaptoethanol (Sigma, Cat. No. M-7522) and 6x SDS Protein Loading Buffer pH 6.8 (Morganville Scientific, Cat. No. LB0100), heated at 95°C for 10 min, then loaded on to NuPAGE 4-12% gels (Invitrogen, Thermo Fischer, Cat. No. NPO321Box) with the PageRuler Prestained protein ladder (Thermo Scientific, Cat. No. 26616) for separation. The gel was then stained using Coomassie Brilliant Blue R-250 Staining Solution (BioRad, Cat. No. 1610436) for 1-2 hours. Gels were then destained overnight using a destaining solution (5% methanol, 7.5% acetic acid, 87.5% H_20).

3.5 EV-DNA Transfer-related Assays

In this section, methods used for the investigation of transfer of EV-DNA to recipient cells are described. A workflow of EV-DNA labelling, recipient cell education and downstream confocal microscopy analyses can be seen in Figure 3.2.

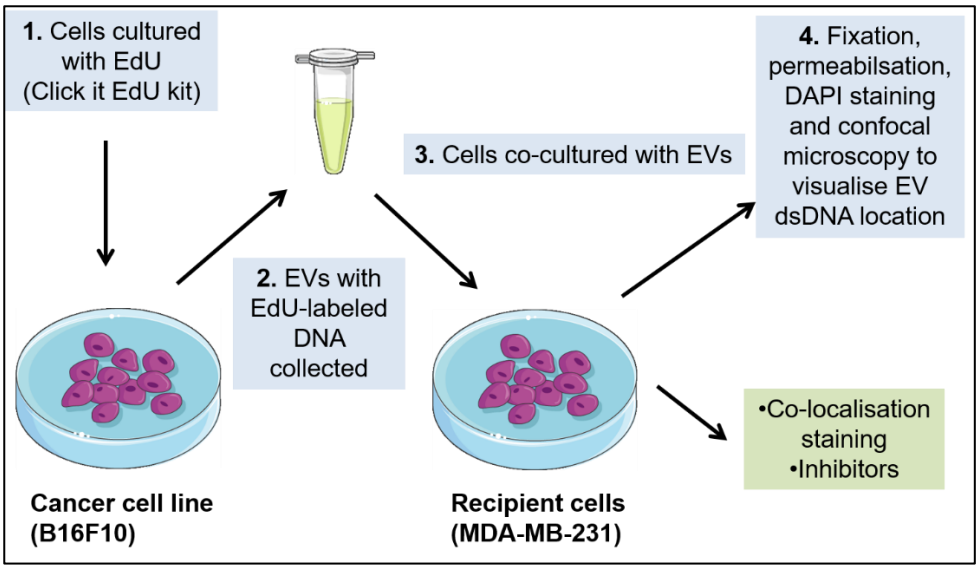

Figure 3.2: Investigating EV-DNA Transfer Work Flow. General overview of the methods used for EV-DNA labelling and recipient cell education for the investigation of EV-DNA transfer. Image created using smartservier.com and PowerPoint.

3.5.1 Generation of EdU-labelled EVs

Cells were seeded at the desired number in 145 cm well plates containing 30 mL EV-depleted media. Four hours after seeding, 2 µM 5-ethynyl-2'-deoxyuridine (EdU) from a Click-iT EdU Alexa Fluor 647 Imaging kit (ThermoFisher) was added to each plate (Fig. 3.2). It was expected that this EdU would integrate with newly synthesized gDNA in the cell, which would then be subsequently packaged inside EVs. This EdU-labelled EV-DNA could then be detected using an Alexa Fluor 647 florescent label.

3.5.2 Education of recipient cells

For education of recipient cells with EVs, 50,000 cells were seeded in to each well of a 24-well plate, with each well containing an autoclaved glass cover slip and 500 µl media. Cells were allowed to adhere to the cover slips overnight, after which media was removed and replaced with FBS-depleted media. B16-F10 derived EVs were then added to each well at desired time points- 1.6 x 10^9 particles per well as determined by NTA (Fig. 3.3). In some experiments inhibitors were added, this was always just before the 48h EV education time point (section 3.5.8). Knockdown experiments (section 3.5.10) were performed directly before the 48h time point. Cells were then incubated for the desired length of time at 37 °C and 5 % CO2.

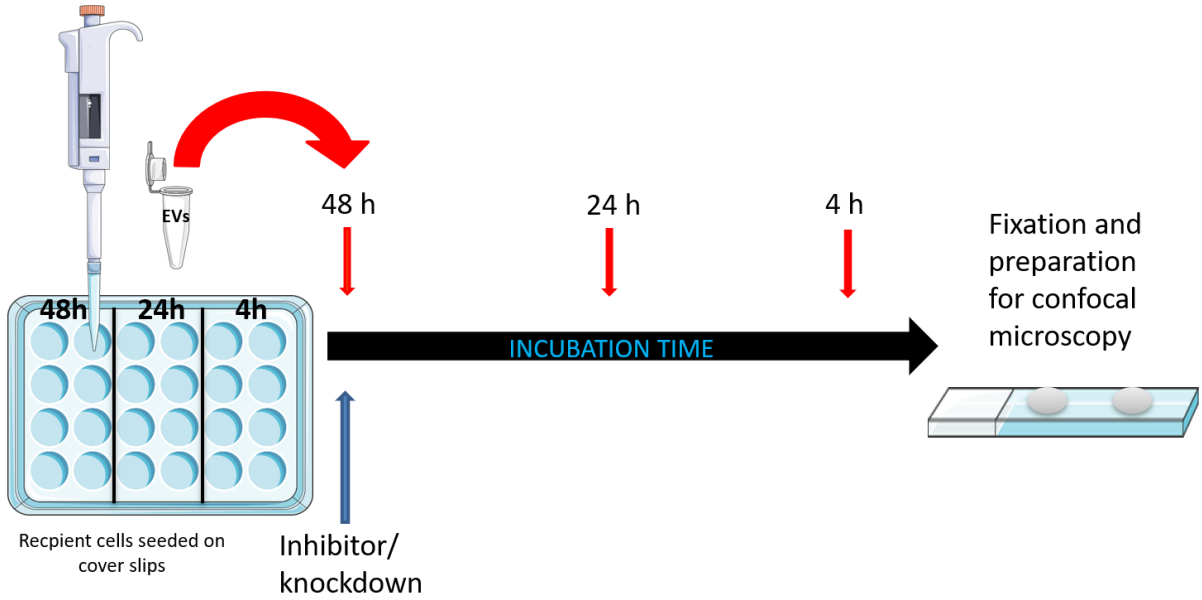

Figure 3.3: EV Education Time Line. Cells were seeded on cover slips in a 24-well plate in EV-depleted medium. Cells in all wells were seeded at the same timepoint, one day before the start of the education. Cells were treated with EVs at desired time points. The numeration of time points reflects the number of hours before the fixation the EVs were added i.e. 48h = EVs were added to cells 48h before fixation. In experiments where inhibitors were added or knockdowns were performed, this was always performed just prior to the 48h time point and the EVs were added as usual. Graphic created with smartservier.com and PowerPoint.

3.5.3 Fixation and permeabilization of recipient cells

Before fixation, cells were washed with 300 µl PBS per well, followed by 300 µl 0.01 % PBS-T. To fix the cells, 200 µl 4 % Paraformaldehyde (PFA) (ThermoFisher, Cat. No. J61899) were added per well. The plate was then incubated for 15 minutes at room temperature, after which the PFA was removed and the cells were washed with 200 µl sterile filtered 3 % bovine serum albumin in PBS (3 % BSA). The cells were then washed twice with 300µl PBS before 200 µl 0.5 % Triton-X100 were added for permeabilization. The plate was then incubated for 20 minutes at room temperature. Afterwards, the Triton-X100 was removed and 200 µl sterile filtered 3 % BSA were added. The cells were then washed a further two times with PBS.

3.5.4 Detection of EdU-labelled EV-DNA

A Click-iT™ EdU Alexa Fluor 647 Imaging kit from ThermoFisher Scientific was used to detect EdU-labelled EV-DNA in recipient cells. The stock solutions and reaction mixture were prepared according to manufacturers' instructions. A piece of Parafilm was placed into a plastic dish on to which 30 µl of the reaction mixture per coverslide was pipetted. The cover slips were then carefully transferred out of the well plate and placed cell-side down onto the reaction mixture drops. The samples were then incubated for 30 minutes at room temperature in the dark, after which the cover slips were transferred back into the 24-well plate and washed with 200 µl 3 % BSA, then 300 µl PBS.

3.5.5 Immunohistochemistry

Some recipient cell features were also labelled with antibodies. Cells on the coverslips were blocked for 30 minutes with 200 µl 1 % BSA in the dark. Parafilm was prepared, as mentioned previously, with 30 µl of primary antibody staining solution per coverslip. Primary antibodies used were anti-LaminB1 (1:500), anti-beta-Tubulin (1:200), anti-LAMP1 (1:1000), anti-Rab5 (1:1000) and anti-Rab7 (1:100). The coverslips were placed on to the primary antibody and incubated for 70 minutes at room temperature in the dark. The cells were then washed three times with 300 µl PBS-T. Parafilm was then prepared with 30 µl of a staining solution containing an Alexa Fluor-488 conjugated secondary antibody (1:1000 in 3% BSA). Coverslips were then placed on to the secondary antibody solution and incubated for 45 minutes in the dark. Cells were then washed three times with PBS-T.

3.5.6 DAPI staining

DAPI (4′,6-Diamidin-2-phenylindol) staining was performed so that the nucleus of the recipient cells could be visualised. For each coverslip, 200 µl of a 0.4 µg/mL DAPI solution was added and incubated for 10 minutes on a shaker at room temperature protected from light. Coverslips were then washed with PBS and mounted on to microscope slides using Fluoromount-G® mounting medium (Southern Biotech, Cat. No. 0100.01). Slides were left to dry for at least 48 hours before microscopy.

3.5.7 Confocal fluorescence microscopy

Confocal fluorescence microscopy was performed using a Leica TCS SP8 confocal microscope with a 1.3 N.A., 63 x glycerin immersion objective (HC PL APO CORR CS2). AF647 and AF488 were excited with a white light laser (WLL2) at 633nm and 488nm, respectively, while DAPI was excited with a 405 nm diode laser. For detection, a spectral confocal detection channel (HyD) was used, set at at 643-720 nm for AF647, 498-580 nm for AF488 and 416-480 nm for DAPI. Image capture settings were as follows: pixel dwell time of 1.2 µs, pixel size of approximately 180 nm and a line average of 4 using the Leica LAS AF 3 software. All confocal fluorescence microscopy was performed at IMCES of the University Hospital Essen. ImageJ was used for the processing of images.

3.5.8 Addition of inhibitors for confocal microscopy

In order to assess the effects of three inhibitors on EV-DNA uptake by MDA-MB-231 cells, 50,000 MDA-MB-231 cells were seeded in a 24-well plate with coverslips with 500 µL of DMEM medium. After 24 hours, the medium was removed, cells were washed with PBS, and 500 µL EV-depleted medium was added. Next, aphidicolin (8.5 µg/mL), ivermectin (10 µg/mL) or hydroxyurea (2.5 µM) was added to the cells and incubated for 48 hours at 37°C, 5% CO_2. Slides were then fixed and processed for confocal microscopy as previously described.

3.5.9 Addition of inhibitors to recipient cells for FACS analysis

In order to assess the effects of three inhibitors on MDA-MB-231 cells, 2 x 10^5 MDA-MB-231 cells were seeded in a 6-well plate with 1 mL of DMEM medium. After 24 hours, the medium was removed, cells were washed with PBS, and 1 mL EV-depleted medium was added. Next, aphidicolin (8.5 µg/mL), ivermectin (10 µg/mL) or hydroxyurea (2.5 µM) was added to the cells and incubated for 48 hours at 37°C, 5% CO_2. The medium was removed and collected in 5 mL FACS tubes, while the cells

were washed with PBS. Then, 200 µl Trypsin-EDTA were added to each well and the plate was incubated for 3 min at 37°C, 5% CO_2. The previously collected medium was added to the cells to deactivate the trypsin, after which the cell-containing medium was returned to the FACS tubes. The cells were then centrifuged at 1300 x g for 5 min at 4°C, after which the supernatant was discarded, and the cells resuspended in PBS. The centrifugation step was repeated, and the cell pellet was then used for cell cycle or apoptosis assay.

3.5.9.1 **Cell cycle assay**

The previously prepared cell pellet was resuspended in 800 µl ice cold ethanol (100 %) dropwise while vortexing, after which the cells were incubated on ice for 30 min. The cells were suspended in PBS and then pelleted by centrifugation at 1300 x g for 5 min at 4 °C. The supernatant was discarded, and the wash step repeated. After the second centrifugation step, the supernatant was discarded, leaving a residual 200 µl to which 12.5 µl RNAse A (10 mg/mL) were added. Cells were incubated for 30 min at 37 °C, after which 500 µl PBS and 20 µl of Propodium Iodide (PI) (1 mg/mL) were added. The samples were then analysed using a FACS CANTO FC500.

3.5.9.2 **Apoptosis assay**

To assess cell death, a BD Annexin V: FITC Apoptosis detection kit I (BD Bioscience) and flow cytometry analysis were used. The cell pellet was resuspended in 100 µl 1x Binding Buffer. Then, 2 µl FITC Annexin V and 5 µl PI were added and incubated for 20 minutes at room temperature in the dark. Next, 300 µl 1x Binding Buffer were added to each sample and flow cytometry analysis was performed with a FACS CANTO FC500.

3.5.10 Transfection using lipofectamine RNAiMAX

Cells were seeded in a 6- or 24- well plate, with or without microscopy cover slips. When the cells were 70-80 % confluent, the cells were transfected with siRNA intended to knockdown Rab5A (Santa Cruz, Cat. No. sc-36344) or Rab7 (Santa Cruz, Cat. No. sc-29460), or a siRNA control with or without a GFP tag, using a Lipofectamine RNAiMAX reagent (ThermoScientific, Cat.No. 13778030). In each well intended for knockdown, 30 pmol of siRNA and desired volume (depending on well size)of Lipofectamine RNAiMAX were added in Opti-MEM medium (Gibco), with a final well volume of 500 µl in a 24-well plate or 1500 µl in a 6-well plate. After 5 hours of incubation at 37 °C with 5 % CO_2 the Opti-MEM medium was replaced with normal

growth medium. If education of the transfected cells was desired, the medium would be replaced with EV-depleted growth medium and EVs would be added at this point. After the desired incubation period, the transfected cells were collected and lysed in preparation for western blot analysis, or the coverslips were collected and prepared for confocal microscopy.

3.5.11 Nuclear extraction

The nuclei of recipient cells that had been educated with EVs were extracted using a nuclear extract kit (Active Motif, Cat No. 40010). Step 1 and 2 were performed according to the manufacturer's instructions for preparation of a nuclear extract from cells. After step two, the supernatant (cytoplasmic fraction) was stored and 25-30 µL of the nuclear fraction was kept aside for western blotting analysis. The rest of the nuclear fraction was used for DNA extraction. The nuclear fraction that had been previously stored was then further processed according to step 3 of the manufacturer's protocol for preparation of a nuclear extract from cells, in order to obtain nuclear protein for western blotting analysis. In addition, whole cell extracts of untreated recipient cells were prepared according to the manufacturer's instructions for preparation of whole-cell extract from cells for western blotting analysis.

3.5.12 STR DNA fingerprinting

DNA extracted from MDA-MB-231 cells that had been educated with B16-F10 EVs, was sent for STR DNA fingerprinting to confirm the presence of donor cell EV-DNA in recipient cell nuclei. DNA fingerprinting was performed by IDEXX. For the assay, samples containing 15 µL of DNA at a concentration of 25 ng/µL were prepared, as determined by Nanodrop.

3.5.13 Fluorescence microscopy

To confirm uptake of GFP-labelled HEK-CD63-GFP EVs, fluorescence microscopy was performed using an AMG EVOS light microscope with GFP filter. Microscopy was performed at the Imaging center Essen (IMCES), University hospital Essen.

3.6 Statistical Analysis

All statistical analyses were performed using Students T-test with Microsoft Excel software.

4. Results

4.1 EV Nucleic Acid Cargo as a Diagnostic Tool

In order to explore the diagnostic potential of EV-DNA and EV-RNA, the first part of this project focussed on the detection of *SMARCB1* mutations in DNA extracted from EVs of AT/RT cell lines, mouse plasma or patient samples, and the detection of the *EWS-FLI-1* mutation in RNA extracted from EVs isolated from a Ewing Sarcoma cell line.

4.1.1 Detection of SMARCB1 mutations in AT/RT cell line EV-DNA

Cell lines containing known *SMARCB1* mutations were used to establish the idea that EV-DNA could be used as a diagnostic marker in AT/RT. This part of the project was begun by a former colleague, and was taken over by myself at the commencement of my Ph.D. After 72 hours of cultivation in EV-depleted medium, the supernatant of AT/RT cell lines ATRT-SHH-311, A204 and BT16 were exposed to ultracentrifugation in order to isolate EVs. EVs fractions were characterised using nanoparticle tracking analysis (NTA) for EV concentration, BCA for protein content, and EV-DNA was then extracted and quantified (Table 4.1).

Table 4.1: AT/RT EV Fraction Characteristics. EV fractions were isolated from cell line-conditioned media using ultracentrifugation. Fractions were analysed using NTA, BCA and DNA extraction and quantification..

Cell line	EV Concentration (particles/mL)	Protein (µg/µl)	dsDNA (ng/µl)
BT16	$5.8x10^{10}$	0.24	8.94
A204	$3.75x10^{10}$	0.15	0.83
ATRT-SHH-311	$2.7 x 10^{10}$	0.12	34

The extracted and quantified DNA was then sent to a collaborator, Florian Oyen, University hospital Hamburg-Eppendorf, for the detection of expected mutations or deletions using an MPLA kit or Sanger sequencing. It was found that in all tested cell lines, the expected *SMARCB1* mutations were detectable from the isolated EV-DNA (Table 4.2).

Table 4.2: Detection of SMARCB1 Mutations in AT/RT Cell Line EV-DNA. Mutations were detected using MPLA kit or Sanger sequencing, performed by Florian Oyen, University hospital Hamburg-Eppendorf.

Cell Line	*Known SMARCB1* Mutation	Detected
BT16 EVDNA	Homozygous mutation: c.178_179delAGp.Arg60Glufs*10	+
A204 EVDNA	Hemizygous mutation: c.543_544delTCp.Gln182Alafs*28(LOH) and delPPIL2_SMARCB1	+
ATRT-SHH-311 EVDNA	Homozygous mutation: c.618G>Ap.Trp206*	+

4.1.2 Detection of SMARCB1 mutations in AT/RT mouse plasma

After laying the foundation at a cell line level, in the next phase, mice models were adopted in order to further investigate the effectiveness of using EV-DNA as a diagnostic marker in AT/RT. The plasma of NODSCID mice which had tumours consisting of human AT/RT cells containing either a whole *SMARCB1* gene depletion (G401) or a hemizygous 2-base-pair deletion in exon 5 (A204) was sent to us from a collaboration partner, Dr. Natalia Moreno Galarza, University hospital Münster, who had carried out the mice experiment. The plasma was exposed to ultracentrifugation and EVs were isolated (Table 4.3). The DNA of the EVs was extracted and quantified, and sent to a collaboration partner, Florian Oyen, University hospital Hamburg-Eppendorf, for detection of mutational status. The assay used for mutational detection was a Multiplex-PCR (MLPA) for exon 5 of the *SMARCB1* gene. Unfortunately, none of the expected mutations or deletions could be detected (Fig. 4.1).

Table 4.3: Mouse Plasma EV Fraction Characteristics.The plasma of NODSCID mice, that had been transplanted with AT/RT A204 or G401 cells after which a tumour formed, was subjected to ultracentrifugation for EV isolation. The EV fractions were then analysed using NTA and DNA was extracted. dsDNA was quantified and sent to Florian Oyen, University hospital Hamburg-Eppendorf, for mutational detection of AT/RT specific mutations. indicates DNA was amplified.*

Mouse ID	Mouse Type	Injected AT/RT Cells	Concentration (Particles/ml)	dsDNA (ng/ul)
828	NODSCID	A204	$1.10x10^{7}$	2.01
829	NODSCID	A204	$1.40x10^{7}$	3.13
830	NODSCID	A204	$3.80x10^{7}$	1.95
861	NODSCID	G401	$1.30x10^{7}$	1.81
866	NODSCID	G401	$1.90x10^{7}$	1.41
877	NODSCID	G401	$8.30x10^{6}$	1.31
874+721+832	NODSCID	A204	$9.80x10^{10}$	171.26*
857+833+835	NODSCID	A204	$8.10x10^{10}$	150.70*
862+863+876	NODSCID	G401	$3.40x10^{10}$	147.09*

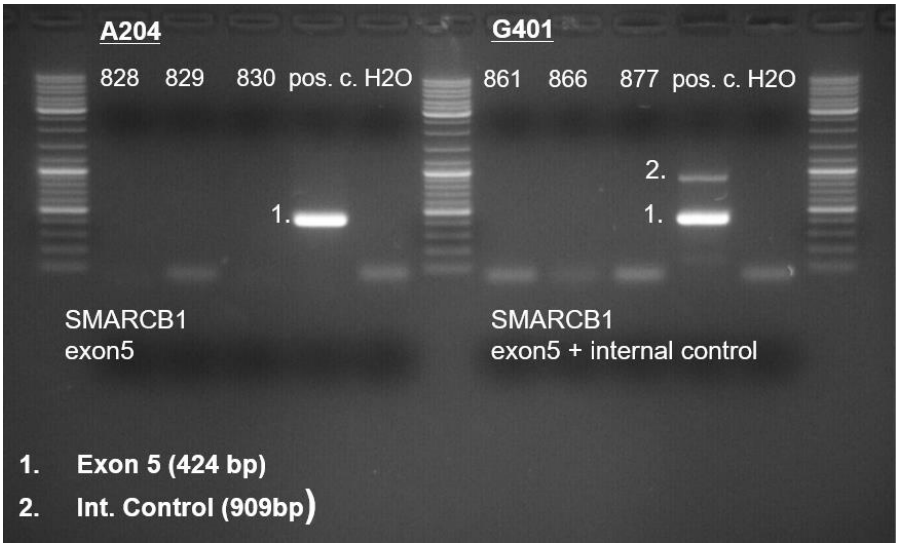

Figure 4.1: Detection of SMARCB1 Mutations in Mouse Plasma EV-DNA. EVs were harvested from the plasma of mice containing A204 (828,829,830) or G401 (861,866,877) ATRT tumours. The EV-DNA was extracted and sent to collaboration partner, Florian Oyen, University hospital Hamburg-Eppendorf for mutational analysis using multiplex PCR. The expected SMARCB1 deletions could not be detected in any of the samples. As G401 contains a whole gene deletion, a second positive control was also used for analysis. Picture provided by Florian, Oyen.

As it was suspected that the EV content and, therefore, the EV-DNA content may have been too low for effective analysis, we repeated the experiment with plasma pooled from three mice per mutation to try and increase the number of EVs. We also used a different isolation method of size exclusion chromatography (SEC) with sepharose beads with hope of increasing the EV yield. The DNA was also amplified using a REPLI-g Single Cell Kit (Qiagen) in order to increase the amount of DNA for analysis. Despite these efforts, the expected mutations could not be detected in the mouse EV-DNA samples. In an attempt to remedy this situation, our collaborators tried to establish different methods of mutational detection for EV-DNA, such as OncoScan, however, the EV-DNA did not appear to be efficient for this detection method.

4.1.3 Detection of SMARCB1 mutations in AT/RT patient plasma

The third part of the AT/RT project plan was to also assess the biomarker potential of the EV-DNA in AT/RT patient plasma. Unfortunately, enough patient plasma samples were not collected within the time-frame of this project; therefore, patient plasma analysis could not be performed.

4.1.4 Detection of EWS-FLI-1 fusion gene in Ewing Sarcoma Cell line EV-RNA

In order to evaluate the biomarker potential of EV-RNA in the cancer model of Ewing sarcoma, Ewing Sarcoma cell line, TC-71, containing a EWS-FLI-1 fusion oncogene,

and negative control HEK-293 cells were cultured in EV-depleted medium for 72 hours. The supernatant was collected and EVs were extracted using a PEG/SEC method as described in section 3.2. The PEG/SEC EV fractions 4 and 5 were characterised using NTA, BCA and TEM (Table 4.4; Fig 4.2)

Table 4.4: Characteristics of TC-71 and HEK-293 EV Fractions. EVs were isolated using PEG/SEC, the 4th (F4) and 5th (F5) EV fractions were characterised using NTA and BCA.RNA concentration was determined using RNA quantifluor assay.

Sample	Particle/mL	Protein (mg/mL)	RNA (ng/µL)
TC-71 F4	$3.30x10^9$	0.01	0.38
TC-71 F5	$1.30x10^9$	0.04	0.20
HEK 293 F4	$6.60x10^8$	0.01	0.57
HEK 293 F5	$9.10x10^8$	0.04	0.32
TC-71 F4	$2.70x10^9$	0.01	0.03
TC-71 F5	$2.40x10^9$	0.08	0.14
HEK 293 F4	$8.30x10^8$	-0.01	0.44
HEK 293 F5	$9.50x10^8$	0.02	0.97

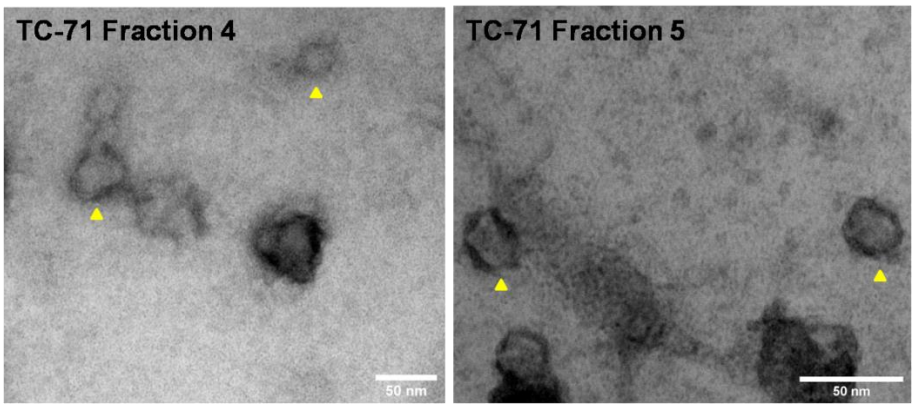

Figure 4.2: Identification of TC-71 EVs Using Transmission Electron Microscopy (TEM). TC-71 PEG/SEC fraction 4 and 5 were analysed using TEM with negative staining. EV-like structures are indicated with yellow arrow heads. Scale bar = 50 nm.

RNA was extracted from 100 µL of each EV fraction and converted into cDNA. A nested PCR approach was then used for the detection of the expected mutation. The PCR approach required optimisation including a change of reagents, editing of the PCR protocol and resolving issues of cross contamination. Finally, in collaboration with members of AG Dirksen, University hospital Essen, it was possible to detect the expected EWS-FLI1 translocation PCR product (228bp) in EV-RNA from PEG/SEC fractions 4 and 5 of the TC-71 cell line, but not in the negative control HEK-293 cell line, using the nested PCR approach (Fig. 4.3).

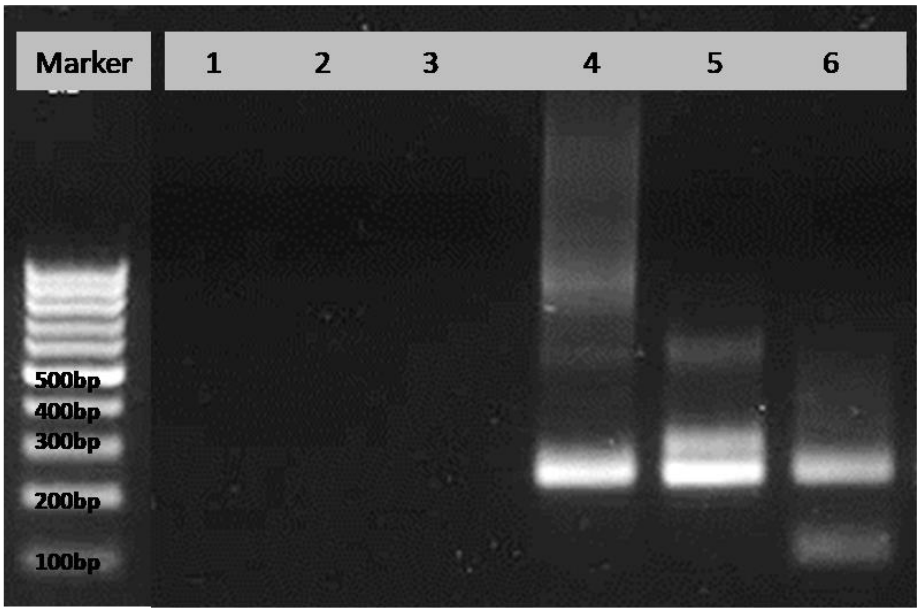

No.	1	2	3	4	5	6
Sample	HEK Cells	HEK EV Fraction 4	HEK EV Fraction 5	TC71 Cells	TC71 EV Fraction 4	TC71 EV Fraction 5

Figure 4.3: Mutational detection of EWS-FLI-1 Mutation in TC-71 EV-RNA. EV-RNA was extracted from PEG/SEC fraction 4 and 5 EVs and cells of Ewing sarcoma cell line TC-71 and negative control HEK cells. cDNA was synthesised from the RNA and a nested PCR was performed in collaboration with AG Dirksen for the presence of the EWS-FLI-1 fusion gene.

These results showed that the principal idea of using EV nucleic acids as diagnostic markers in cancer was viable one.

4.2 Investigation of EV-DNA Transfer to Recipient Cells

This part of the project focussed on investigating the transfer of EV-DNA to recipient cells by optimising a method in which EV-DNA is labelled with EdU. The labelled EV-DNA could then be visualised after being internalised by recipient cells using confocal microscopy. Optimisation of this method allowed us to further investigate certain aspects of EV-DNA transfer and localisation using B16-F10 EVs and MDA-MB-231 recipient cells.

4.2.1 Optimisation of Labelling Methods

Labelling methods were optimized and adopted to allow visualization of EV-DNA.

4.2.1.1 **Labelling of EV-DNA**

In order to track the uptake of EV-DNA into recipient cells, we first had to optimise a method to label DNA inside the EV. Based on the premise that EVs contain gDNA

from the parental cells, we optimised the use of a Click-IT EdU cell proliferation kit in which 5-ethynyl-2'-deoxyuridine (EdU) is incorporated into replicating gDNA. We believed this EdU-labelled gDNA would then be packaged into EVs and would therefore render the EV-DNA identifiable. In the second part of the Click-iT kit reaction, the incorporated EdU is fluorescently labelled with an Alexa Fluor 647 dye, deeming it possible to visualise the DNA using confocal fluorescence microscopy. We found that the EdU was particularly toxic to cells, which led to a period of optimisation of the volume and concentration added to the cells during EV production. Toxicity of the substance had been previously documented (Hong Zhao et al., 2013). Subsequently, we found that 3 million cells per plate with an EdU concentration of 2 µM was sufficient for EV production.

4.2.1.2 **Labelling of the EV membrane**

EV membrane labelling was also attempted, so that it would be possible to visualise the EVs themselves as well as the EV-DNA during EV transfer to recipient cells. To do this, we incorporated the staining of the EV fraction into our PEG/SEC isolation method, by adding PKH67- a green fluorescent cell linker- to the precipitated EV pellet before performing the SEC step. Unfortunately, despite several attempts to optimise this, including changing PKH67 concentration, cell number and fixation methods, it was not possible to consistently visualise the EV membrane staining in confocal microscopy. Therefore, we decided to move forward with only the EV-DNA labelling.

4.2.2 Characterisation of the isolated B16-F10 EVs

B16-F10 EVs were isolated using PEG/SEC as previously described (section 3.2.5/6), and PEG/SEC EV fraction 4 was used for all transfer experiments. To confirm the presence of EVs in our EV fractions before using them in functional assays, EVs were visualised using TEM (Fig. 4.4A). EV fractions were also analysed for their particle number and size using NTA (Fig. 4.4B). EV fractions were also positive for EV markers Hsp70 and TSG101 (Fig. 4.4C). Protein content of EV fractions were also measured using BCA assay (Table 4.5).

*Table 4.5: B16-F10 EV Fractions' Characteristics. All B16-F10 EV fractions used in the transfer project are summarised in the table below. All fractions used were isolated using PEG/SEC, only fraction 4 was used for education. * indiciate measurement with Nanodrop so whole DNA not just dsDNA was measured*

EV Fraction	Date	Concentration particles/ml	Protein Concentration (ug/ul)	dsDNA Concentration (ng/ul)
B16F10 EVs	17.08.18	$6.40x10^{10}$	0.18	-
B16F10 EdU+ EVs	17.08.18	$1.20x10^{11}$	0.08	-
B16F10 EVs	08.10.18	$1.00x10^{10}$	0.12	2.12
B16F10 EdU+ EVs	08.10.18	$1.80x10^{10}$	0,16	20.10
B16F10 EVs	08.10.18	$1.30x10^{10}$	0.14	2.10
B16F10 EdU+ EVs	08.10.18	$2.10x10^{10}$	0.21	21.27
B16F10 EVs	30.10.18	$8.30x10^{10}$	0.45	0.26
B16F10 EdU+ EVs	30.10.18	$1.70x10^{11}$	0.25	9.19
B16F10 EVs	23.11.18	$1.7x10^{11}$	0.04	0.29
B16F10 EdU+ EVs	23.11.18	$8.80x10^{10}$	0.10	9.08
B16F10 EVs	19.11.19	$1.20x10^{11}$	0.02	8.10*
B16F10 EdU+ EVs	19.11.19	$4.70x10^{10}$	0.00	4.10*
B16F10 EdU+ EVs**	12.03.20	$4.20x10^{11}$	0.15	47.7*
B16F10 EVs	26.05.20	$2.30x10^{10}$	0.06	13.10*
B16F10 EdU+ EVs	26.05.20	$5.00x10^{10}$	0,09	9.70*

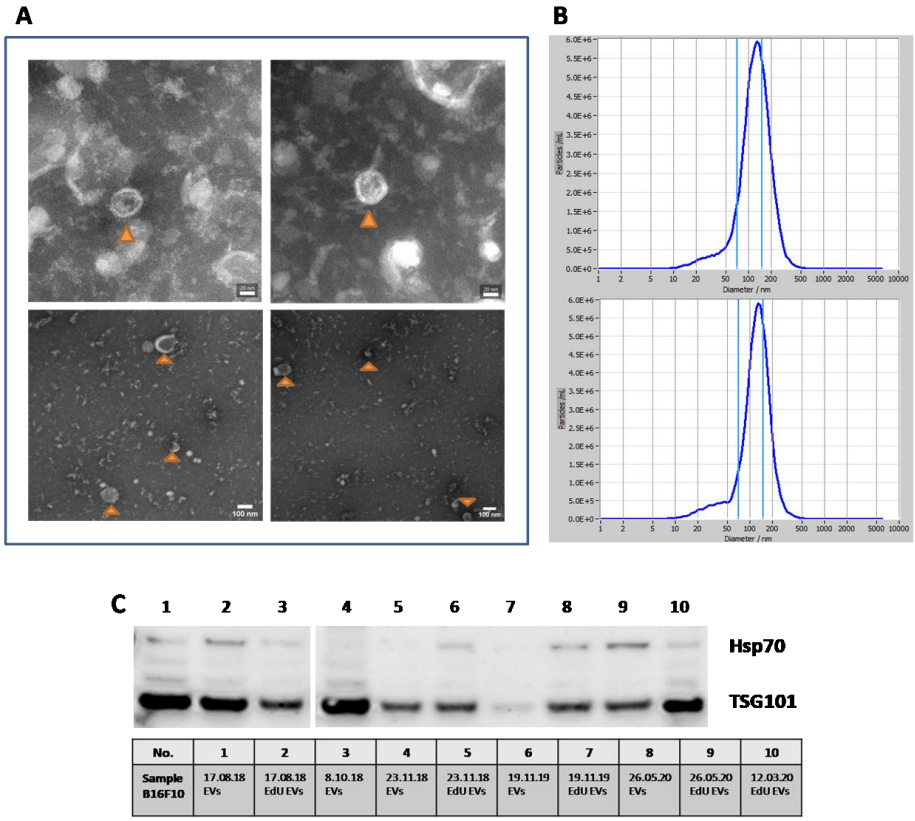

Figure 4.4: Characterisation of B16-F10 EVs. B16-F10 EVs were characterised by (A) TEM, (B) NTA and (C) western blotting. Yellow arrows indicate EV-like structures. Equal volumes of EV fractions were used for western blotting analysis. Samples were processed on the same blot, picture was cropped to exclude irrelevant samples TEM scale bars = 100 µm Images included are representative.

4.2.3 Confirming EV-DNA internalisation using confocal microscopy

After optimisation of the Click-iT kit and microscopy preparation protocol, we wanted to confirm the successful labelling of the EV-DNA and the ability of the EV-DNA to be taken up by recipient cells. We confirmed both of these using confocal microscopy (Fig. 4.5) with the addition of positive and negative controls, which were included in every microscopy experiment thereafter. The AlexaFluor647 (red) signal of the EdU-labelled EV-DNA could clearly be visualised. In addition, it was found that after 48 hours of incubation with the EVs containing the EdU-labelled DNA, the majority of the EdU signal was located in the nucleus of some of the recipient cells suggesting that the DNA was localising there.

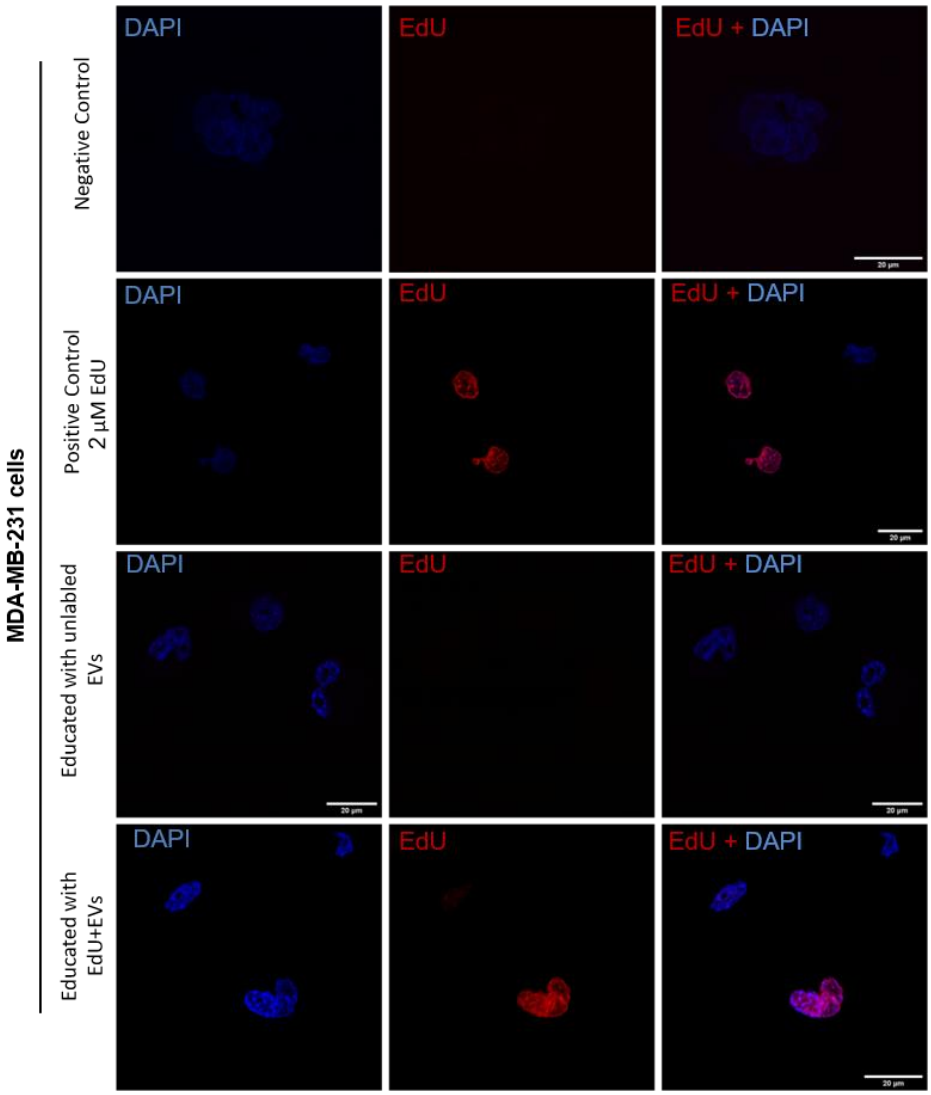

Figure 4.5: Successful EV-DNA Labelling with EdU. MDA-MB-231 cells were educated with B16-F10 EVs containing EdU-labelled DNA for 48 hours. Cells were then visualised using confocal microscopy. Negative control = no addition of EVs of EdU. Positive control = direct addition of EdU 2µM. Unlabelled EVs = addition of EVs without EdU-labelled DNA. Red =EdU-labelled gDNA or EV-DNA, blue = recipient cell nucleus. Scale bar = 20 µm.

4.2.4 EV-DNA uptake time course

In order to get an idea of the course taken by EV-DNA during uptake into the recipient cell, several time courses were performed where EVs were added to recipient cells at various time points and then visualised by confocal microscopy. These time courses revealed the movement of the EdU-labelled EV-DNA from the area of the cell membrane towards the area of the nucleus, with the DNA being located inside the nucleus after 48 hours (Fig. 4.6). In the earliest times points, the EdU appeared to be aggregated and sometimes EdU positive nuclei were seen before the 48h time-point.

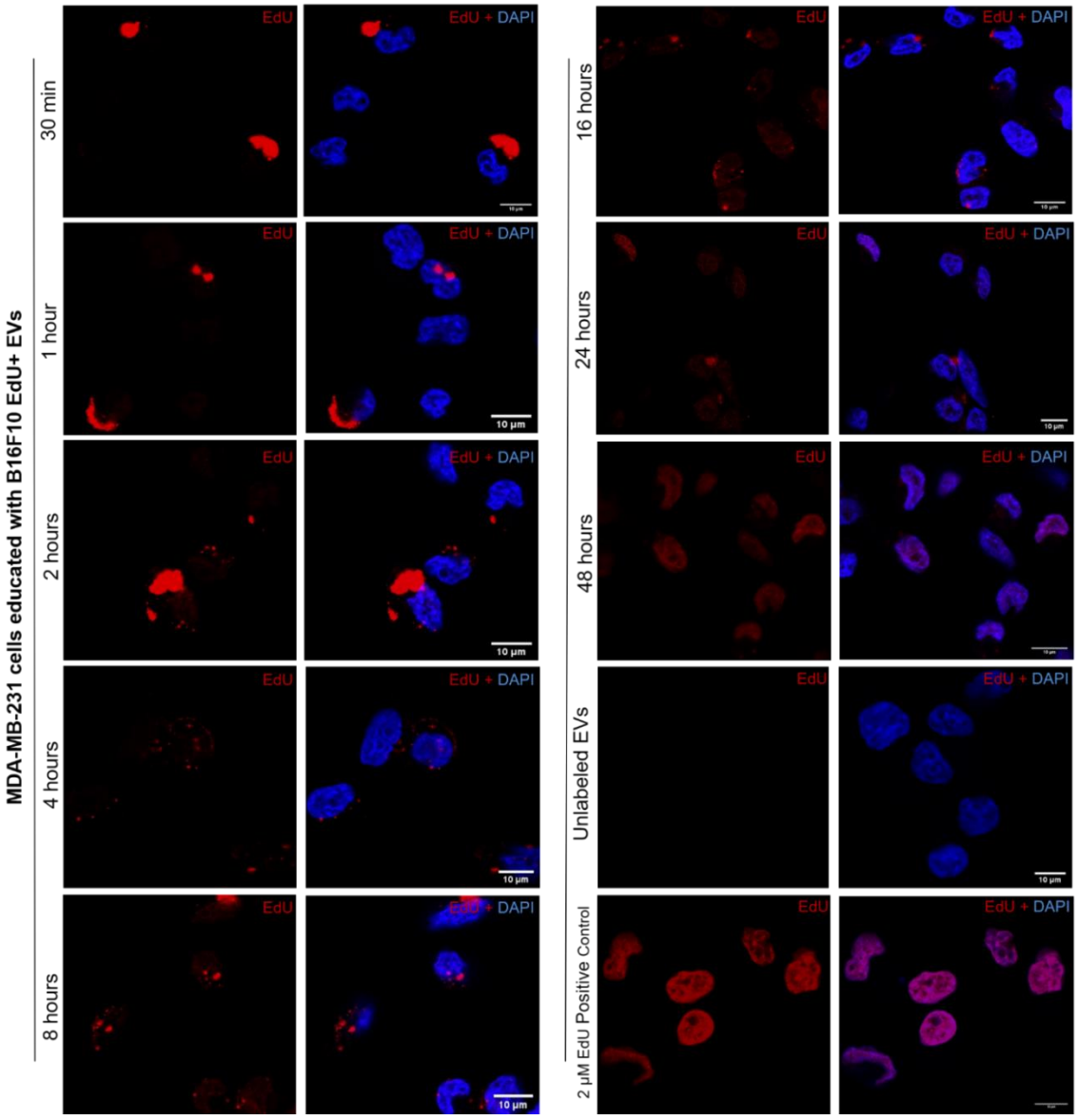

Figure 4.6: EV-DNA Uptake Time-Line. EVs were educated with EVs containing EdU-labelled DNA at indicated time points before cells were fixed for confocal microscopy.2 µM EdU were added as positive control, unlabelled EVs as negative control. blue= cell nucleus, red =EdU-lablled EV-DNA or EdU. Scale bar = 10 µm

4.2.5 Confirming the source of the EdU signal

In order to confirm that the EdU signal was coming from EV-DNA of the donor cells that was internalised by the recipient cells, and not from residual EdU traces potentially present in the EV fraction after isolation, we compared recipient cells that were educated with traditional EdU-labelled EVs or with EVs from a cell line that was not cultured in the presence of EdU, but instead EdU was added to the collected supernatant shortly before the EV isolation was performed. The results showed that the EdU signal could not be detected in the cells where the EdU was added to the supernatant just before EV isolation (Fig. 4.7). This confirms that the isolation method was effective at removing the EdU from the supernatant and that any EdU signal was coming from EdU-labelled EV-DNA.

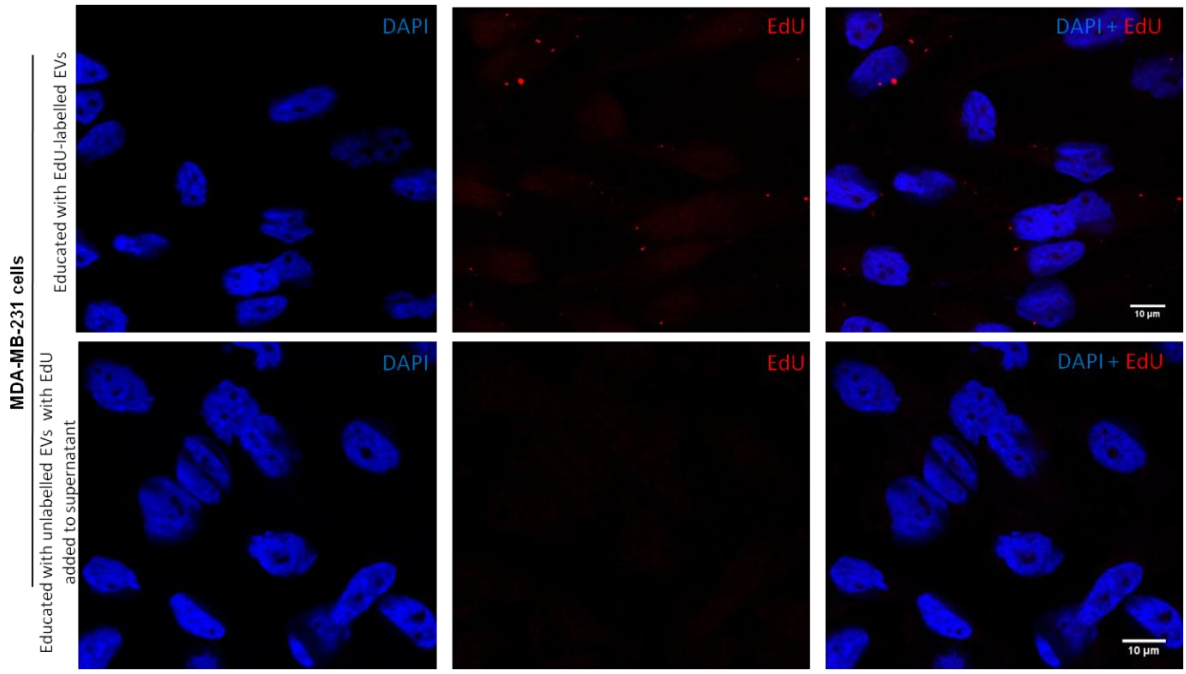

Figure 4.7: Confirmation of the EdU Source. MDA-MB-231 cells were educated with B16-F10 EVs that contained EdU-labelled DNA (upper) or unlabelled DNA (lower). The supernatant of the unlabelled EVs was spiked with EdU after collection, but before isolation. Red =EdU-labelled EV-DNA, blue = recipient cell nucleus. Scale bar =10 µm

Furthermore, the EV fractions were treated with DNase in order to degrade any DNA that was not inside the EVs that may have been remaining after EV isolation. This was to confirm if the DNA being uptaken into the cells was definitely of an internal EV source rather than an EV surface or a cell-free source. In confocal microscopy, EdU was still detectable in recipient cells despite DNase treatment of the EV fraction, with no noticeable reduction in EdU signal (Fig. 4.8B). Additionally, bioanalyser analysis of EV-DNA fractions showed there did not seem to be a difference in the DNA

fragment pattern between EdU-labelled EV-DNA and unlabelled EV-DNA. Treatment with DNase caused an increase in smaller DNA fragments, showing that at least some of the DNA present in the fractions is located outside of the EVs or on the EV surface (Fig. 4.8A).

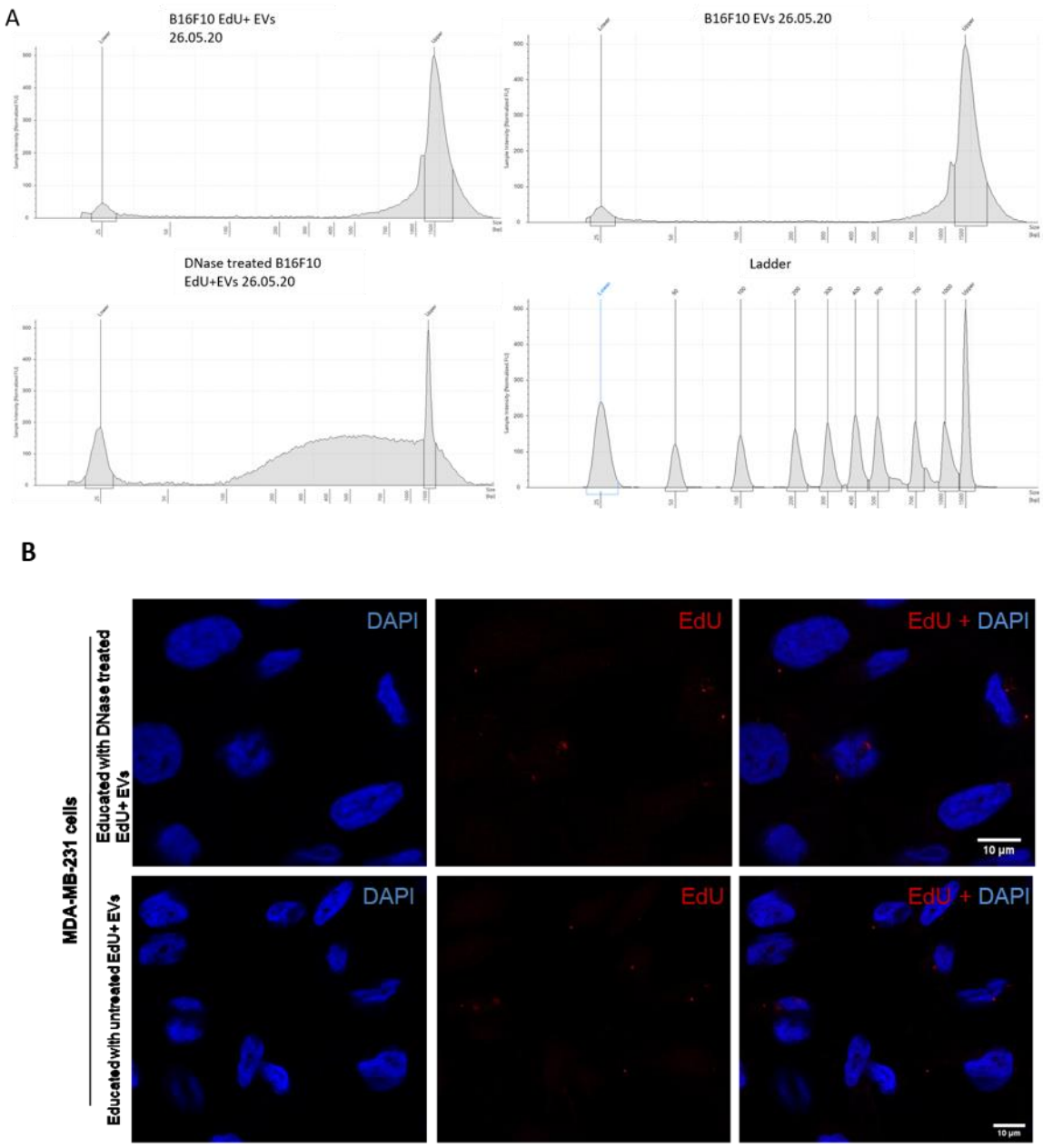

Figure 4.8: Effect of DNase Treatment on EV-DNA. (A) B16-F10 EdU+ EV fractions were treated with DNase or left untreated before DNA extraction and analysed using a DNA bioanalyser. Graphs show fragment sizes (bps) against sample intensity. Fragments up to 1500 bps were measured. (B) MDA-MB-231 cells were educated with B16-F10 EdU+ EVs that had been treated with DNase (upper) or left untreated (lower). Red =EdU-labelled EV-DNA, blue = recipient cell nucleus. Scale bar = 10 µm.

4.2.6 EV-DNA interacts with the cytoskeleton and nuclear envelope

To investigate the trafficking and localisation of the EV-DNA inside the recipient cells, we visualised different components of the recipient cells while simultaneously

visualising the EV-DNA. The first cell component that was considered was the cytoskeleton, more specifically microtubules, which were labelled with an anti-Beta-Tubulin antibody and a secondary AF488 antibody (Fig. 4.9).

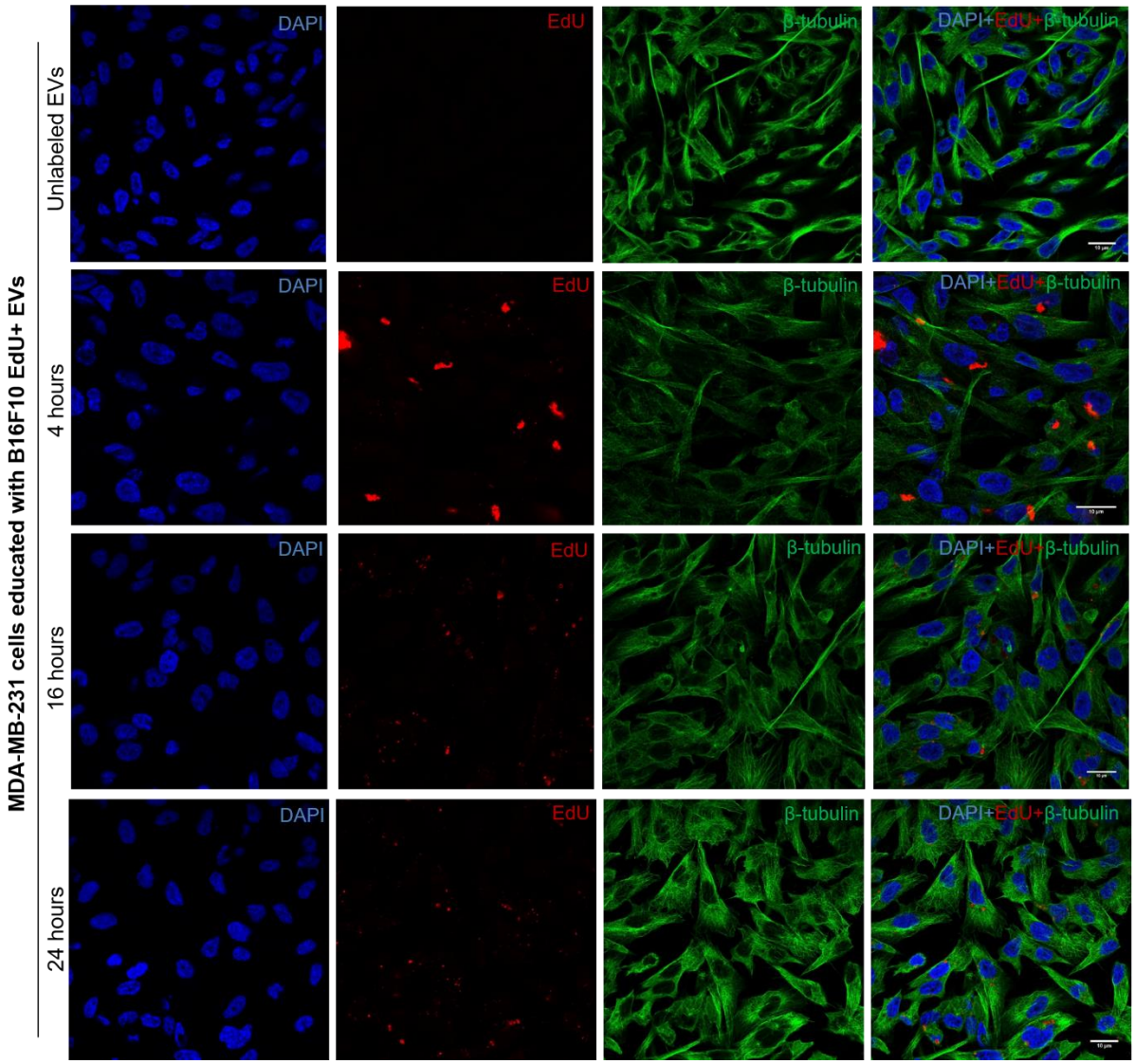

Figure 4.9: Co-localisation of EV-DNA with Beta-Tubulin. MDA-MB-231 cells were educated with B16-F10 EVs that contained EdU-labelled DNA at several time points. Beta-Tubulin was labelled with an anti-beta-Tubulin antibody with a secondary AF488 antibody. Red =EdU-EV-DNA, blue = recipient cell nucleus, green = beta-Tubulin. Scale bar = 10 µm

When comparing the single channel for beta-Tubulin to that of an overlay containing the EdU signal of the DNA, it was observed that there were often gaps or spaces in the beta-Tubulin where the EdU-EV-DNA was located (Fig 4.10). This suggests the EV-DNA is indeed associated with microtubules, which are possibly trafficking it within the recipient cell.

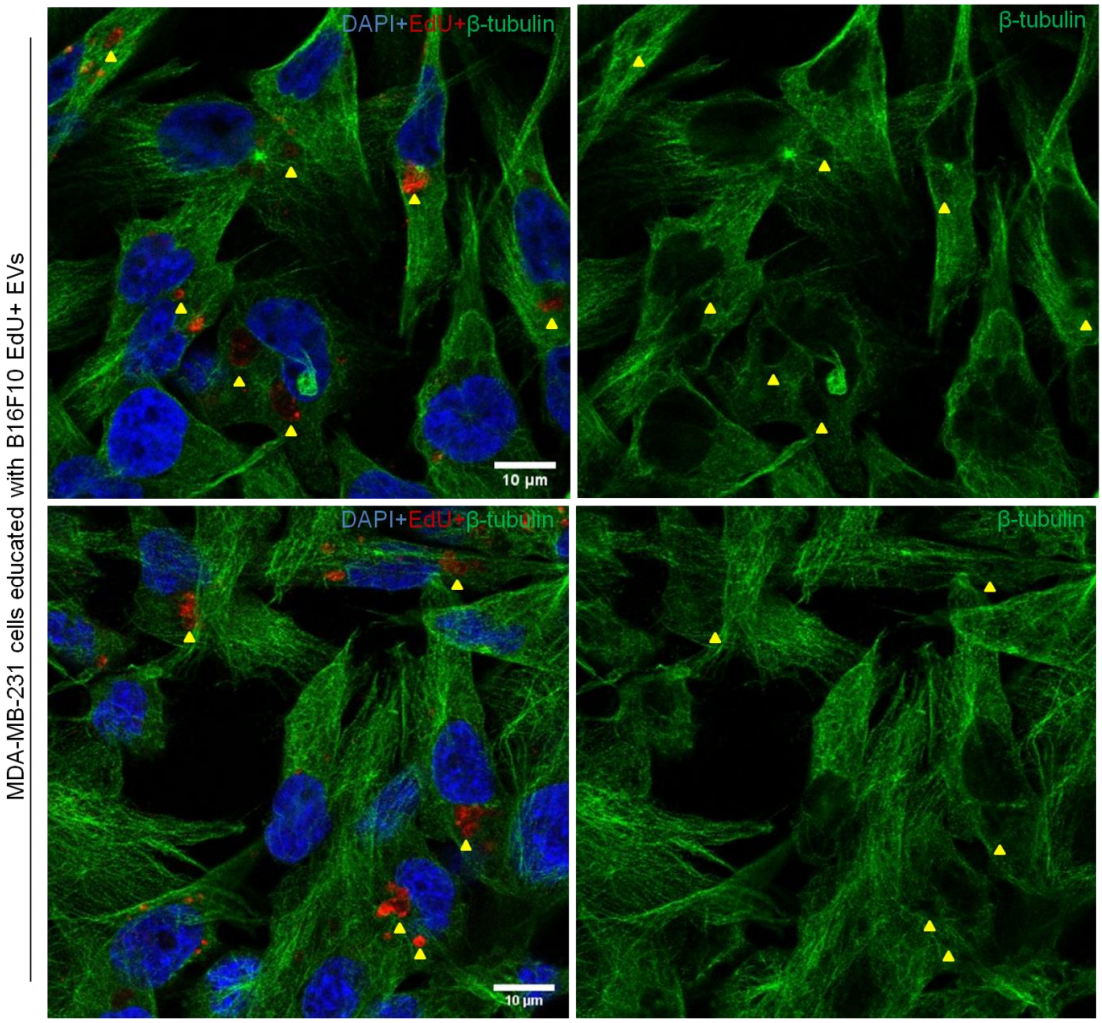

Figure 4.10: EV-DNA Residing in Gaps within Microtubules. MDA-MB-231 cells were educated with B16-F10 EVs that contained EdU-labelled DNA. Gaps or spaces in the beta-Tubulin could be observed where the EdU-EV-DNA was often located. Beta-Tubulin was labelled with an anti-beta-Tubulin antibody with a secondary AF488 antibody. Yellow arrow heads show areas of EdU or gaps where EdU resides.Red =EdU-EV-DNA, blue = recipient cell nucleus, green = beta-Tubulin. Scale bar = 10 µm

The second cell component that was considered was the nuclear envelope, for which lamin was labelled with an anti-LaminB1 antibody and a secondary AF488 antibody, while simultaneously visualising the EV-DNA. In some areas, it was possible to observe some co-localisation between the EdU-EV-DNA signal and the laminB1 signal (Fig. 4.11) suggesting that the EV-DNA does interact with the nuclear envelope.

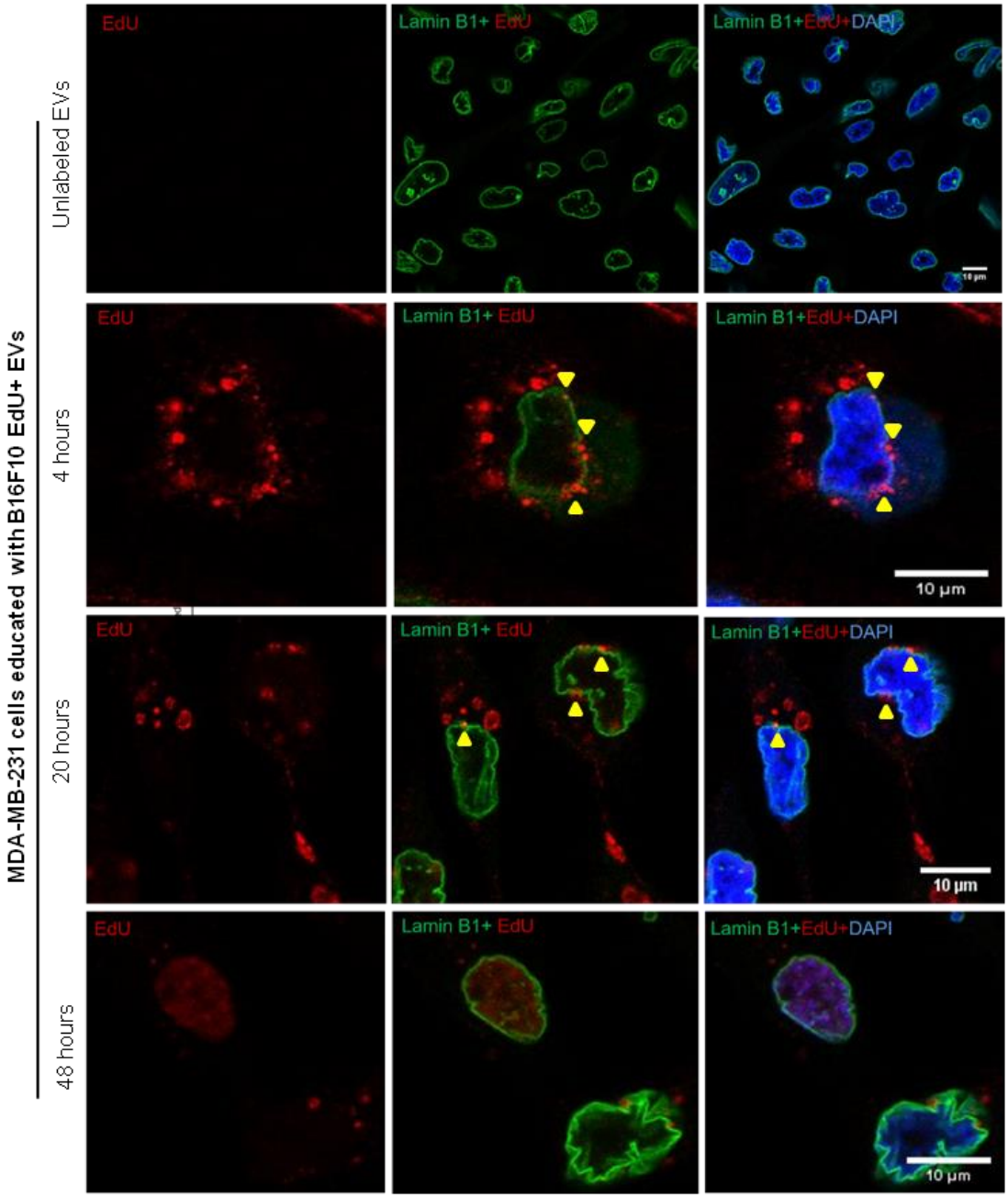

Figure 4.11: Co-localisation of EV-DNA with the Nuclear Envelope. MDA-MB-231 cells were educated with B16-F10 EVs that contained EdU-labelled DNA at indicated time points before fixation for confocal microscopy. Nuclear envelope was labelled with an anti-LaminB1 antibody with a secondary AF488 antibody.Yellow arrow heads show areas of co-localisation. Red =EdU-EV-DNA, blue = recipient cell nucleus, green = LaminB1. Scale bar = 10 µm.

4.2.7 EV-DNA is associated with the endosomal pathway

Additional stainings of early endosomal marker - Rab5, late endosomal marker – Rab7 and lysosomal marker – Lamp1 were performed in the recipient cells in order to identify any possible co-localisation events. These markers were chosen based on the idea that the endosomal pathway could potentially be used in the internalisation and transport of the EV-DNA inside the cells. In the first experiment, no co-

localisation was observed between the EV-DNA and the lysosomal marker, Lamp1 (Fig. 4.12).

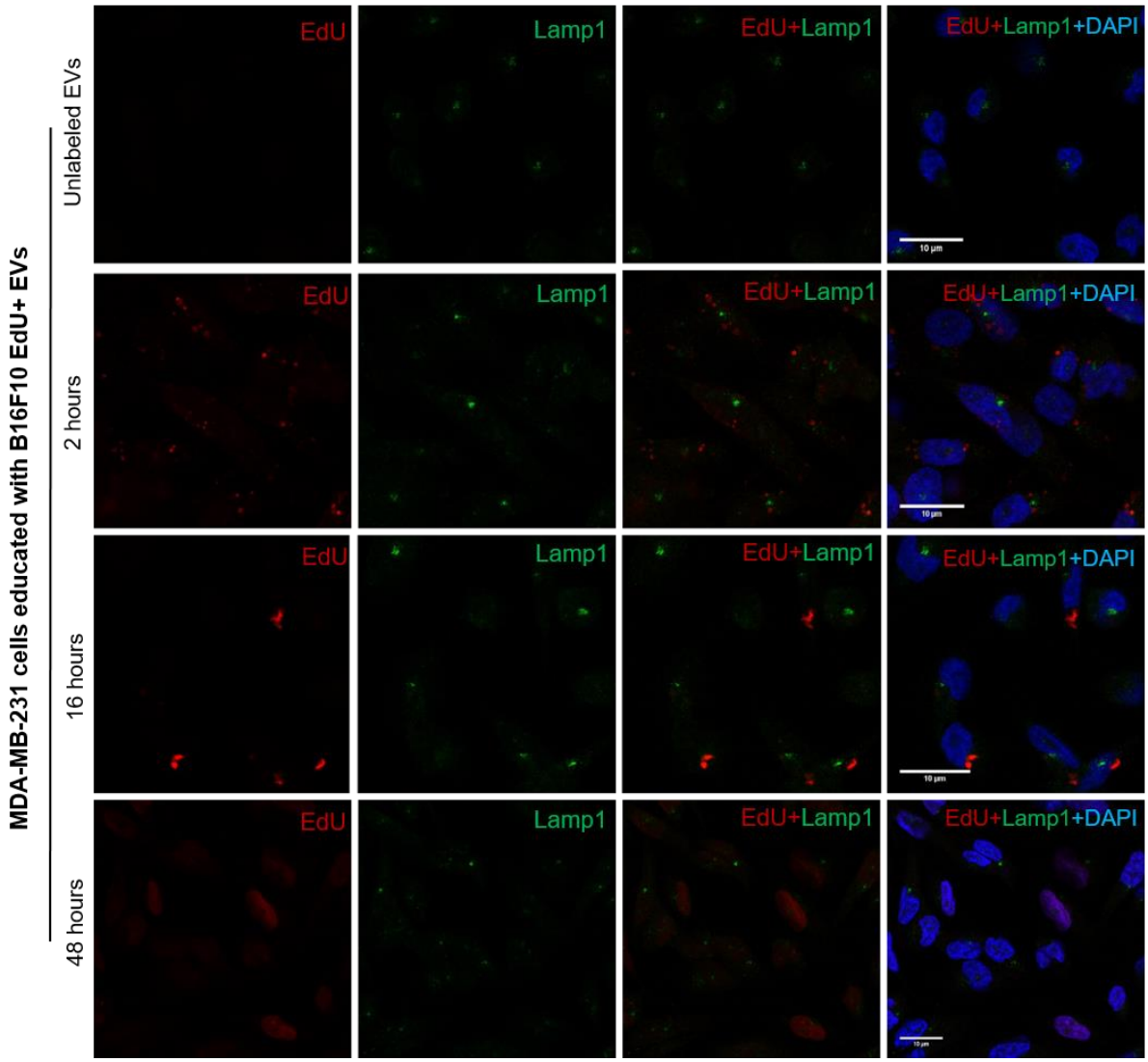

Figure 4.12: No Observed Co-localisation of EV-DNA with Lysosomes. MDA-MB-231 cells were educated with B16-F10 EVs that contained EdU-labelled DNA at indicated time points before fixation for confocal microscopy. Lysosomes were labelled with an anti-Lamp1 antibody with a secondary AF488 antibody. No co-localisation events were observed. Red =EdU-EV-DNA, blue = recipient cell nucleus, green = Lamp1. Scale bar = 10 µm.

Although no co-localisation was observed between EV-DNA and lysosomes, during confocal microscopy some co-localisation was observed between the EV-DNA and the endosomal markers Rab5 and Rab7 (Fig. 4.13/14). At several time points, green circles of $Rab5^{+}$ or $Rab7^{+}$ molecules could be observed, inside of which an EdU signal could be detected. The colocalization events were observed at almost every time point that was investigated, except 48h. These circles were also observed when cells were treated with Rab5 or Rab7 antibodies only, which confirms the signals were coming from endogenous Rab5/7, rather than any internalised EVs. Not all EV-

DNA was associated with Rab5/7^{+} endosomes, as EdU molecules without Rab5/7 co-localisation were also observed.

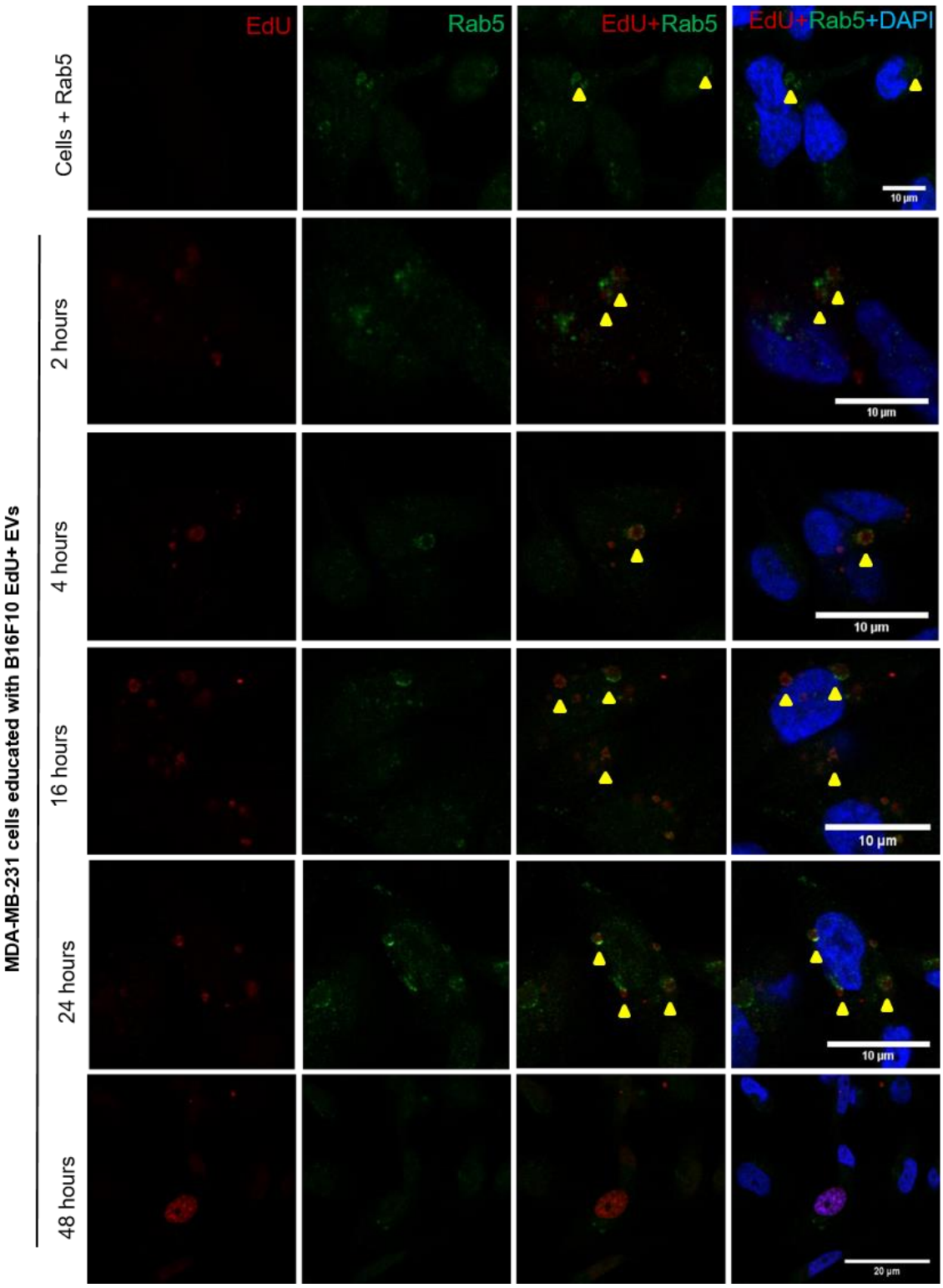

Figure 4.13: Co-localisation of EV-DNA with Early Endosomes.MDA-MB-231 cells were educated with B16-F10 EVs that contained EdU-labelled DNA at indicated time points before fixation for confocal microscopy. Early endosomes were labelled with an anti-Rab5 antibody with a secondary AF488 antibody. Yellow arrow heads show areas of co-localisation. Red =EdU-EV-DNA, blue = recipient cell nucleus, green = Rab5. Scale bar = 10 µm.

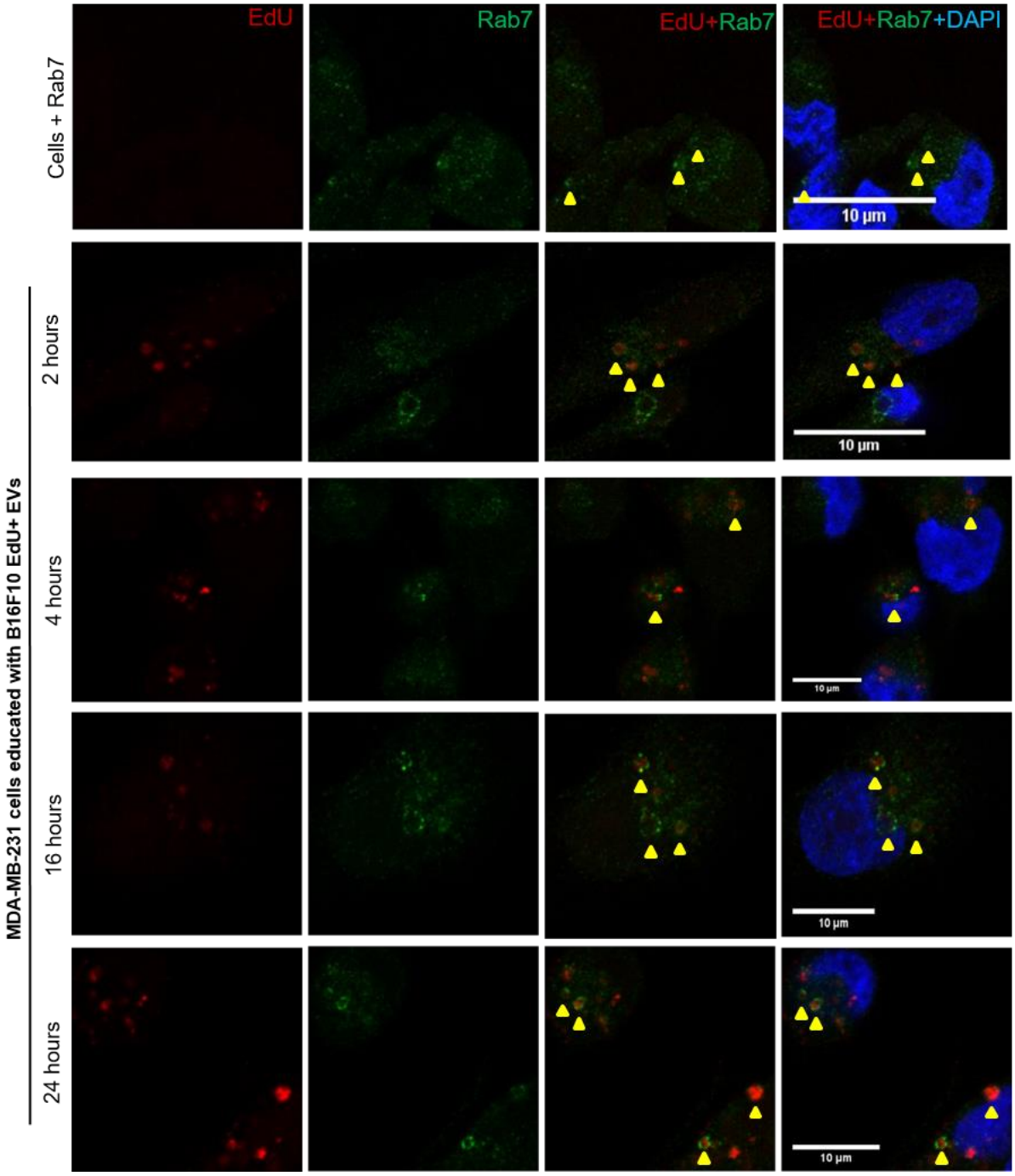

Figure 4.14: Co-localisation of EV-DNA with Late Endosomes.MDA-MB-231 cells were educated with B16-F10 EVs that contained EdU-labelled DNA at indicated time points before fixation for confocal microscopy. Late endosomes were labelled with an anti-Rab7 antibody with a secondary AF488 antibody.Yellow arrow heads show areas of co-localisation. Red =EdU-EV-DNA, blue = recipient cell nucleus, green = Rab7. Scale bar = 10 µm.

Z-stacking was also performed during confocal microscopy experiments to further investigate the co-localisation of the EdU-EV-DNA signal and the Rab5/Rab7 signals. The Z-stacking images confirmed that the areas of observed co-localisation were true co-localisation events, as they could still be observed at different depths within the recipient cells.

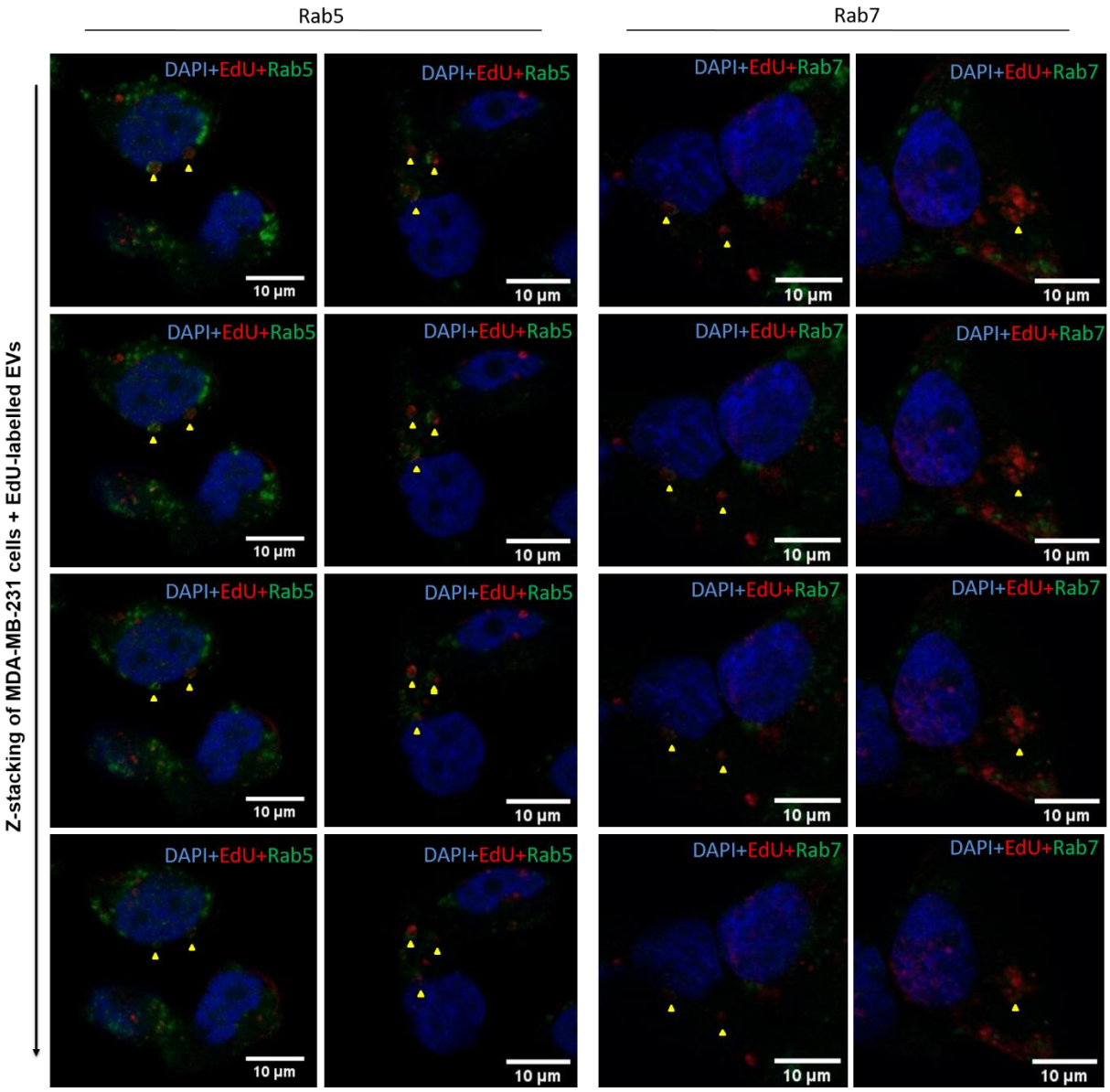

Figure 4.15: Z-stacks of Rab5 and Rab7 Labelling. MDA-MB-231 cells were educated with B16-F10 EdU+ EVs for 24 hours and labelled with anti-Rab5 or anti-Rab7antibodies.Z-stacking confocal microscopy was performed to confirm co-localisation of EV-DNA and Rab5/7. Yellow arrow heads indicate areas of co-localisation. Blue = recipient cell nucleus, red = EdU-labelled EV-DNA, green = Rab5 or Rab7.Scale bar = 10 µm.

4.2.8 Assessing the role of Rab5⁺ and Rab7⁺ endosomes in EV-DNA uptake

After the observation that EV-DNA appeared to be associated with Rab5$^+$ and Rab7$^+$ endosomes, it was decided to further investigate the role of Rab5$^+$ and Rab7$^+$ endosomes in the internalisation and trafficking of EV-DNA by performing a knockdown of endogenous Rab5 and Rab7 in the recipient cells using short interfering RNA (siRNA) before education with EdU-labelled EVs. When siRNA enters the cell it interacts with RISC (RNA-induced silencing complex) and directs it to cleave the target mRNA, which has a complementary sequence to the siRNA (Dykxhoorn et al., 2006).This results in knockdown of gene expression.

4.2.8.1 **Confirmation of knockdown method**

Firstly, in order to confirm that the knockdown of Rab5 and Rab7 was possible, recipient cells were seeded in a six-well plate and were transfected with siRNA against Rab5 and Rab7 using lipofectamine as mentioned in section 3.5.10. The protein from these transfected cells was subjected to western blotting, where it was possible to see that Rab5 knockdown had been successful (Fig. 4.16) with only a faint signal remaining. Unfortunately, the western blot for the Rab7 knockdown showed no signal for Rab7 at all, even in control samples. Additional positive staining with ß-actin confirmed that transfer of proteins was successful (Fig. 4.16).

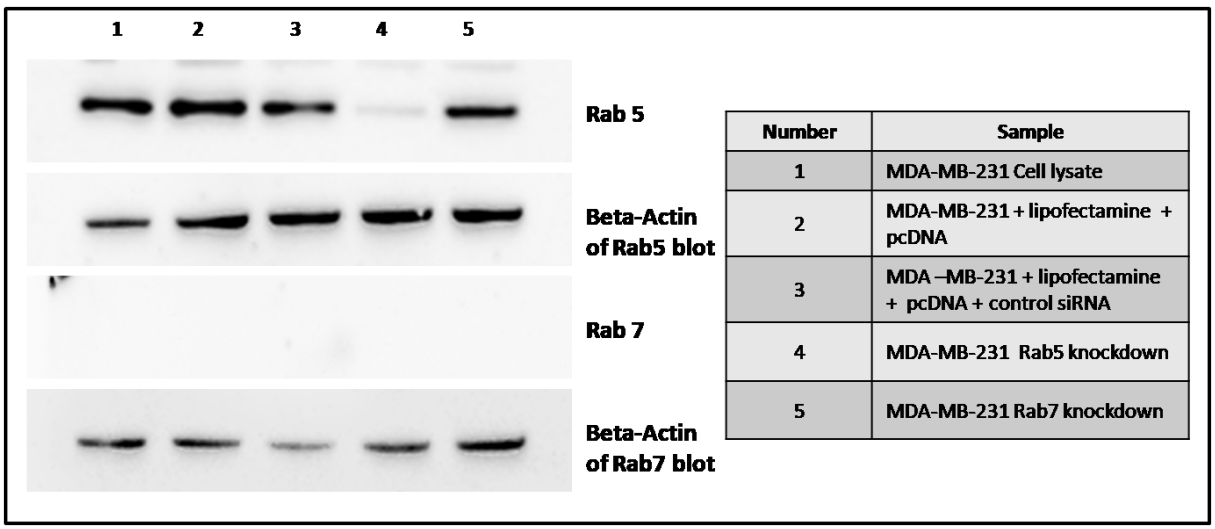

Number	Sample
1	MDA-MB-231 Cell lysate
2	MDA-MB-231 + lipofectamine + pcDNA
3	MDA –MB-231 + lipofectamine + pcDNA + control siRNA
4	MDA-MB-231 Rab5 knockdown
5	MDA-MB-231 Rab7 knockdown

Figure 4.16: Rab 5 and Rab 7 Knockdown Confirmation. Rab 5 and Rab 7 were knockdown in MDA-MB-231 cells using siRNA. Western blotting was used to confirm the knockdown.

The western blot was repeated several times, and the concentration of the antibody was increased, however, the signal was still absent. The transfection experiment was repeated using a semi-dry western blotting process with a PVDF membrane, an increased amount of protein and a new anti-Rab7 antibody, however, again the Rab7 signal was not detectable while the ß-actin signals were present. These western blots confirmed the knockdown of Rab5, but not Rab7; however, as Rab5 knockdown was successful and the exact same method of transfection was used for the Rab7 knockdown, it would be highly likely that this knockdown was successful as well.

4.2.8.2 **Rab5/Rab7 knockdown in confocal microscopy**

The next step in assessing the importance of Rab5 and Rab7 in EV-DNA uptake was to educate MDA-MB-231 cells that had been transfected with siRNA against Rab5 or

Rab7 with EdU-labelled EVs. As control, untreated MDA-MB-231 cells were simultaneously educated with the same EdU-labelled EVs, at the same time points. A further control was used to confirm that the siRNA uptake was not altering the cells, in the form of a scrambled siRNA, which would have no knockdown effect. The knockdown protocol was performed directly before the first time point of addition of EdU-labelled EVs (48 h).

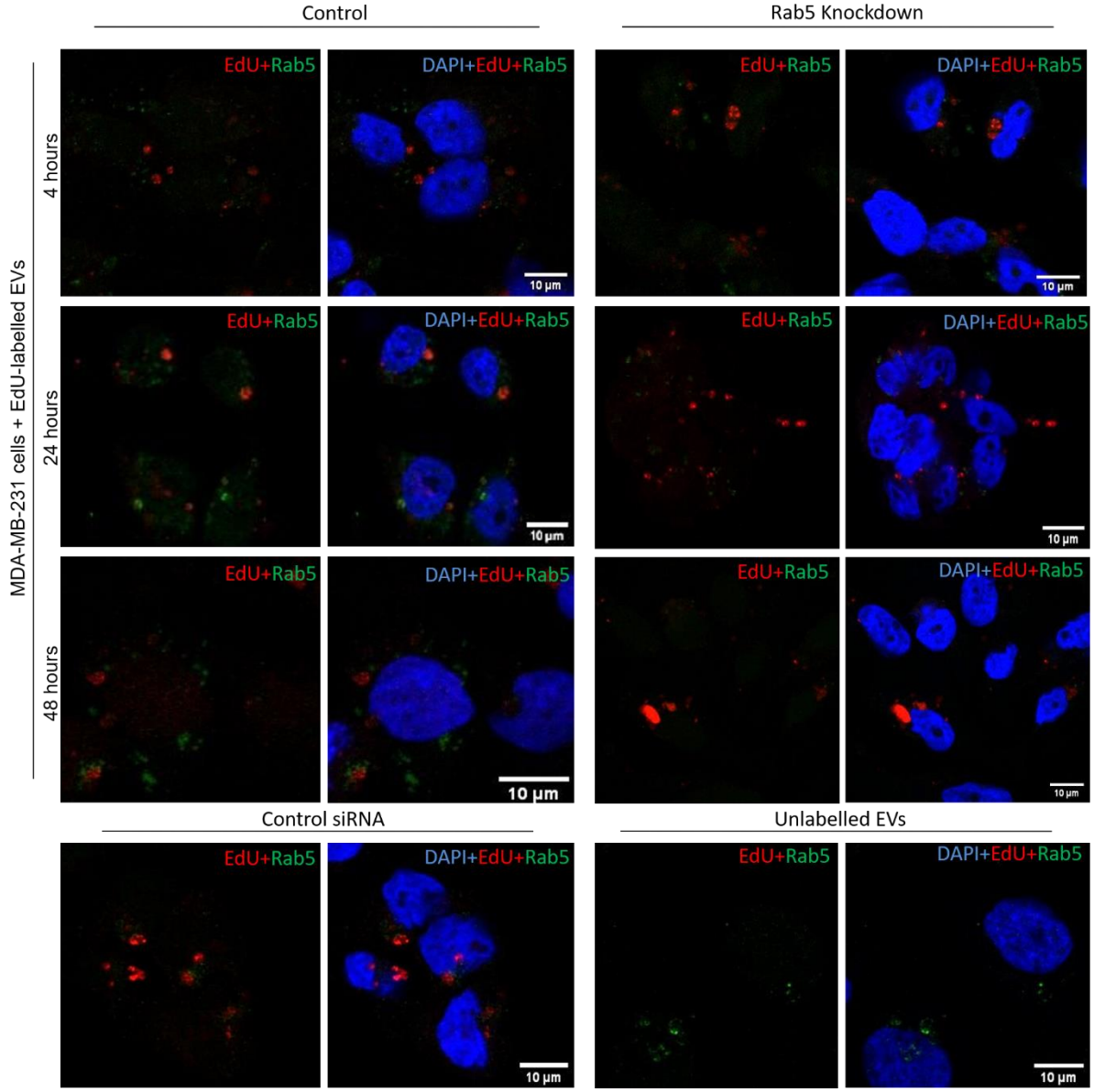

Figure 4.17: Assessing the Effects of Rab5 knockdown on EV-DNA Uptake. MDA-MB-231 underwent a knockdown procedure using siRNA against Rab5A. Cells were subsequently educated with EdU-labelled EVs to assess effects of the knockdown on EV-DNA uptake. Time points show addition of EVs before fixation for confocal microscopy. Early endosomes were labelled with an anti-Rab5 antibody with a secondary AF488 antibody. Yellow arrowheads show areas of co-localisation. Red =EdU-EV-DNA, blue = recipient cell nucleus, green = Rab5. Scale bar = 10 µm.

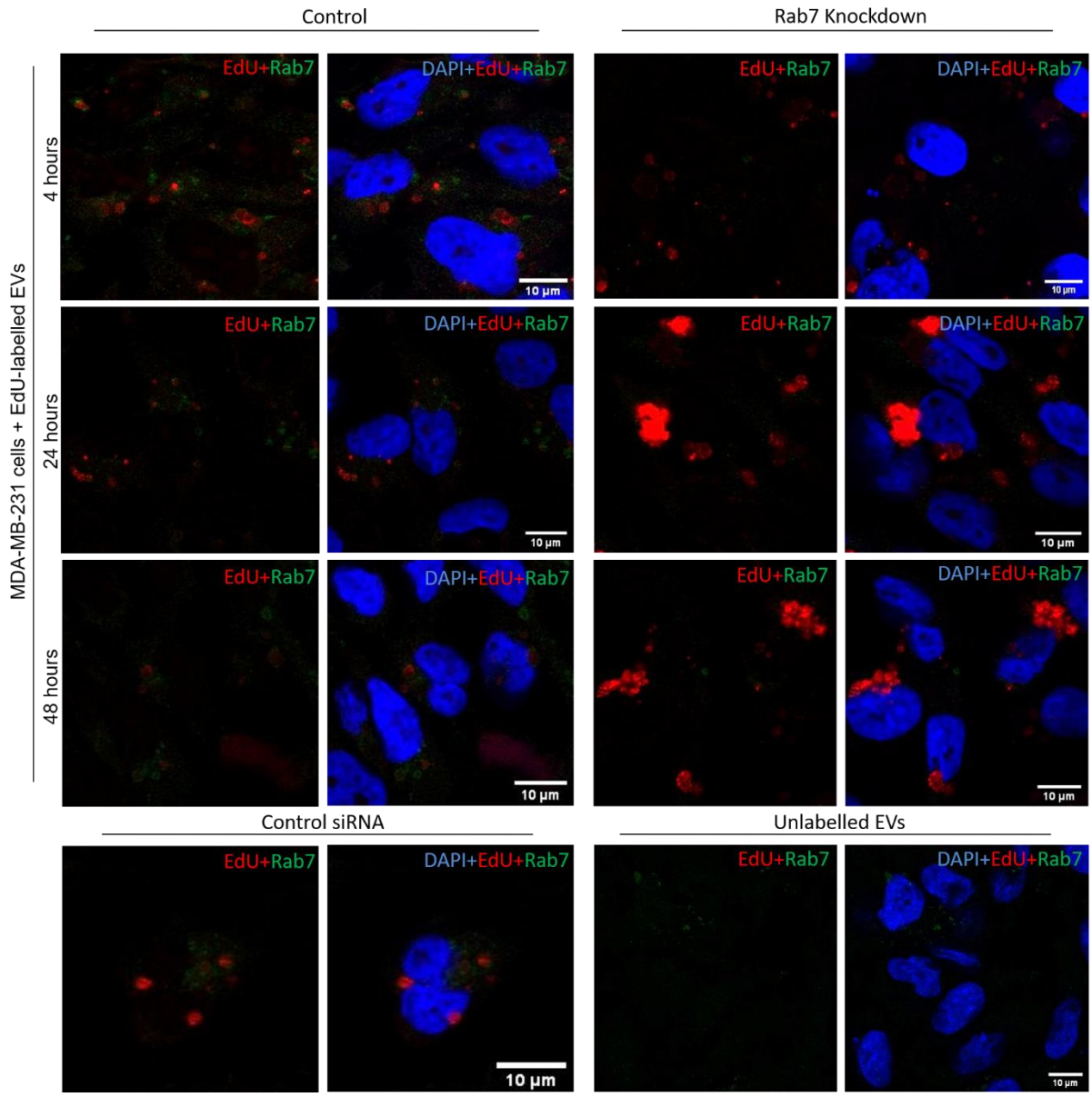

Figure 4.18: Assessing the Effects of Rab7 Knockdown on EV-DNA Uptake. MDA-MB-231 underwent a knockdown procedure using siRNA against Rab7. Cells were subsequently educated with EdU-labelled EVs to assess effects of the knockdown on EV-DNA uptake. Time points show addition of EVs before fixation for confocal microscopy. Early endosomes were labelled with an anti-Rab7 antibody with a secondary AF488 antibody. Yellow arrowheads show areas of co-localisation. Red =EdU-EV-DNA, blue = recipient cell nucleus, green = Rab7. Scale bar = 10 µm.

In the Rab5 knockdown model, the results showed that despite the knockdown, Rab5 was still detectable, and some co-localisation between Rab5 and EV-DNA could still be observed. At the 48h time point, the Rab5 signal was highly reduced suggesting that the knockdown had been partially successful at this time of EV education (Fig. 4.17). This EV addition time point was directly after the knockdown had been performed, suggesting that the knockdown effect was lost over the course of the experiment. At this time point, it was observed that some the EV-DNA appeared to be in aggregates, which is something that was previously seen at earlier

EV education time points (Fig. 4.6). In the Rab7 knockdown model, there was a clear reduction in Rab7 signal when compared to control cells at all time points, but not a complete absence (Fig 4.18). Additionally, EdU signal appeared more abundant in knockdown samples than in control samples at most time points; however, the EV-DNA appeared to be aggregated in the knockdown samples, which is something that was previously observed at early EV education time points. This suggests that the knockdown of Rab7 was influencing EV-DNA uptake, perhaps causing DNA accumulation, but complete inhibition of EV-DNA uptake was not observed.

4.2.9 Inhibition of EV-DNA uptake

To further understand the process of EV-DNA uptake into the recipient cells, recipient cells were exposed to three substances, aphidicolin (8.5 µg/mL), ivermectin (10 µg/mL) and hydroxyurea (2.5 µM). Aphidicolin is known to inhibit DNA polymerase, which in turn prevents DNA replication and halts the cell cycle in early S-phase (Baranovskiy et al., 2014). Similarly, Hydroxyurea is also known to inhibit DNA replication and halts the cell cycle in G1 or S phase (Koç et al., 2004). Ivermectin elicits a different effect than the aforementioned substances. It is thought to inhibit the import of macromolecules to the nucleus through the nuclear pore complex (NPC) (Wagstaff et al., 2012).

4.2.9.1 **Effects of three substances on EdU incorporation by recipient cells**

To assess the effects of aphidicolin (8.5 µg/mL), ivermectin (10 µg/mL) and hydroxyurea (2.5 µM) on the MDA-MB-231 recipient cells ability to incorporate EdU in to its nuclear DNA, cells were treated with the three substances for 48 hours, while 2 µM of EdU was added directly to the supernatant for 24 hours - the normal preparation process of the microscopy EdU positive control which is used to assure the EdU kits is always functioning optimally. These cells were then visualised using confocal microscopy. The cells treated with aphidicolin for 48 hours had no EdU signal, whereas cells treated with the other two substances looked similar to the untreated control cells (Fig. 4.19). As EdU is incorporated into DNA as it is being replicated, it was expected that the aphidicolin treated cells would have a reduced EdU signal. The same had been hypothesized for the hydroxyurea treated cells, as it also supposed to halt DNA replication; however, this was not observed.

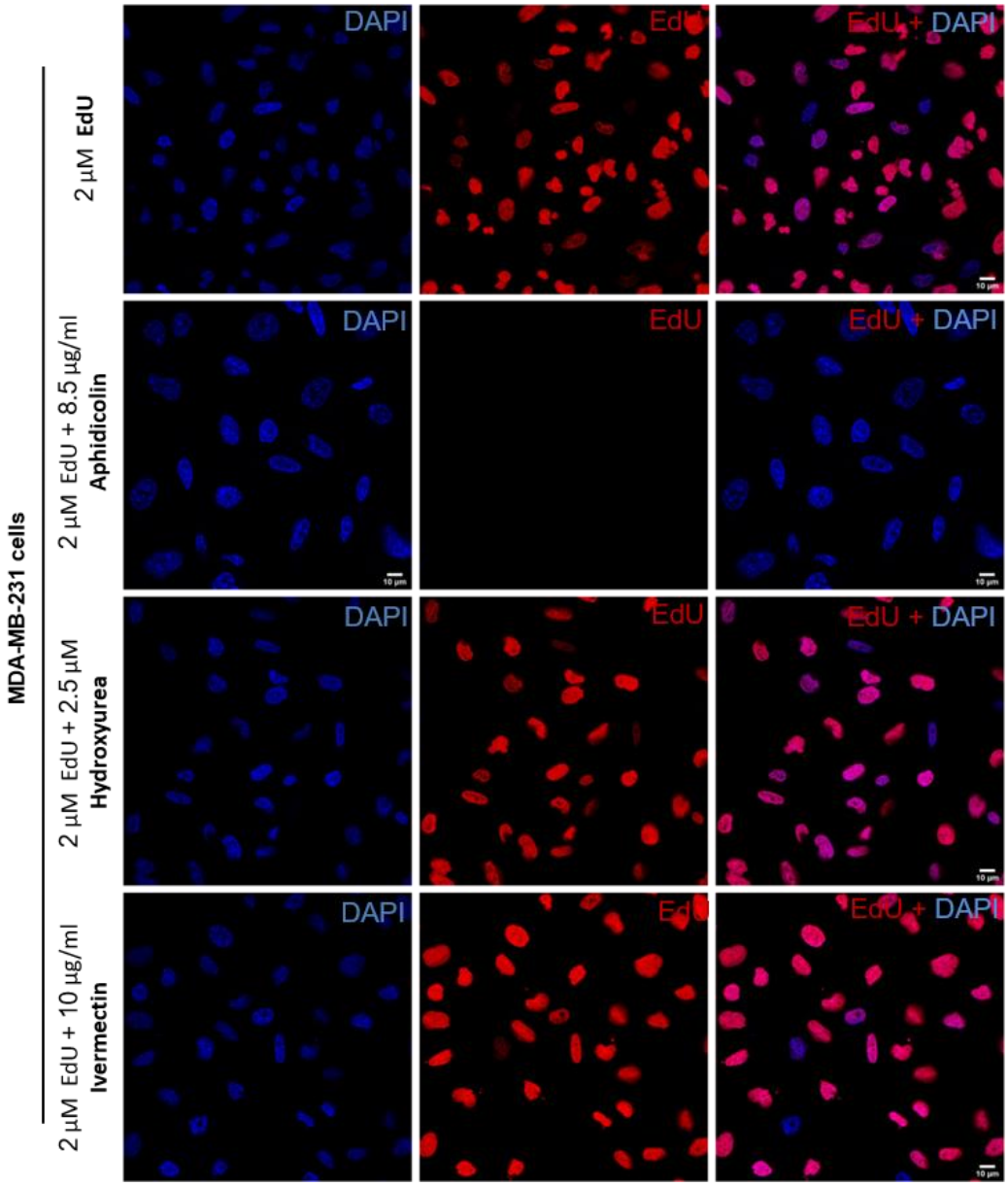

Figure 4.19: Effects of Three Substances on EdU Incorporation by Recipient MDA-MB-231 Cells. Recipient cells were exposed to three substances: aphidicolin (8.5 µg/mL), ivermectin (10 µg/mL) and hydroxyurea (2.5 µM), after which EdU (2.5 µM) was added and incubated for 24 hours before fixation for confocal microscopy. Red =EdU labelled gDNA, blue = recipient cell nucleus. Scale bar = 10 µm.

4.2.9.2 **Effects of three substances on EV-DNA uptake by recipient cells**

In parallel, the effect of the same substances on the uptake of B16-F10 EVs containing EdU-labelled DNA was investigated by treating the cells with the substances before education with EdU-EVs. After 48 hours of treatment, the cells were visualised using confocal microscopy. Two of the substances, ivermectin and hydroxyurea, did not appear to majorly affect internalisation of EV-DNA as the AF647 (red) signal of EV-DNA could still be observed in some of the EV-educated recipient cells' nuclei (Fig. 4.20). Conversely, aphidicolin appeared to inhibit the uptake of EV-

DNA into the recipient cells (Fig 4.20), as no EdU positive nuclei were observed as seen in the other conditions.

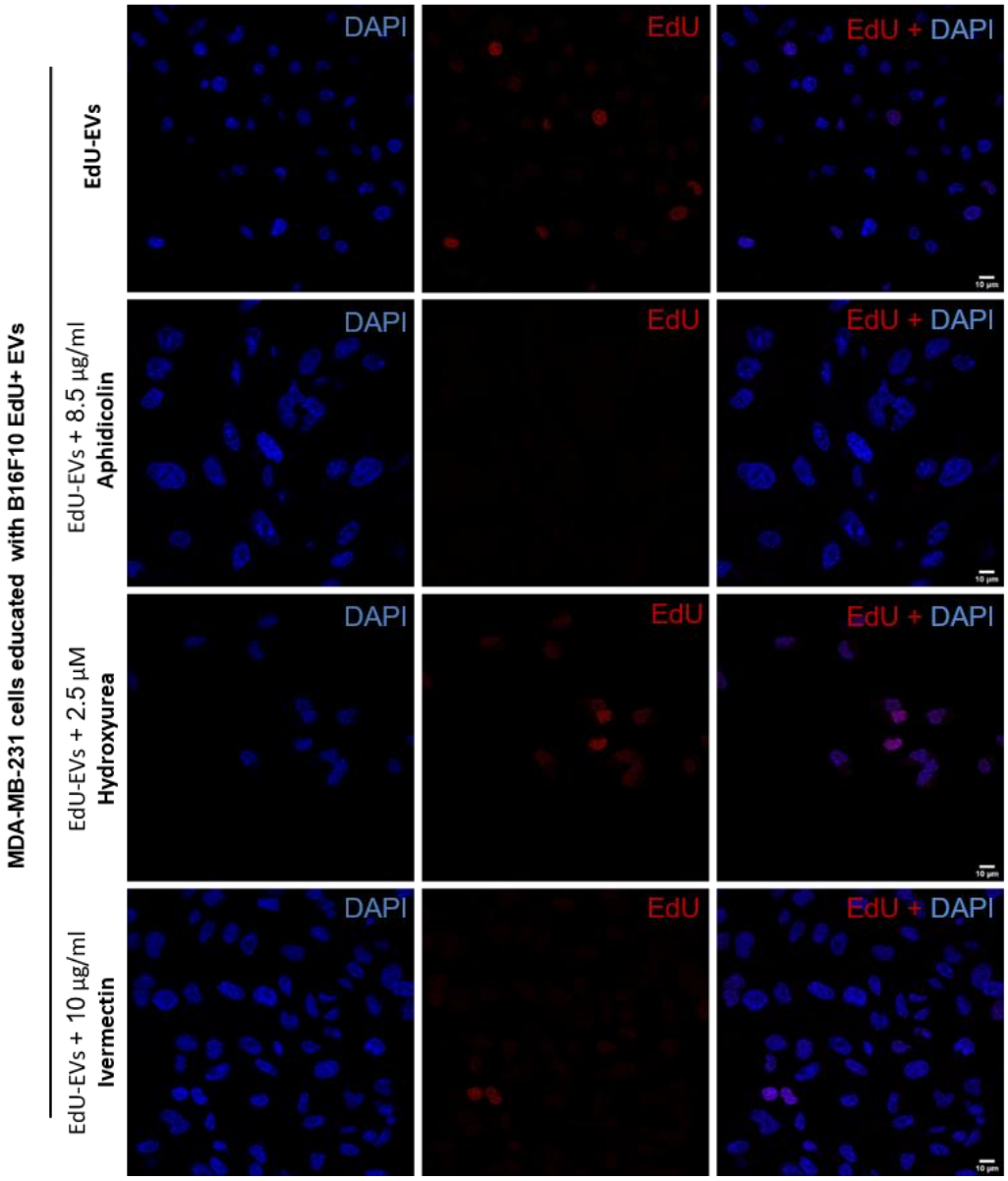

Figure: 4.20: Effects of Three Substances on Uptake of EdU-labelled EV-DNA by Recipient MDA-MB-231 Cells. Recipient cells were exposed to three substances: aphidicolin (8.5 µg/mL), ivermectin (10 µg/mL) and hydroxyurea (2.5 µM), after which B16-F10 EVs containing EdU-labelled DNA were added and incubated for 48hours before fixation for confocal microscopy. Red =EdU-labelled EV-DNA, blue = recipient cell nucleus. Scale bar = 10 µm.

After this observation, it was decided to test the same substances at the same concentrations on the uptake of EV-DNA over a time course. Cells were treated with one dose of the three substances for 48 hours, with EdU-EVs being added at the same time point (48 hours), as well as at 24-,16- and 4 hours before fixation for microscopy. As previously observed, the addition of hydroxyurea and ivermectin did not seem to majorly affect EV-DNA uptake at any observed time point (Fig. 4.21)

Interestingly, EV-DNA signals were detected in recipient cells treated with aphidicolin at some of the observed time points, however, its presence appeared reduced in comparison to the control untreated cells. There was still no signal observed in the aphidicolin treated recipient cells that had been incubated with EdU-labelled EVs for 48h, as previously observed. As the aphidicolin was added to the recipient cells at the same time point as the 48h EdU-EV education, it could indicate that the aphidicolin loses its effect on inhibition of EV-DNA uptake over time.

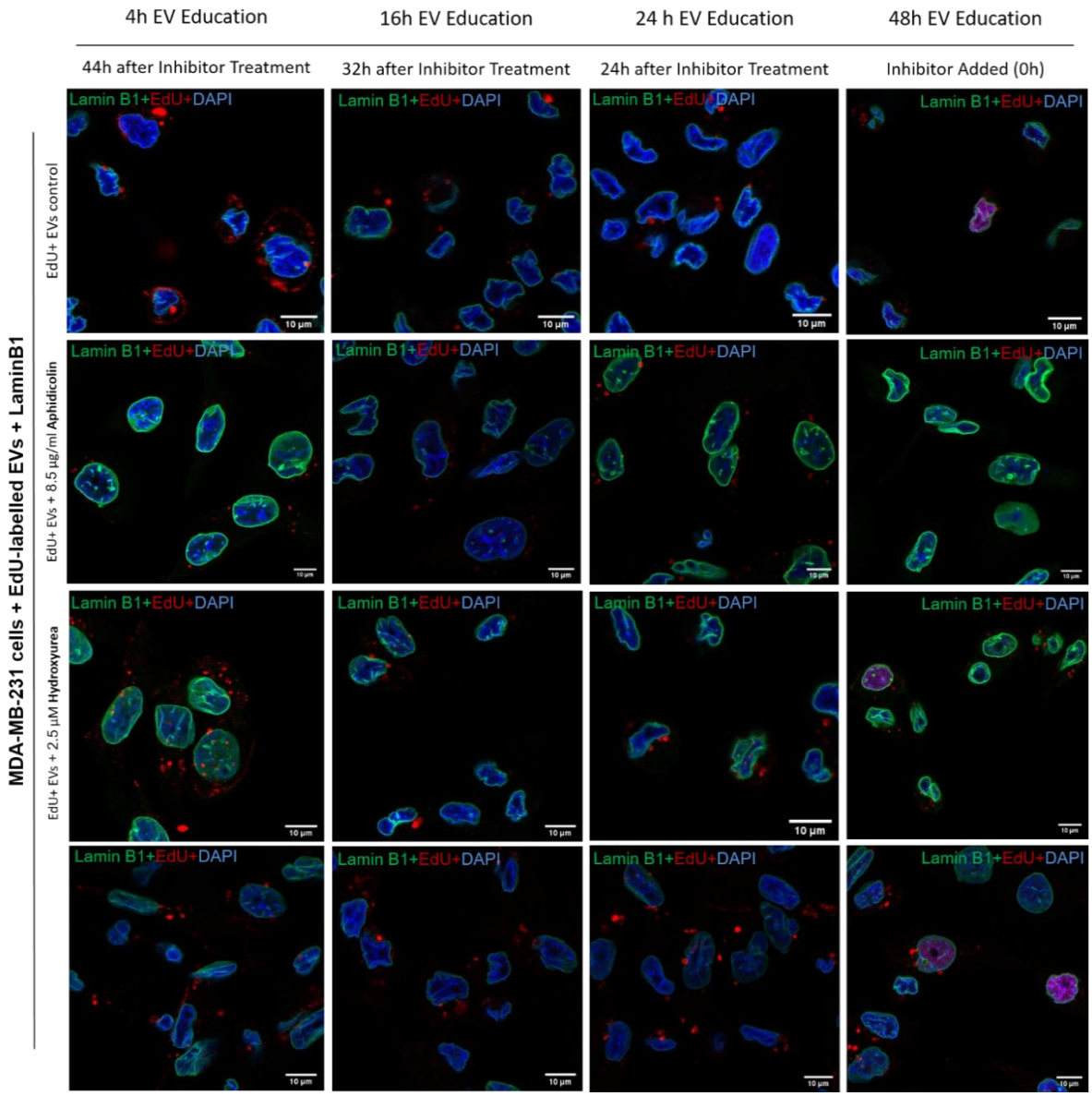

Figure 4.21: Effects of Inhibitor Treatment on EV-DNA Uptake at Different Time Points. Recipient cells were exposed to three substances: aphidicolin (8.5 µg/mL), ivermectin (10 µg/mL) and hydroxyurea (2.5 µM). Inhibitor substances were added once, 48 hours before fixation for confocal microscopy. EV-DNA was added 4, 16, 24, and 48 hours before fixation for microscopy. Blue = recipient cell nucleus, red = EdU-labelled EV-DNA, green = LaminB1 staining. Scale bar = 10 µm.

4.2.9.3 **Effects of three substances on recipient cell homeostasis**

As the ivermectin and hydroxyurea substances did not appear to be eliciting an effect, assays to investigate cell homeostasis were performed. The effects of aphidicolin (8.5 µg/mL), ivermectin (10 µg/mL) and hydroxyurea (2.5 µM) on the recipient MDA-MB-231 cells were analysed using cell cycle and apoptosis flow cytometry assays.

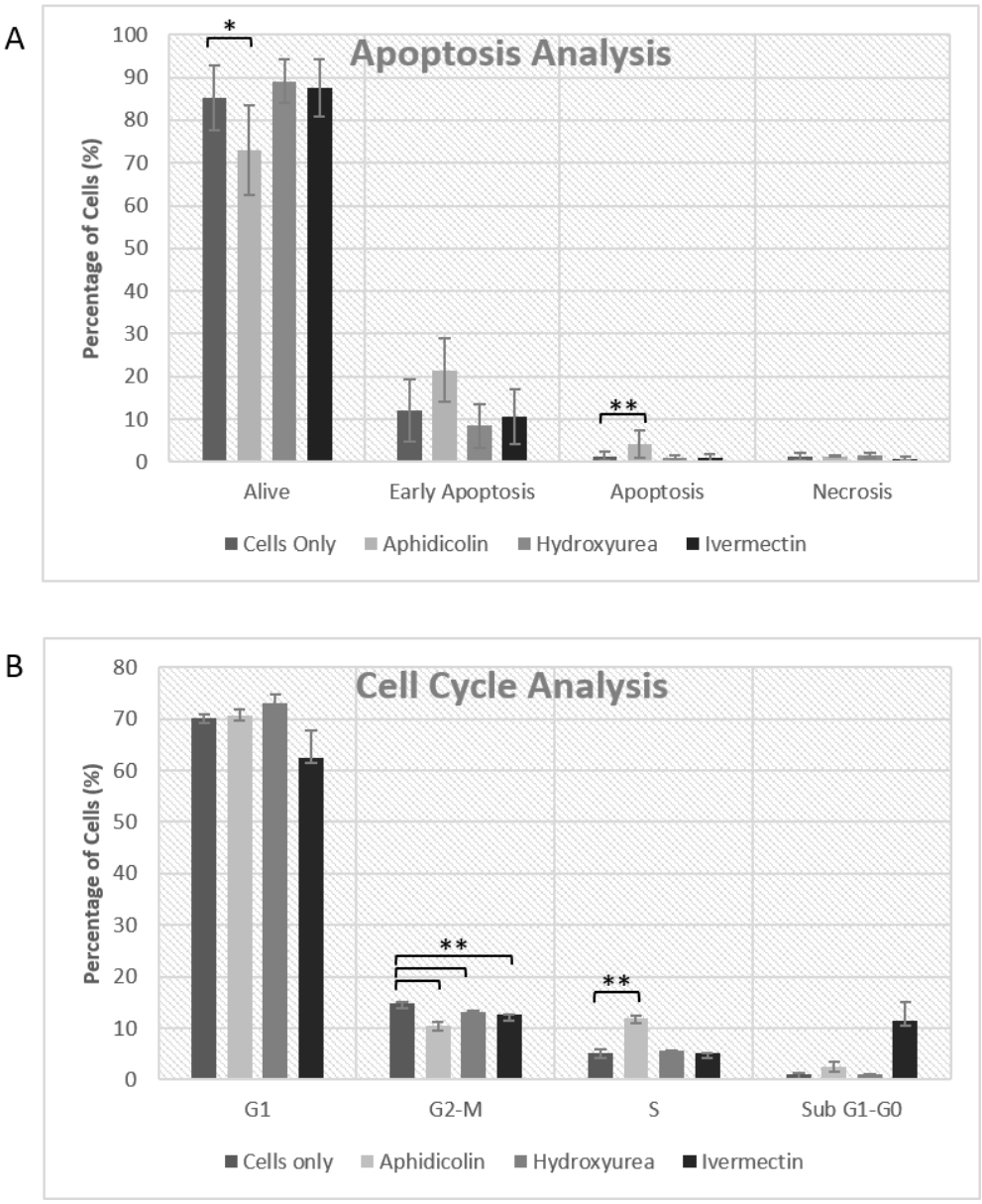

*Figure 4.22: Effects of Three Substances on Cell Homeostasis. MDA-MB-231 cells were treated with aphidicolin (8.5 µg/mL), hydroxyurea (2.5 µM) or ivermectin (10 µg/mL) for 24h. Cells were then assessed using (A) apoptosis assay and (B) cell cycle assay, using flow cytometry. Figures show mean with standard deviation. n = 2. *= p ≤ 0.05, **= p≤ 0.01. Statistics performed using students T-test.*

Cells were treated with the three substances for 48 hours, after which they were collect and prepared for FACS analysis as previously described (section 3.5.9). The apoptosis analysis showed that only cells that had been treated with aphidicolin (8.5 µg/mL) displayed any significant difference in comparison to the untreated cells. The number of alive cells were significantly lower in aphidicolin treated cells, while the number of cells in apoptosis increased. The other two drugs did not appear to effect cell vitality (Fig. 4.22A). The cell cycle analysis showed that in comparison to untreated cells, aphidicolin treated cells had a significant increase in the number of cells in S-phase (Fig. 4.22B) and a decrease of the number of cells in G2-M phase, which had been expected Ivermectin treated cells had an increase in the number of cells in subG1-G0, and is not known to inhibit cell cycle. Hydroxyurea has been reported to elicit the same effects as aphidicolin, however, this was not reflected in any of the experiments presented here. This either demonstrates that other experimental conditions are needed for it to be functional or that it was not viable. Nevertheless, the aphidicolin results seem to show that actively replicating cells are needed for EV-DNA uptake.

4.2.10 EV-DNA is transported to recipient cell nucleus

To further establish the finding that EV-DNA is transported to the nucleus after internalisation by recipient cells, three different approaches were adopted. Two types of recipient cells were educated with EVs of a different cell line with mutations, or EVs from another species. MDA-MB-231 cells were educated with B16-F10 EVs, while HeLa cells were educated with EVs of AML origin or melanoma origin, containing known mutations The nuclei of the recipient cells were then removed and DNA was extracted for analysis. Western blotting was performed to confirm that no cytoplasmic elements were present in the nuclear extracts. This was confirmed by the lack of beta-Tubulin signals in the nuclear fractions which were subsequently used for analysis (Fig. 4.23).

A

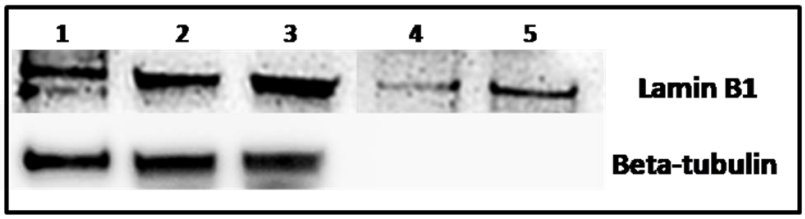

No.	1	2	3	4	5
Sample: MDA-MB-231	Whole cell extract	treated with 1X B16F10 EVs Supernatant	treated with 4X B16F10 EVs Supernatant	treated with 1X B16F10 EVs Nuclear fraction	treated with 4X B16F10 EVs Nuclear fraction

B

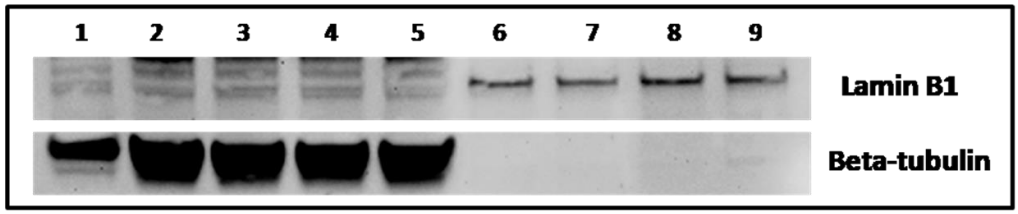

No.	1	2	3	4	5	6	7	8	9
Sample: HeLa	Whole cell extract	treated with 1X SKmel28 EVs Supernatant	treated with 4X SKmel28 EVs Supernatant	treated with OCIAML3 EVs Supernatant	treated with MV411 EVs Supernatant	treated with 1X SKmel28 EVs Nuclear fraction	treated with 4X SKmel28 EVs Nuclear fraction	treated with OCIAML3 EVs Nuclear fraction	treated with MV411 EVs Nuclear fraction

Figure 4.23: Confirmation of Nuclear Extraction. MDA-MB-231 cells were educated with B16-F10 EVs (upper), HeLa cells were educated with SK-MEL-28 EVs, MV4-11 EVs or OCI-AML3 EVs (lower). The nuclei of the recipient cells were removed using a nulcear extract kit. Whole cell protein extract, the supernatants containing cytoplasmic components and nuclear pellet fractions were analysed using western blotting. Beta-Tubulin antibody was used to confirm that no cytoplasmic components were remaining in the nuclear fraction. Lamin B1 was used to identify presence of nuclear components.25 µg or 25 µL of the preparations were added in accordance to the results of BCA assay.'4x' indicates the four-times the amount of EV particles were used for education in comparion to the '1x' indicators. Samples were processed on the same blot, picture was cropped to exclude irrelevant samples

4.2.11 DNA fingerprinting confirms presence of donor DNA in recipient cell nuclei

As used in the previous microscopy experiments, human MDA-MB-231 cells were educated with mouse B16-F10 EVs for 48 hours. The number of particles that were used in the microscopy experiments were scaled up for education of recipient cells in a 6-well plate. Additional recipient cells were also educated with 4-times this particle number, to overcome the possibility of EV concentration being a factor. After education, the nuclei of the recipient cells were removed from the cells and the DNA extracted. The DNA was then sent to IDEXX for cell line identification using STR DNA fingerprinting. The results showed that traces of mouse donor DNA could be detected in the DNA extracted from the nuclei of the human recipient cells. This suggests that the donor EV-DNA had indeed been transported to the recipient cell

nucleus (Table 4.6.). No cross-contamination was detected in the control DNA samples.

Table 4.6: Donor EV-DNA Detectable in Recipient Cell Nucleus. Using STR fingerprinting it was possible to confirm the presence of mouse DNA in the DNA extracted from recipient human MDA-MB-231 cell nuclei after education with B16-F10 EVs for 48 hours.'4X' indicates that 4-times the amount of EVs were used for education. The gDNA of the respective cell lines were used as positive and negative controls.

Species	MDA-MB-231 gDNA	MDA-MB-231 nuclear DNA +B16F10 EVs	MDA-MB-231 nuclear DNA +B16F10 EVs (4X)	B16F10 gDNA
Human	+	+	+	-
Mouse	-	+	+	+

4.2.12 GeneScan-based fragment-length analysis

Once we had confirmed that the donor DNA was reaching the recipient cell nucleus, we were interested to see if donor cell-specific mutations could also be detected in the nucleus of recipient cells. As we had previously optimised fragment-length analysis for our AML mutational studies, it was decided to utilise this technique for the mutational transfer investigation. In this approach, HeLa cells were educated with EVs from AML cell lines OCI-AML3 and MV4-11 which contained AML-specific mutations nucleophosmin (NPM1) and FMS-like tyrosine kinase 3 internal tandem repeats (FLT3-ITD), respectfully. DNA was extracted from educated whole cells as well as the nuclei only, and quantified using Nanodrop. This DNA was analysed for the aforementioned mutations using GeneScan-based fragment-length analysis (Fig. 4.24). A positive NPM1 signal was represented by a double peak, as the WT-allele showed a peak around 221-223 bp, with a second larger peak at 225-226 bp being observed if the mutated allele was present. A positive FLT3-ITD mutation was represented by a peak at a fragment size of 372 bp which is larger than the WT FLT3 allele seen here at 342 bp. Despite repeat analysis, the mutations could not be detected in recipient cell whole cell DNA or nuclear DNA.

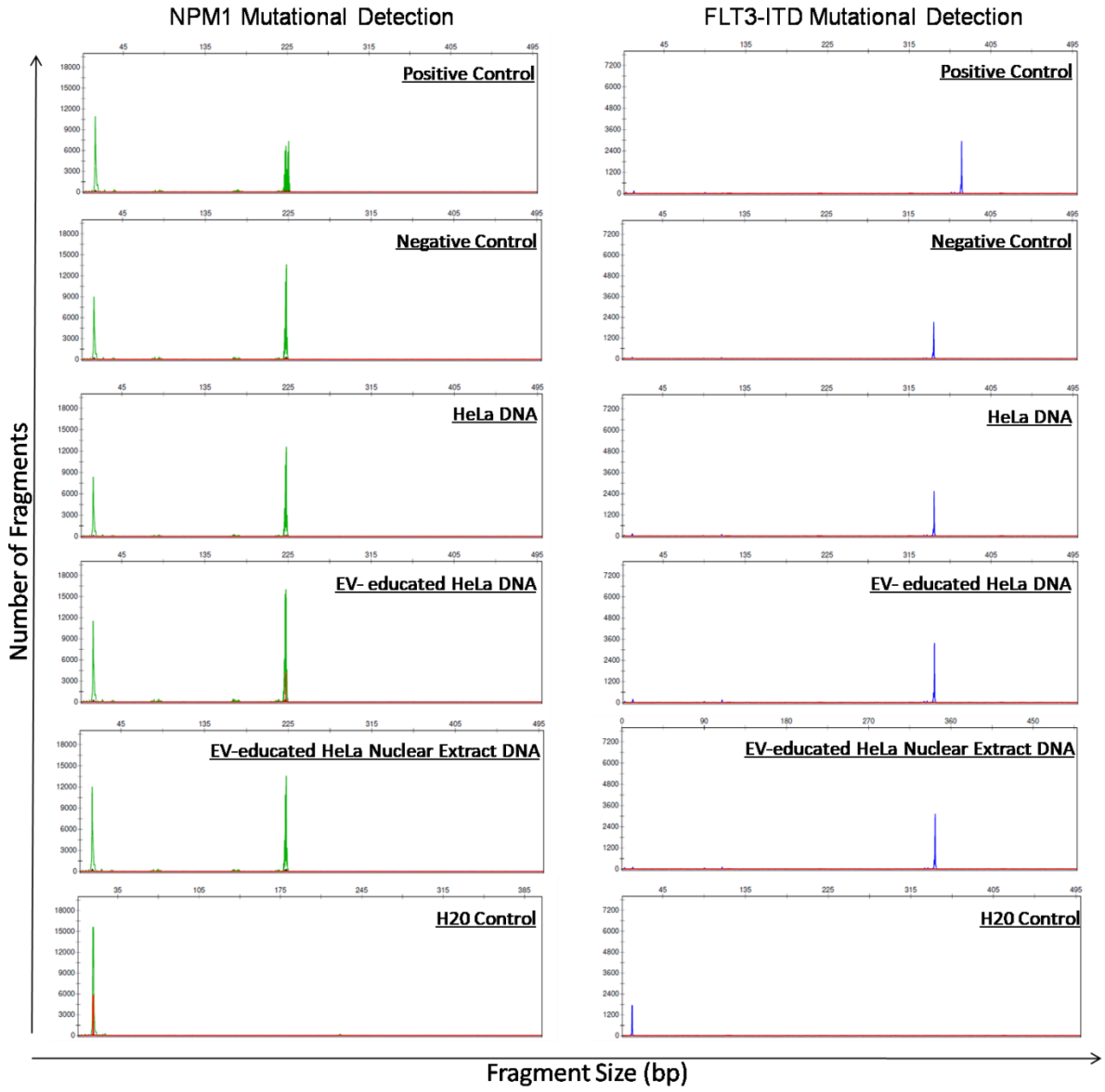

Figure 4.24: Mutational Analysis of EV-educated HeLa cells. The DNA of HeLa cells that had been educated by OCI-AML3 or MV4-11 EVs containing NPM1 or FLT3-ITD mutations, respectfully, were analysed by GeneScan-based Fragment-length analysis. The positive and negative controls were the OCI-AML3 and MV4-11 cells gDNA.

4.2.13 Allele-specific RTPCR

In another approach, HeLa cells were educated with EVs from melanoma cell line SK-MEL-28 containing a *BRAF*V600E mutation. DNA was extracted from educated whole cells as well as the nuclei only, and quantified using Nanodrop. This DNA was analysed for the aforementioned mutation using an allele-specific real-time PCR with primers for the mutated *BRAF* gene (primer E) or the WT *BRAF* gene (primer V). This approach did not turn out to be reliable, as there was amplification with mutant primers in samples which should be negative for the mutation. The amplification of negative samples always appeared much later in the assay reflected by a higher CT

mean (Fig. 4.25) usually around 28, whereas the positive control cell line, SK-MEL-28, saw earlier amplification with a CT in the early 20's. Based on this idea, it can be seen that the DNA of EV-educated HeLa cells showed a similar pattern to the negative samples, giving the impression that any EV-DNA transferred by the EVs could not be detected in the recipient cell DNA using this approach.

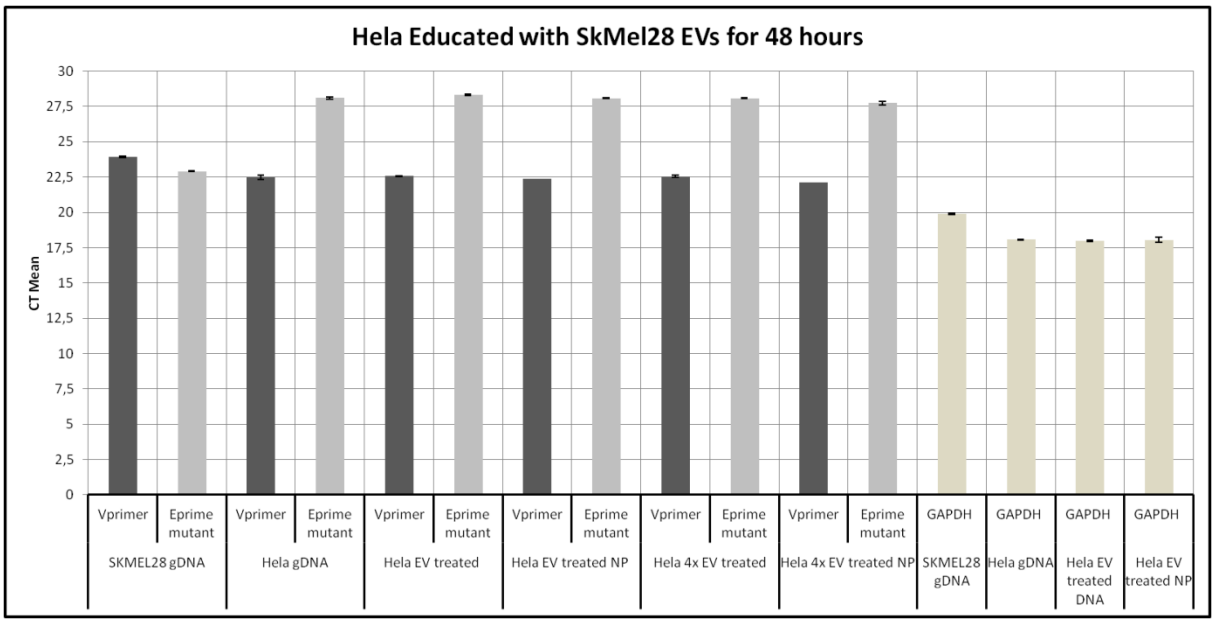

Figure 4.25: Dectection of BRAF V600E Mutations Using Allele-specific RT-PCR. HeLa cells were educated with EVs from cell line SK-MEL-28 which contains a BRAF V600E mutation. Either the whole cell DNA or the nuclear DNA(NP) were used for amplification. Two concentrations of EVs were used for education, '4x' indicates the cells were treated with 4-times the amount of EVs. Two primers were used, one for the WT (Vprimer) and one for the mutant (Eprimer). SK-MEL-28 gDNA was used as a positive control. GAPDH was used as a housekeeping gene. Error bars show standard deviation. n=3.

4.2.14 Assessing different combinations of donor and recipient cell lines

For the establishment of the methods, we had focussed on B16-F10 as the EV donor cell line and MDA-MB-231 as the recipient cell line. In order to determine that this DNA-labelling method was also applicable to other cell lines, and ones that had more of a relation, we harvested EVs from different cell lines using the same EdU-based labelling system and placed them on various recipient cells. Here, we saw that in other cell lines it was also possible to visualise the EdU-EV-DNA using confocal fluorescence microscopy and that the DNA appeared to have been taken up by the recipient cells (Fig. 4.26). High cell loss was observed when different recipient cells were used with this protocol, suggesting the method should be adjusted according to the recipient cell line of choice.

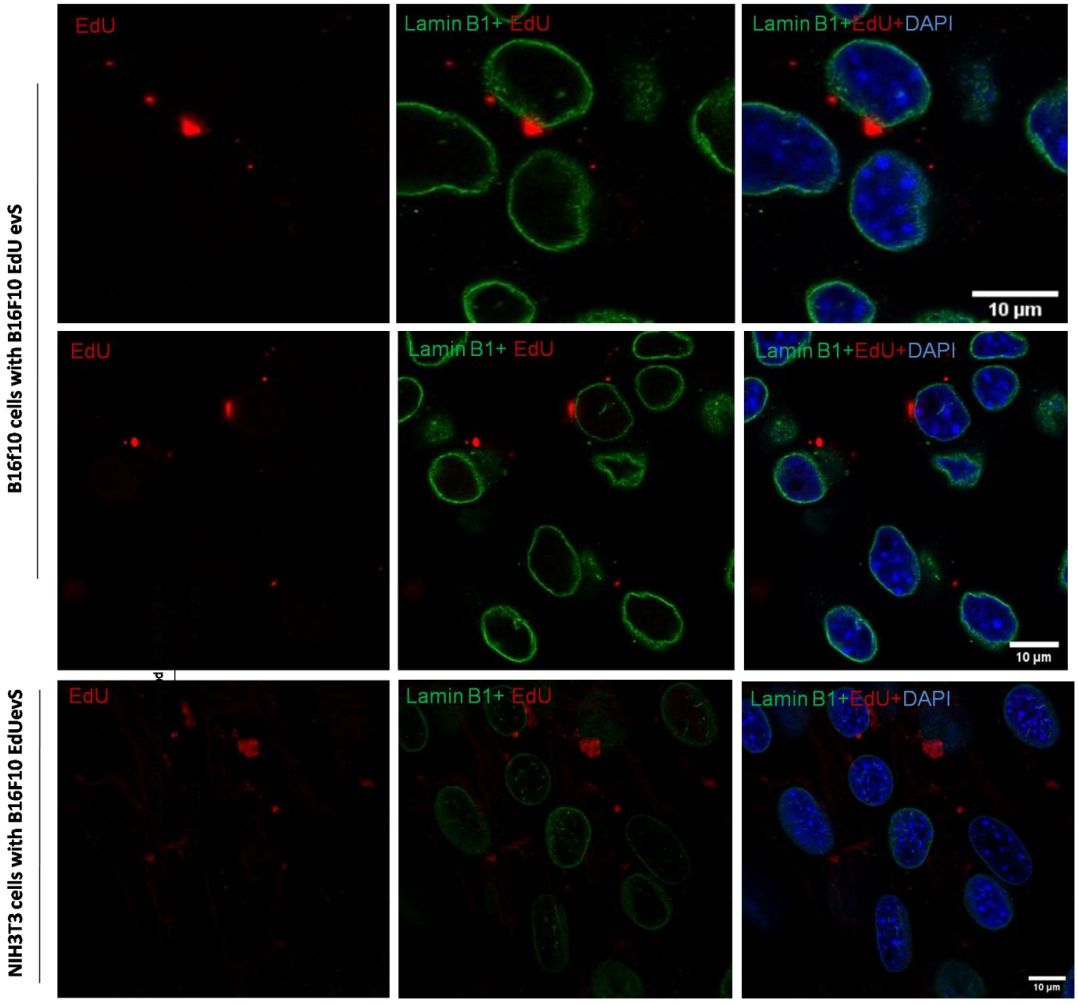

Figure 4.26: The EdU-Labelling Protocol is Applicable to Other Cell Lines. B16-F10 cells and NIH/3T3 cells were educated with B16-F10 EVs that contained EdU-labelled DNA and analysed by confocal microscopy. Blue = recipient cell nucleus, green= LaminB1, red = EdU-labelled EV-DNA. Scale bar = 10 µm.

4.2.14.1 HEK-CD63-GFP EVs: new opportunity for EV membrane labelling

As mentioned in section 4.2.1.2, our attempts to label the EV surface with PKH67 had been unsuccessful. At a later stage of this current project, a HEK cell line which had been engineered to produce EVs with a GFP-tag attached to the tetraspanin CD63 found in the EV membrane became available to us from the working group of AG Giebel, University hospital Essen. If successful, this GFP tag would allow visualisation of the EV membrane without having to take extra steps to incorporate a label in to the EV membrane. To assess if GFP-tagged EVs could be detected, EVs from HEK-CD63-GFP were added to B16-F10 cells and incubated for 24h. The EVs had been isolated using a different isolation method, TSC, which will be presented later (*section 4.3.3*). EVs from TSC fractions 2 and 3 were used for education. The presence of GFP-tagged EVs in the preparations was confirmed using fluorescence microscopy of the live cells (Fig. 4.27).

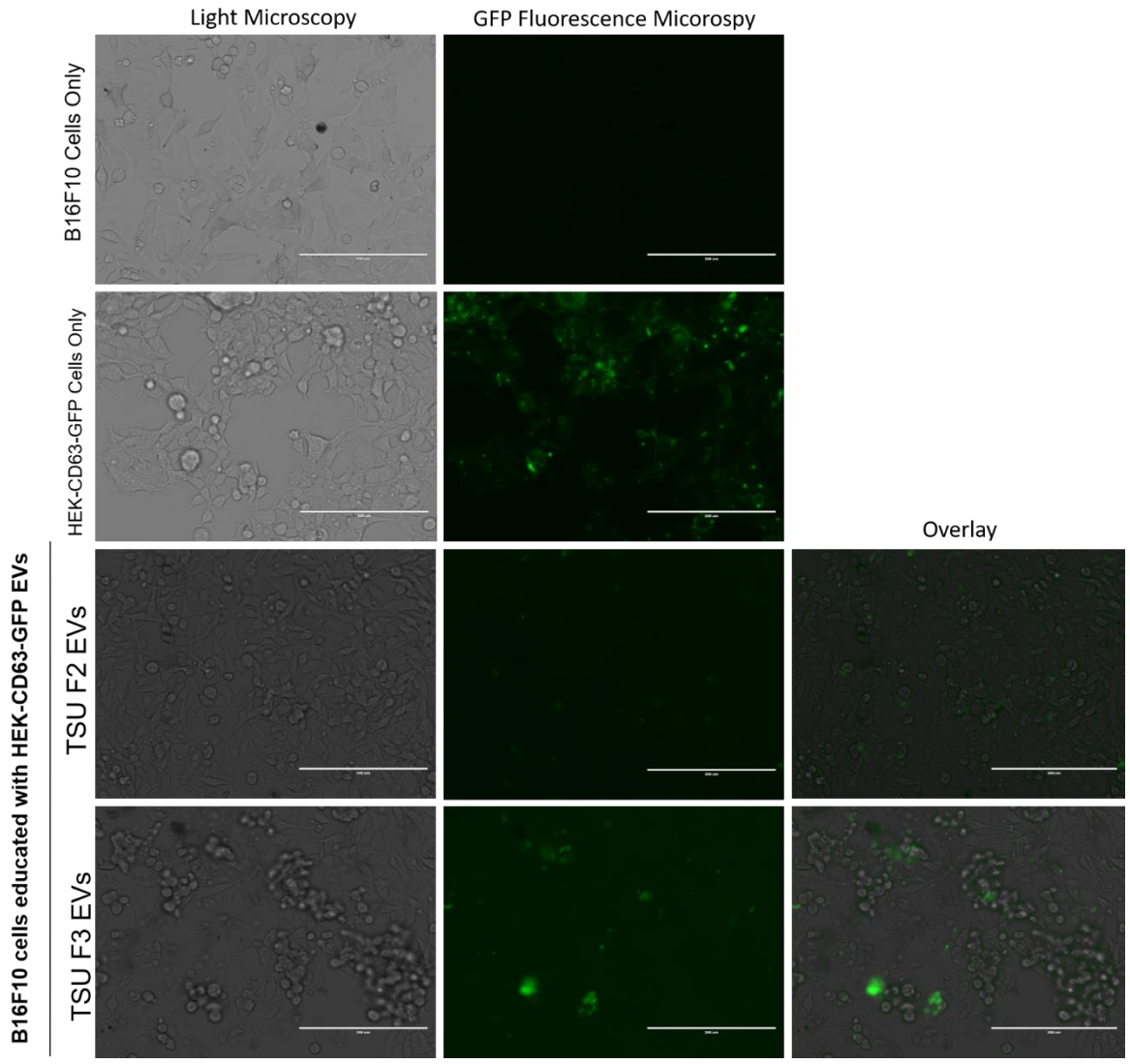

Figure 4.27: B16-F10 Cells Educated with HEK-CD63-GFP EVs. B16-F10 cells were treated with EVs from HEK-CD63-GFP cell line for 24 hours. EVs were isolated by TSU, fractions 2 and 3 (20 µL) were used for education .GFP was visualised using fluorescence microscopy on an AMG light microscope. Scale Bar = 200 µm.

To further investigate the presence of the CD63-GFP-tagged EVs, the same samples shown above were fixed and prepared for confocal microscopy. The confocal microscopy analysis confirmed the presence of the CD63-GFP-tagged EVs in some of the B16-F10 cells (Fig. 4.28). As with the previous experiments where different recipient cells were used, the B16-F10 cells in this experiment didn't survive the microscopy preparation as well as MDA-MB-231 cells had, as reduced amount of cells were seen in the confocal microscopy analysis. Nevertheless, this experiment confirmed that use of CD63-GFP-tagged EVs could be a viable alternative to labelling of the EV membrane. The future steps would be to combine this cell line with EdU for detection of EV-DNA and the EV membrane simultaneously.

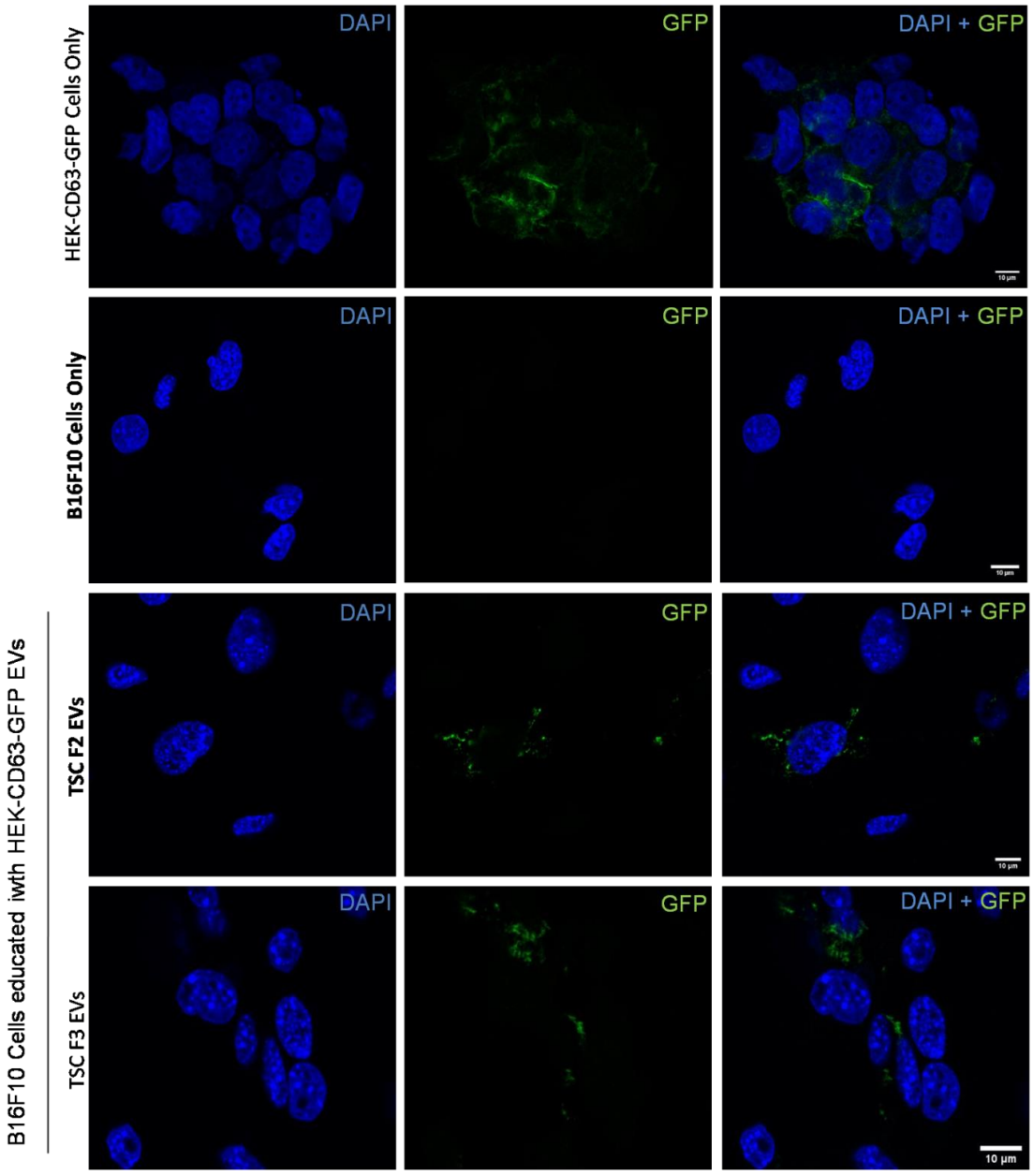

Figure 4.28: Confocal Microscopy B16-F10 Cells Educated with HEK-CD63-GFP EVs. B16-F10 cells were treated with EVs from HEK-CD63-GFP cell line for 24 hours before fixation for confocal microscopy. EVs were isolated by TSU, fractions 2 and 3 were used for education. Blue = cell nucleus, green = GFP-tagged CD63 EVs or HEK-CD63-GFP cells. Scale Bar = 10 µm.

4.3 Optimisation of an EV Isolation Method for Cell Line-Conditioned Media

Due to increasing disadvantages surrounding the gold-standard ultracentrifugation (UC) method for EV isolation, several other isolation techniques have been developed. However, until now there is still no universally recognised isolation method. Here, we optimised a method to circumvent UC use which combined polyethylene gycol (PEG) precipitation and size exclusion chromatography (SEC) for

the isolation of EVs from large volumes of cell line-conditioned media, and compared it to the gold-standard UC method.

4.3.1 Isolation of EVs from healthy donor plasma samples

The effectiveness of SEC alone was firstly confirmed using healthy donor plasma samples, before its combination with PEG for cell line supernatant analysis.

4.3.1.1 **Characterisation and comparison of plasma EVs isolated by mini-SEC or ultracentrifugation**

EVs from healthy donor plasma were isolated by both mini-SEC and ultracentrifugation and compared with regards to their yield, protein content, morphology and their EV-dsDNA and RNA contents. The fourth mini-SEC EV fraction was previously established by Hong et al. (2016) as the optimal EV fraction for plasma samples, containing a high number of EVs with low protein contamination. Therefore, only EVs from fraction 4 were used for analysis and comparison to the EVs that were isolated by UC. In all samples, EV fractions isolated by mini-SEC revealed a higher number of particles and lower protein concentration levels in comparison to the EV fractions of the same samples isolated by UC *(Table 4.7)*.

Table 4.7: EV Yield and Protein Comparison. Comparison of EV fractions isolated from plasma of 5 healthy donors by mini-SEC (fraction 4 only) and UC with regards to EV yield and protein-based purity.

Sample	Yield (particles per mL)		Protein (mg/mL)	
	SEC	UC	SEC	UC
Healthy Donor 1	**$3.20x10^{9}$**	$1.80x10^{9}$	**0.014**	0.269
Healthy Donor 2	**$1.0x10^{11}$**	$2.90x10^{9}$	**0.025**	0.107
Healthy Donor 3	**$2.00x10^{11}$**	$9.90x10^{9}$	**0.017**	0.072
Healthy Donor 4	**$7.90x10^{10}$**	$4.20x10^{9}$	**0.027**	0.106
Healthy Donor 5	**$7.30x10^{10}$**	$5.60x10^{9}$	**0.072**	0.118

A representation of the results of the NTA analyses of EVs from the fourth mini-SEC fractions and UC fractions are shown in Figure 4.29. Peaks show the most common diameter of EVs in the sample. The most common diameter of EVs isolated by mini-SEC ranged from 98 to 113nm, and most common diameter of EVs isolated by UC ranged from 105 to 139nm, which fit within the 30-150nm sEV diameter size range.

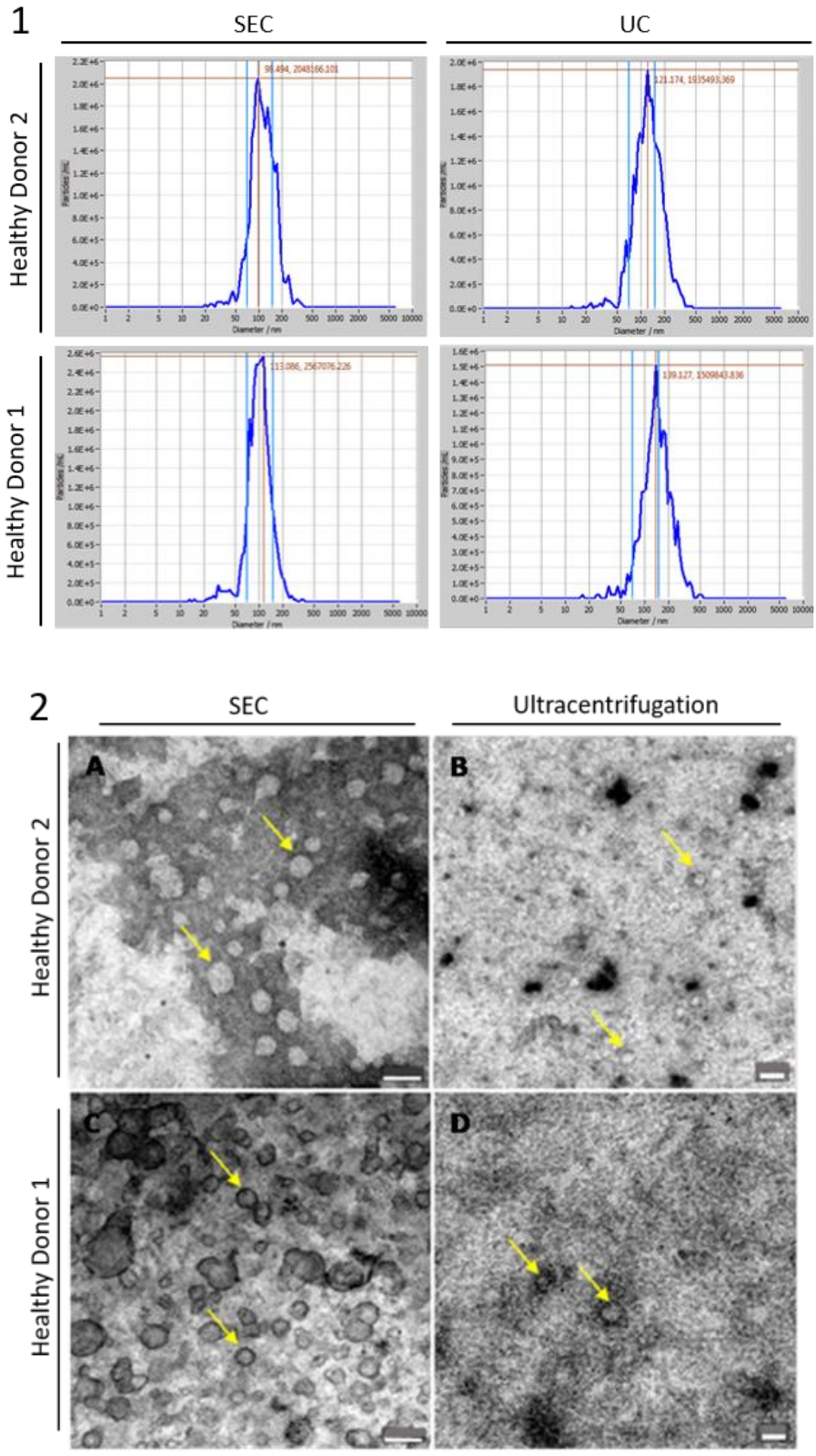

*Figure 4.29: EV Characterisation. Quantification and diameter analysis of particles by Nanoparticle Tracking Analysis (NTA) (**1**) Peaks show most common diameter of tracked particles. Confirmation of EV-like structures using Transmission electron microscopy (TEM) (**2**). EVs were isolated from plasma of 5 healthy donors by mini-SEC (2A&C) and UC (2B&D), images representative of two healthy donors. Representative images of unconcentrated aliquots of EV-containing fractions that were negatively stained using uranyl acetate. Scale bars = 50 nm.*TEM analysis of the healthy donor EV fractions confirmed the presence of EV-like structures in both mini-SEC and UC

fractions (Fig. 4.29). It was also easier to locate the EV-like structures in the mini-SEC fractions than in the UC fractions. This could be a reflection of the NTA results which showed that the mini-SEC fractions contained more particles than the UC fractions.; however, a quantitative assay would have been needed for confirmation.

4.3.1.2 Characterisation and comparison of nucleic acids from plasma EVs isolated by mini-SEC or ultracentrifugation

Double-stranded DNA and RNA were extracted from EVs isolated by mini-SEC and UC to compare the dsDNA and RNA concentrations obtained from both methods. DNA and RNA quantification were performed by dsDNA quantifluor and RNA quantifluor. It was possible to recover both dsDNA and RNA from EVs isolated by both isolation methods. No overall trend could be identified as neither of the two isolation methods consistently yielded higher dsDNA or RNA amounts (Fig. 4.30). It was also observed that dsDNA and RNA concentration did not reflect EV number detected by NTA.

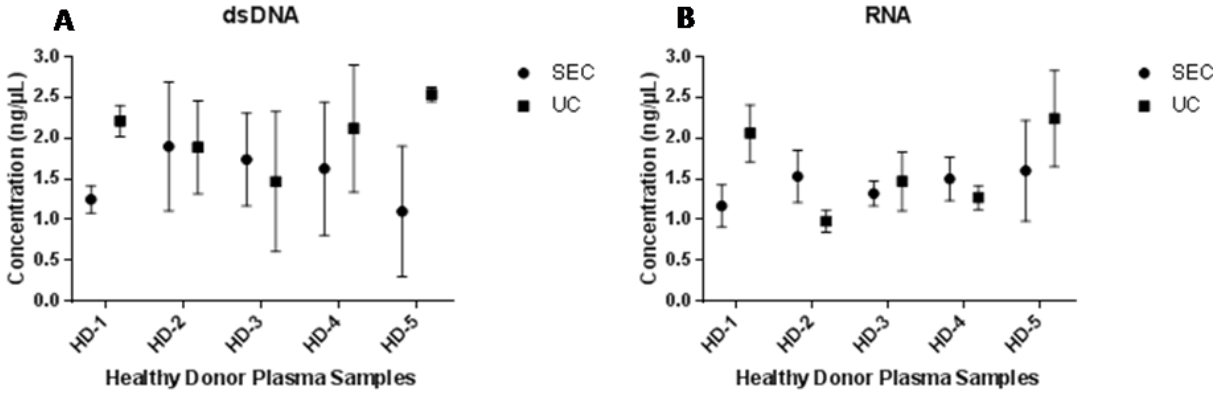

Figure 4.30: EVdsDNA and RNA Comparison. A) dsDNA concentration of EVs isolated from healthy donor plasma by mini-SEC (fraction 4) and UC. B) RNA concentration of EVs isolated by mini-SEC (fraction 4) and UC. Error bars show standard deviation, n=3.

4.3.2 Isolation of EVs from cell line-conditioned media

Once we had confirmed that the SEC method was working as expected for low volume plasma samples, we then moved on to combining this SEC method with an EV precipitation method using polyethylene gycol (PEG) for larger volumes of cell line-conditioned media.

4.3.2.1 **Characterisation of cell line EVs isolated by PEG/SEC**

EVs were isolated from the conditioned media of three cell lines, NB4, OCI-AML3 and HT-29, by both UC and PEG/SEC isolation techniques, to be compared for EV yield, protein co-isolation, morphology and dsDNA and RNA contents. Firstly, although fraction 4 had been previously established as the optimal EV fraction for plasma samples, an optimal fraction needed to be confirmed for cell lines using the PEG/SEC isolation method before comparison to the UC samples. Particles were detected in fractions 3-6 using NTA, therefore, fractions 1 and 2 were excluded from further analysis. From the three cell lines, there was not one fraction that consistently contained the highest number of particles (Fig. 4.31A) although fraction 3 never contained the highest concentration. To further investigate the purity of the different EV fractions in terms of protein co-isolation, BCA and coomassie blue staining were performed. Using BCA a clear pattern was observed with the sixth fraction of each cell line having the highest concentration of co-isolated protein in the cell lines, with the third having the lowest concentration (Fig.4.31B). Coomassie blue also reflected that fraction 6 had higher protein than fraction 4 and 5 (Fig.4.31D). In TEM analysis, it was observed that EV-like structures were harder to find in the PEG/SEC third fraction, and they still appeared to contain visible protein aggregations, despite the BCA results showing fraction 3 as the purest fraction (Fig. 4.31C). Fractions 4 and 5 of the PEG/SEC isolation method appeared to contain fewer co-isolated proteins than fraction 6. Due to the higher protein content in fraction 6 and lower number of particles and EV-like structures in fraction 3, we decided to perform further comparative analysis with fractions 4 and 5.

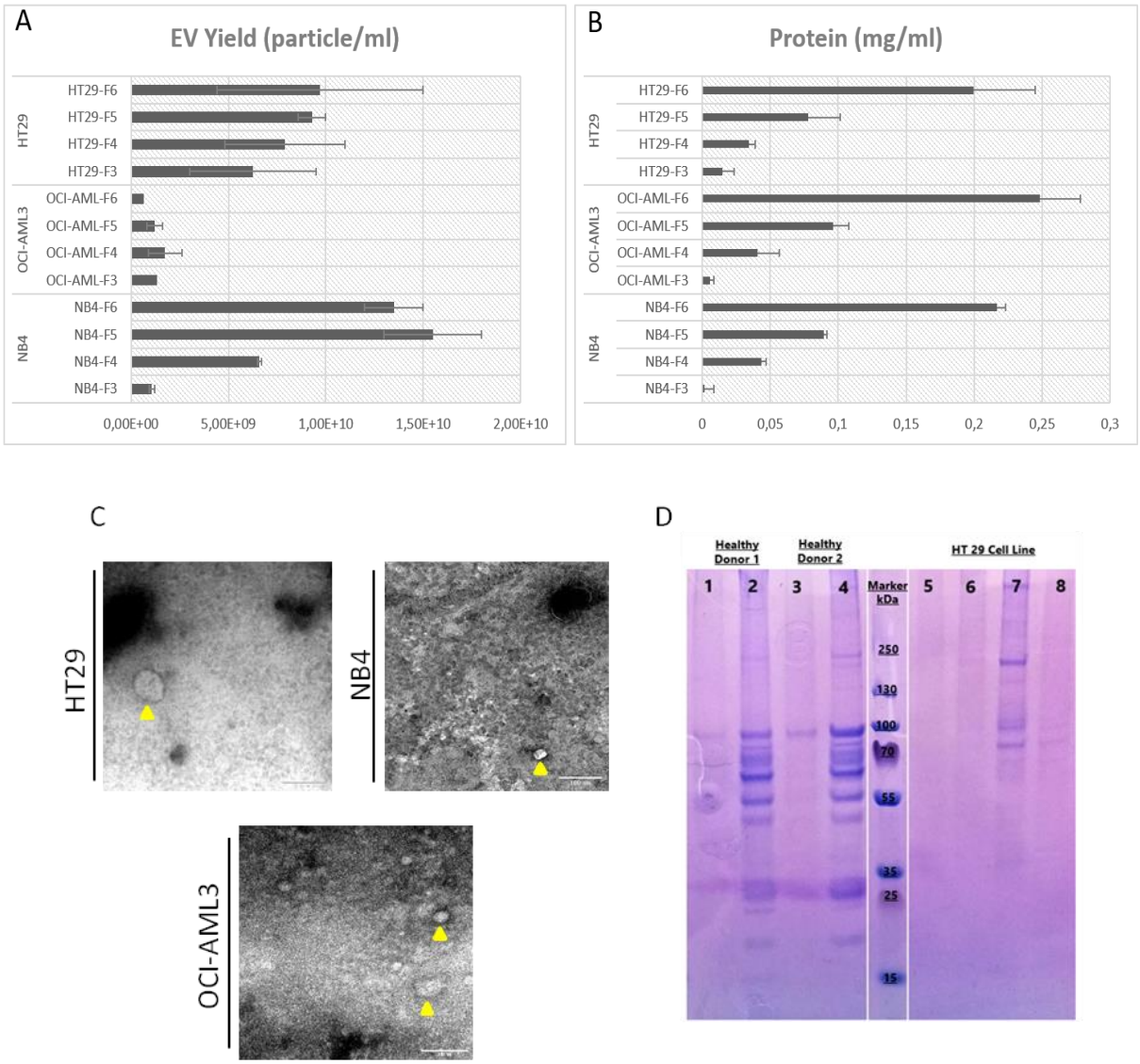

*Figure 4.31: Comparison of PEG/SEC EV fractions. EV yield (**A**) and protein content (**B**) of PEG/SEC fractions 3-6 of the three cell lines were compared. n=2. Data shows mean with standard deviation. (**C**) TEM imaging of the PEG fractions 3. Scale bar = 100 nm (**D**)Coomassie blue staining was performed to assess protein presence in the EV fractions. (1+2) Concentrated mini-sec fractions 4 and 5, respectively, from healthy donor plasma. (3+4) Concentrated mini-sec fractions 4 and 5, respectively, of a second healthy donor. (5-7) Unconcentrated EV PEG/SEC fractions 4-6 and (8) unconcentrated UC EV fraction, from the HT-29 cell line.*

4.3.2.2 **Characterisation and comparison of cell line EVs isolated by PEG/SEC or ultracentrifugation**

When PEG/SEC fraction 4 and 5 were compared to the UC fractions for EV yield and protein content, the results were again variable. In cell lines, HT-29 and OCI-AML3, the UC fraction had a higher number of particles than the PEG/SEC fractions 4 and 5, with a large difference seen in HT-29 (Fig. 4.32A). In terms of protein co-isolation,

in two cell lines, HT-29 and NB4, PEG/SEC F4 had lower protein concentration than the UC samples (Fig. 4.32B).

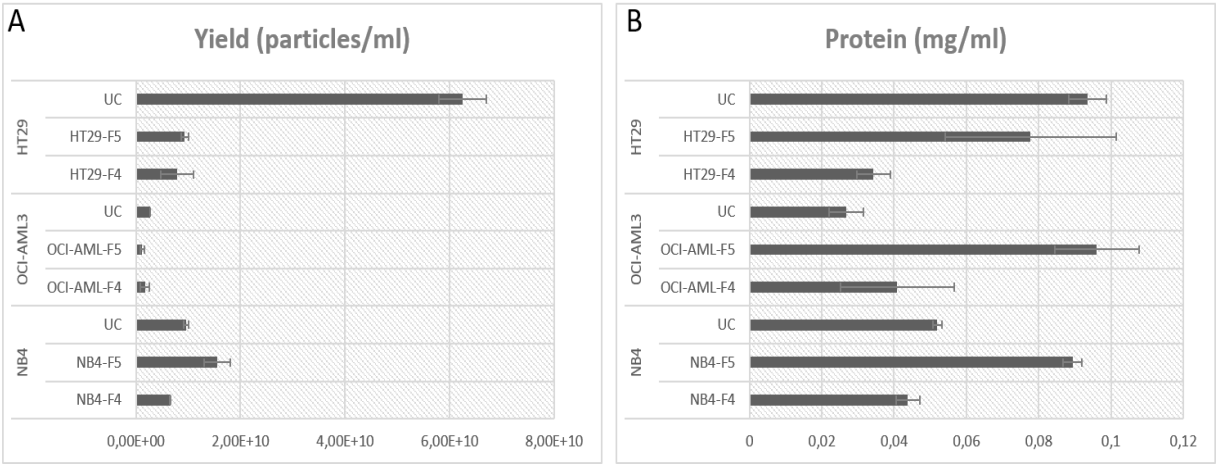

Figure 4.32: Comparison of EV Yield and Protein Content. of EV fractions. PEG/SEC fractions 4 and 5 were compared to UC fractions for EV yield and protein content in three cell lines. n=2. Data shows mean with standard deviation.

Additionally, NTA analysis showed that the most common diameter of EVs isolated by PEG/SEC in F4 and F5 ranged from 129 to 171 nm, and most common diameter of EVs isolated by UC ranged from 129 to 149 nm (Fig. 4.33). TEM analysis of the PEG/SEC EV fractions 3-6 and UC EV fractions was carried out. Similarly to the plasma samples, TEM confirmed that EV-like structures of various sizes were present in fractions isolated using both the PEG/SEC and UC method (Fig. 4.34), although a quantitative analysis could not be made.

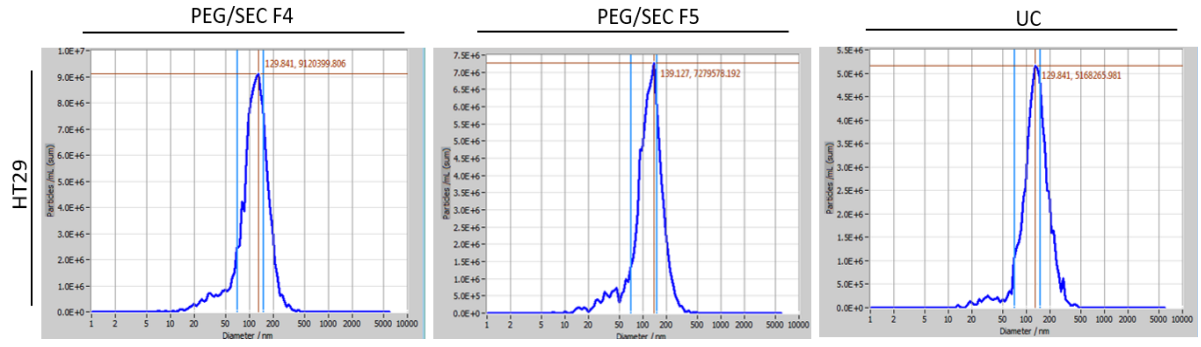

Figure 4.33: EV Size Analysis. Representative images of NTA analysis diameter peaks of HT29 cell line EV fractions isolated by PEG/SEC or UC. Peaks show most common diameter of tracked particles (nm).

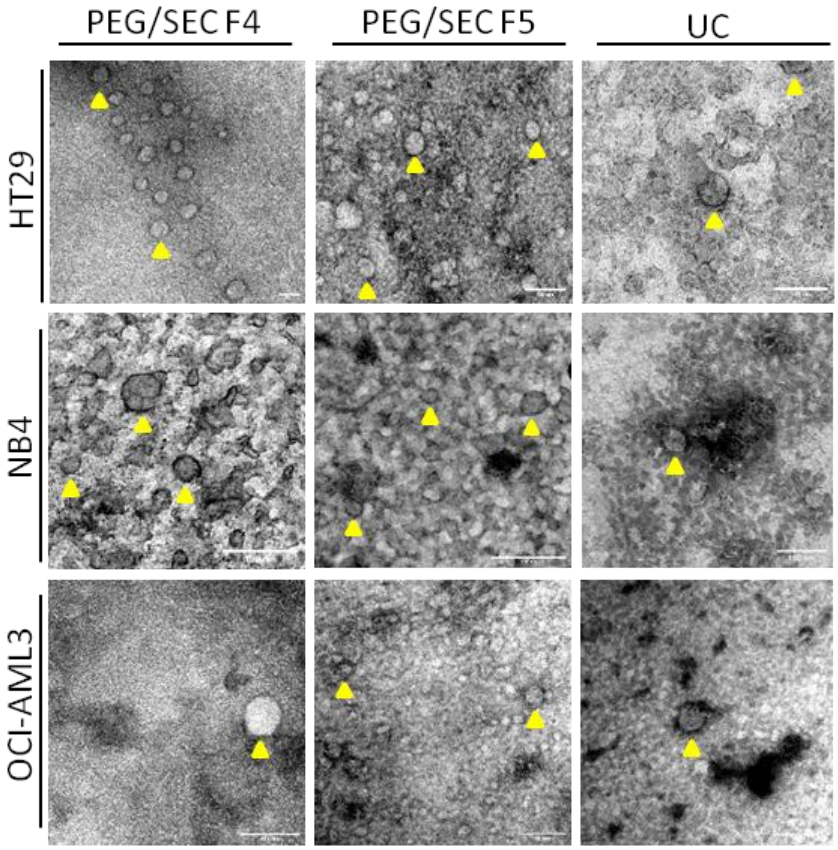

Figure 4.34: EV Visualisation. Representative transmission electron micrographs of EV fractions from cell lines HT-29, NB4 and OCI-AML3 eluted via PEG/SEC (fractions 4 and 5) or by UC. Unconcentrated aliquots of EV-containing fractions were negatively stained using uranyl acetate. Scale bars = 100 nm

Furthermore, DNA and RNA were isolated from PEG/SEC fractions 4, 5 and the UC fraction for comparison. Results showed it was possible to extract dsDNA and RNA from EVs isolated by both methods. Two out of three cell lines showed higher dsDNA concentration in the UC fraction than PEG/SEC fraction 4 or 5, with the third cell line, OCI-AML3, showing the opposite trend (Fig.4.35A). Two out of three cell lines showed higher RNA concentration in the fourth PEG/SEC fraction than in the fifth fraction or UC fraction, with the third cell line, OCI-AML3, showing highest RNA concentration from the fifth PEG/SEC fraction (Fig. 4.35B).

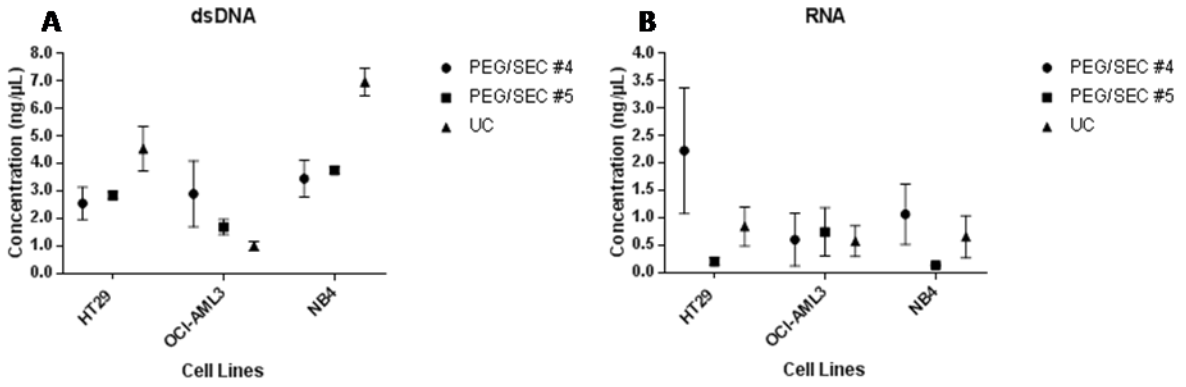

Figure 4.35: EVdsDNA and RNA Comparison. (A) dsDNA concentration from cell line-derived EVs isolated by PEG/SEC (fraction 4 and 5) and UC. (B) RNA concentration from cell line-derived EVs isolated by PEG/SEC (fraction 4 and 5) and UC. Error bars show standard deviation, n=3.

4.3.2.3 **Comparison of diagnostic potential of nucleic acids from cell line EVs isolated by PEG/SEC or ultracentrifugation**

Additionally, dsDNA was extracted from MV4-11 EVs and OCI-AML3 EVs that were isolated by UC or PEG/SEC (fraction 4) and was analysed for the detection of the FLT3/ITD and NPM1 mutations, respectively. The cell line gDNA was used as positive control and the gDNA from the opposite cell line was used as negative control in both cases. The results show it was possible to successfully detect the mutations in the gDNA and the EV-DNA isolated by both the UC method and the PEG/SEC method, but not in the negative control (Fig.4.36).This reflected that both isolation methods were capable of supplying nucleic acids which could be utilised in a diagnostic capacity.

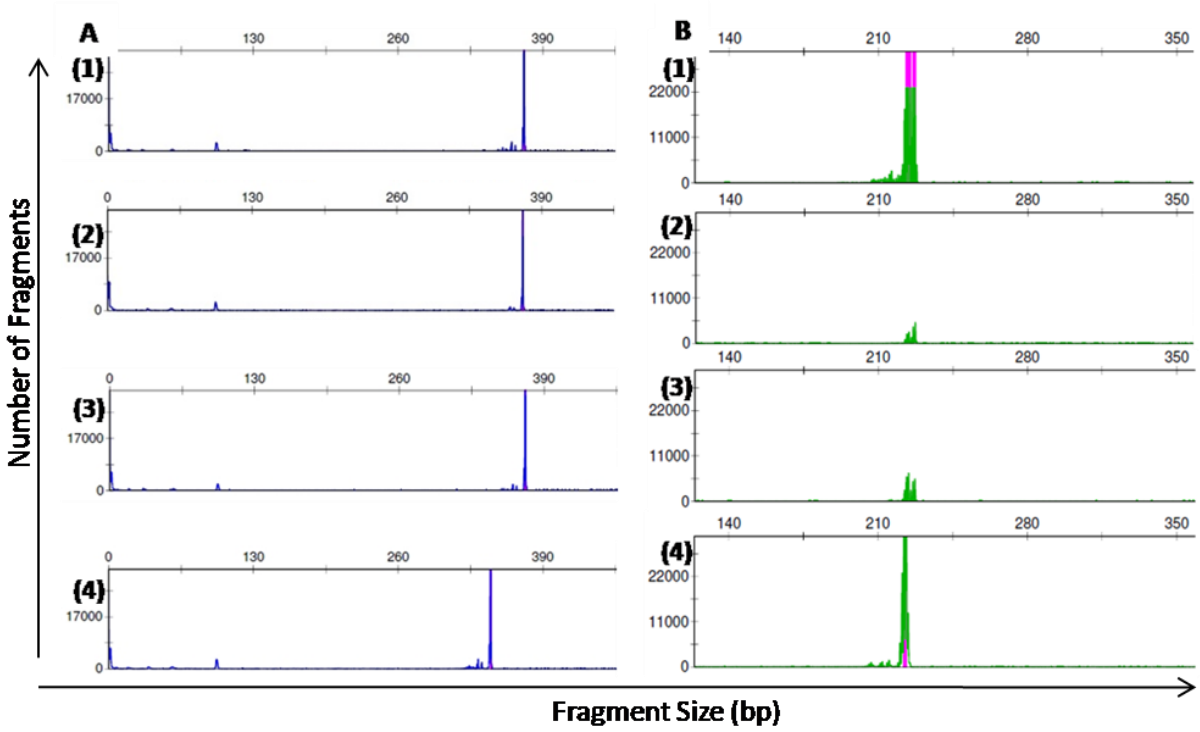

Figure 4.36: EVdsDNA Mutational Analysis Using GeneScan-based Fragment-length Analysis. (A) Detection of FLT3/ITD mutation in dsDNA from (1) MV4-11 cells, (2) MV4-11 EVs isolated by PEG/SEC, (3) MV4-11 EVs isolated by UC and (4) OCI-AML3 cells (negative control). (B) Detection of NPM1 mutation in dsDNA from (1) OCI-AML3 cells, (2) OCI-AML3 EVs isolated by PEG/SEC, (3) OCI-AML3 EVs isolated by UC and (4) MV4-11 cells (negative control). Both negative controls show only one peek for the WT.

Considering the results of the three cell lines, it was clear that SEC in combination with PEG, was not as effective as SEC alone. The yield of the PEG/SEC fractions didn't show a definitive trend, and in two cell lines the UC samples had a higher particle yield than PEG/SEC fraction 4 and 5 samples. In two out of three cell lines, PEG/SEC fraction 4 still showed less co-isolated protein, and more RNA than the UC samples. Oppositely, dsDNA was higher in the UC samples in two out of 3 cell lines. Although the PEG/SEC F4 and F5 results were not consistently better than the UC samples, it was observed that DNA and RNA with mutational information could be recovered from the EVs, which was a main focus of our laboratory at the time of this comparative study. Therefore, for our laboratory practices, it was a suitable alternative to UC for EV isolation. However, it was clear that a period of optimisation was needed to improve upon reproducibility.

4.3.3 Further investigation of PEG/SEC fractions

Due to the varied results of the cell line fractions in terms of yield and protein content, we spent some time optimising the PEG/SEC method. A colleague then proceeded in the comparison of the PEG/SEC isolation with a different isolation

method. After this optimisation period, with four cell lines - MV4-11, OCI-AML3, SK-MEL-28 and MeWo, the results showed that EV fraction 4 of the PEG/SEC method consistently contained the highest particle concentration when analysed with NTA, with fractions 4 and 5 having a lower protein content than fraction 6 (Appendix Fig. 1). Considering these combined results it was decided that fraction 4 would be the optimal working fraction, due to high yield, lower protein and that nucleic acids were present in the fractions - with fraction 5 being the second most optimal fraction.

Sometime after implementing PEG/SEC as our main method of EV isolation from conditioned media in our laboratory, a new EV characterisation technology became available in the form of flow cytometry using an Amnis Image StreamX MkII instrument (Gorgens et al. 2019). This is a flow cytometry approach which should be able to detect EVs by their traditional tetraspanin markers (CD9, CD63). Attempts at western blotting with EV fractions in this comparison project had been difficult. While some EV markers such as Hsp70 could be detected, it was never possible to detect traditional tetraspanin EV markers even after EV concentration attempts, which we had always assumed was due to low EV content. A colleague who was collaborating on this PEG/SEC isolation method brought PEG/SEC samples for AMNIS analysis, which appeared to show a low level of CD9 or CD63 EV markers (Data not shown), which was a disappointing result.

Due to these more recent results, our laboratory is now attempting to optimise an alternative EV isolation technique which combines tangential flow filtration (TFF) with size exclusion chromatography using IZON columns, followed by a concentration step using amnicon columns. At the time that this method emerged I was working with B16-F10 EVs, therefore, I performed a comparison of the PEG/SEC method with the new TSC method. As the TSC protocol uses 8 plates of cells for EV isolation, I increased the number of plates for the PEG/SEC isolation from 4 to 8. TSC fraction 2-5 and PEG/SEC fractions 4 and 5 were analysed using NTA, BCA and a beads-based FACS assay for the tetraspanin markers CD9 and CD63, which a colleague had newly optimised. Additionally, apolipoprotein content was also assessed, due to more recent literature identifying their co-isolation in EV fractions (Table 4.8; Appendix Fig. 2). As they showed the highest particle number with NTA, DNA was also extracted from TSC fraction 2 and 3 and PEG/SEC fraction 4, and

these fractions were also assessed using western blotting analysis and TEM (Table 4.8; Fig. 4.37).

Table 4.8: Comparison of PEG/SEC and TSC B16-F10 EV fractions. B16-F10 EVs were isolated using PEG/SEC or TSC methods. Fractions were characterised using NTA, BCA assay, and FACS.

B16F10 EV Sample	Concentration (particles/ml)	Protein (µg/µl)	DNA (ng/µl)	CD9 %	CD63 %	Apo B %
TSC F2	$2.90x10^{11}$	0.38	12.6	69.8	1.77	93.2
TSC F3	$1.40x10^{11}$	0.36	6.1	5.26	1.54	98.9
TSC F4	$1.10x10^{10}$	0.71	-	0.37	0.36	99.5
TSC F5	$4.10x10^{9}$	1.97	-	0.20	0.24	88.2
PEG/SEC F4	$4.20x10^{11}$	0.47	47.7	2.93	0.59	98.4
PEG/SEC F5	$2.50x10^{10}$	0.90	-	1.04	0.55	99.1

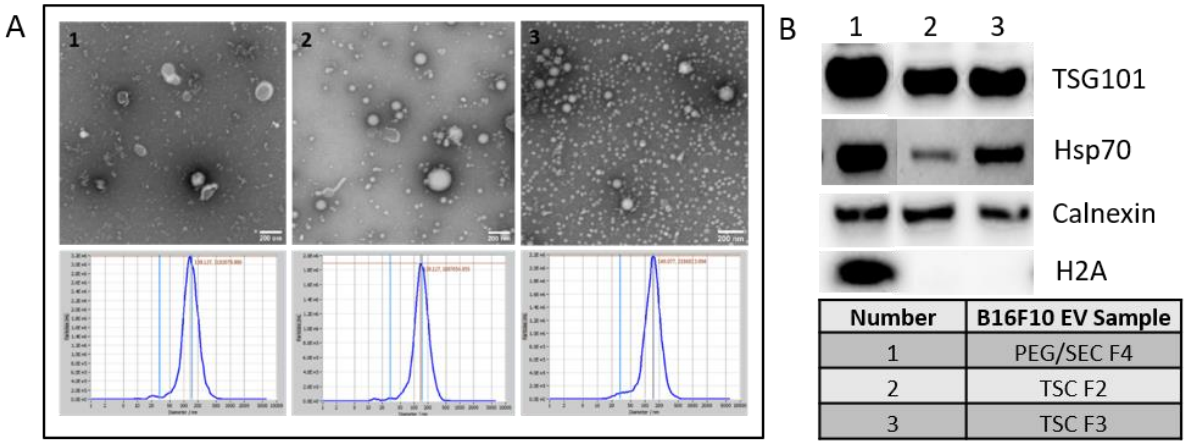

Figure 4.37: Comparison of PEG/SEC EV Fraction 4 and TFF/C EV fractions 2 and 3. B16-F10 EVs were isolated using PEG/SEC or TFF/C methods. Fractions were characterised using (A) NTA, TEM and (B) western blotting. Equal amounts of the EV fractions were used for western blotting. Samples were probed with TSG101, Hsp70, calnexin and H2A antibodies. Samples were processed on the same blot, picture was cropped to exclude irrelevant samples. Scale bar = 200 nm.

Although PEG/SEC fraction 4 had a higher particle concentration, in TEM analysis there was a clear difference between the two methods, with the TSC fractions having a much higher number of EV-like structures. Additionally, TSC fraction 3 appeared to contain an abundance of much smaller spherical structures; however the average particle diameter was larger than the other two fractions, with TSC F3 having a 149 nm average diameter, while the other two fractions both had a 139 nm average diameter. The largest difference was observed in the FACS analysis where TSC F2 had 69.8% CD9 positive events, whereas TSC F3 had only 5.26% and PEG/SEC F4 had only 2.93%. TSC F2 also had the highest percentage of CD63 positive events,

however, CD63 was only present in low amounts in each fraction. Out of the aforementioned fractions, TSC F2 also contained the lowest percentage of apolipoprotein B, although it was present at over 88% in all fractions. With western blotting analysis, TSG101 and Hsp70 were present in all fractions, however, so was calnexin. Histone marker H2A was only present in the PEG/SEC fraction. Due to this finding, the older B16-F10 fractions used in the DNA transfer project (3.2.2.1) were re-probed with antibodies against calnexin and H2A, which showed calnexin was also present in each of the B16-F10 EV preparations tested, although H2A was not detectable (data not shown). Additionally, I compared SK-MEL-28 and HEK-CD63-GFP PEG/SEC fraction 4 with TSC fraction 2 and 3 using western blotting (Fig. 4.38). In this case, all samples were positive for Hsp70, TSG101 and syntenin, but calnexin as well. One tetraspanin marker, CD63, was detectable in HEK-CD63-GFP PEG/SEC and TSC fractions, whereas the only positive signal for CD81 was seen in SK-MEL-28 TSC fractions. However, these fractions were not directly comparable as in the PEG/SEC protocol four plates of cells are used for EV isolation, whereas by TSC 8 plates are used and the same volume of EV fractions were loaded for western blotting.

Number	Sample
1	HEK-CD63-GFP PEG/SEC F4
2	SKMEL28 PEG/SEC F4
3	HEK-CD63-GFP TSC F2
4	HEK-CD63-GFP TSC F3
5	SKMEL28 TSC F2
6	SKMEL28 TSC F3

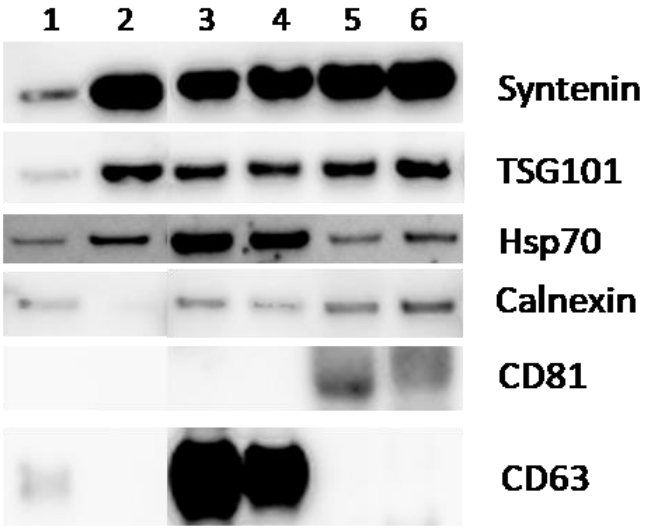

Figure 4.38: Western Blotting Analysis of PEG/SEC and TSC EV Fractions. EV fractions from SK-MEL-28 and HEK-CD63-GFP that were isolated by PEG/SEC (1+2) or TSC (3,4,5+6) were analysed for EV markers using western blotting. Equal volumes of EV fractions were loaded. Samples were processed on the same blot, picture was cropped to exclude irrelevant samples.

These last comparison experiments were just performed out of interest as optimisation of this TSC method is currently the focus of another colleague, who will investigate many different cell lines more thoroughly to establish if this TSC is a

viable alternative for EV isolation. However, these initial experiments show TSC to be a promising isolation technique.

5. Discussion

The field of EVs is a vast one, which is currently rapidly expanding. It is a topic which is still very much in its infancy with new guidelines and regulations emerging frequently. The full potential of these particles is not yet appreciated, and it is the task of the researchers in this field to keep up with the dynamic nature of this research area. This doctoral research project was originally based on the diagnostic potential of EVs in cancer, however, this project expanded in to two other directions along the way resulting in the optimisation of an EV isolation method and the optimisation of an EV-DNA labelling system to help increase the understanding of the functional aspects of EV-DNA transfer. Here, we endeavoured to expand upon current knowledge in these three areas of EV research.

5.1 EV Nucleic Acids as Diagnostic Markers in Cancer

The original outline of this doctoral research project was based on the investigation of EV-DNA as a diagnostic biomarker in AT/RT in collaboration Dr. Kornelius Kerl, University of Münster. It was planned to investigate this on three levels, starting with cell lines, moving on to mouse models and finally paediatric patient samples. Unfortunately, an adequate number of human patient samples to fulfil the planned patient cohort could not be collected within the time-frame of the project. As other collaborators came forward with interest in similar project ideas, this project then expanded to the investigation of EV-RNA as a biomarker in Ewing Sarcoma in collaboration with AG Dirksen, University hospital Essen. In both projects, it was shown on a cell line level, that expected mutations were detectable in EV nucleic acids (Table 4.2).

What has been shown here is a firm foundation at a cell line basis that the principal idea of using EV nucleic acids as diagnostic markers in cancer is possible and plausible. Previous studies have shown that cancerous cells produce more EVs than healthy cells, which makes the idea of using them in diagnostics a positive one (Becker et al., 2016). Although patient sample level was not reached here, during the time-frame of this project other researchers, including our own research group, have since successfully demonstrated the diagnostic potential of EV-DNA and RNA. For example, in the disease model of acute myeloid leukaemia (AML), Kunz et al. (2019) and Kontopoulou et al. (2020) were able to detect disease-related mutations in EV-DNA and EV-RNA from AML cell lines and paediatric patient samples. EV-DNA has

also been identified as having huge potential as a biomarker in pancreatic cancer (Malkin & Bratman, 2020). Additionally, Garcia Romero et al. (2017) demonstrated that EVs derived from neurological malignancies were able to cross the blood-brain barrier and be detected in peripheral blood, further promoting the idea of using EVs as biomarkers for neurological tumours. These results suggest that this method would also be successful in detecting the cancer-related mutations of the cancer models of interest in this project, namely AT/RT and Ewing Sarcoma, in human plasma.

In terms of the impact of this research on the field of diagnostics, the use of EVs in a liquid biopsy-type assay could massively change the face of cancer diagnostics. In solid cancers, such as AT/RT or other tumours of the brain and CNS - which are sensitive, difficult-to-access areas for biopsies - a liquid biopsy could be life changing (Boire et al., 2019). Not only could this save time for health organisations by avoiding full scale operations to perform tumour or tissue biopsies, but it could also improve the quality of life of patients. Patients would no longer have to undergo potentially painful, invasive operations and the stress that goes hand-in-hand with anticipation of such procedures (Fig. 5.1).

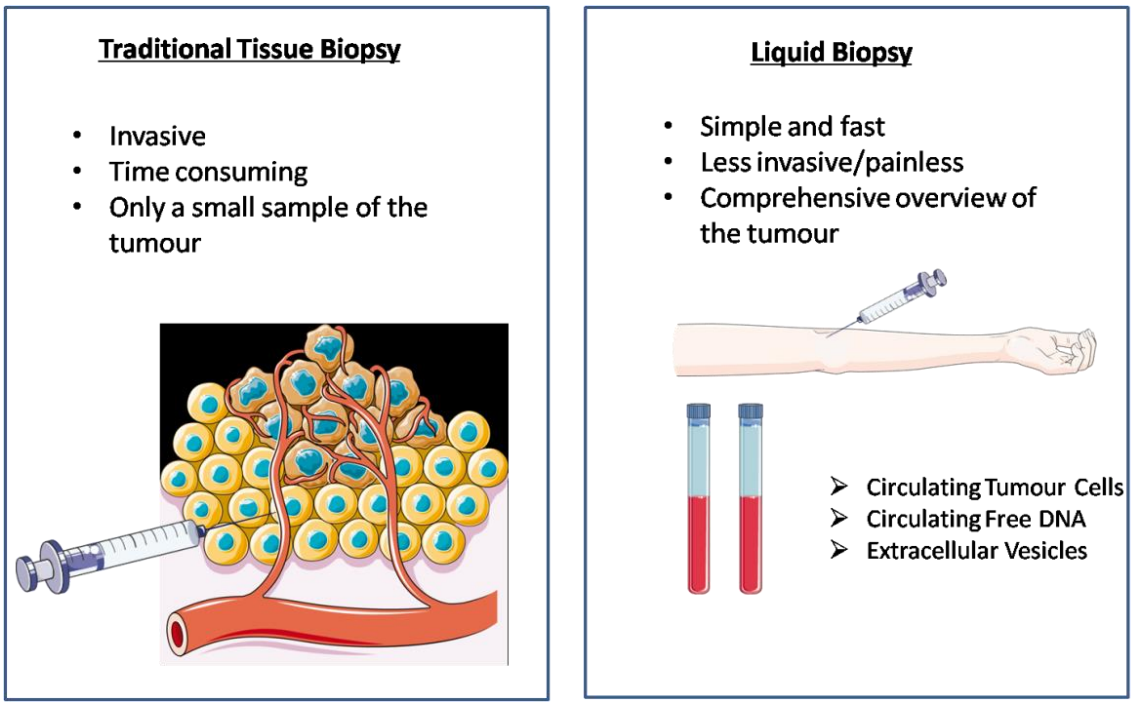

Figure 5.1: Overview of the Advantages of Liquid Biopsies. Image created using smartservier.com and PowerPoint software.

Patients would also receive results faster, as a blood draw can be performed instantaneously by any health professional, which would reduce the anxiety-filled waiting time for an allotted surgical procedure, and could potentially be lifesaving with treatment being prescribed earlier. It's thought that liquid biopsies may be more effective at giving an overview of the tumour composition as well, as EVs from all cell types within the tumour could potentially be collected and analysed, while a tissue biopsy may only contain a small sample of the heterogenic cancerous entity (Arneth, 2018).

However, as positive as this sounds, there are still many issues to be addressed before this can become a routine process in clinical settings. Issues with sensitivity with such methods are clear. In this project alone, we were unable to detect expected mutations in the EV-DNA from the AT/RT mice models. Despite taking steps to try and improve the outcome, such as pooling the plasma of several mice together to increase starting material volumes and the amplification of the EV-DNA to try increase the amount of DNA for detection, the assay was still unsuccessful. It is of course possible that this could be an issue with the mice models in this case; however, sensitivity issues have also been shown in other studies with patient plasma material. Although Kunz et al. (2019) and Kontopoulou et al. (2020) were able to detect AML-specific mutations in before-treatment patient samples, this was not in 100% of the cases. Accuracy is a necessity when diagnosing patients (Arneth, 2018). Another contender in the development of liquid biopsy-based diagnostic and prognostic methods is cell-free or circulating tumour DNA or RNA (cf/ctDNA or cf/ctRNA). Several research groups are demonstrating the cfDNA diagnostic potential with some promising results having been already published (Nguyen et al., 2020; Schneegans et al., 2020). It would be thought that being inside the EV would give the EV-DNA and RNA an advantage as they are more protected from degradation; however, cfDNA is looking promising with reported higher sensitivity (Nguyen et al., 2020), perhaps due to the amount of the material being larger than what is contained inside the EVs. Although one study showed that cfDNA in plasma would not serve as a good biomarker for neurological malignancies, like AT/RT, as DNA was only able to cross the blood-brain barrier when connected with EVs (Noemí García-Romero et al., 2017; Malkin & Bratman, 2020), it has been proposed that cerebral spinal fluid (CSF) could be a better liquid biopsy starting material for tumours of the CNS. It has been shown that CSF contains higher amounts of

tumour-specific cfDNA, which lowers the background signal of genomic DNA from non-cancerous cells (Boire et al., 2019). In Ewing sarcoma, ctDNA and ctRNA have been repeatedly shown to be effective biomarkers for several distinct Ewing Sarcoma mutations, fusions and gene breaks, and they have even observed a correlation between ctDNA levels and tumour burden (Salguero-Aranda et al., 2020). One attractive diagnostic idea combines these EV and cell-free potential biomarkers as well as circulating cancer cells to make a 'single tube' multi-compartmental diagnostic assay, which would of course increase sensitivity and accuracy of diagnostics by utilising all three potential diagnostic materials while requiring only one blood draw (Schneegans et al., 2020).

With such issues in mind, the most that an EV-nucleic acid-based detection method can offer at the moment is complementary information, perhaps becoming a part of a diagnostic panel supporting current diagnostic methods, until the current draw-backs of the assay can be overcome. Indeed, one such draw-back in need of a lot of consideration is the lack of a uniform isolation method that can be used routinely in clinical or research settings - a problem we also attempted to address in this doctoral project.

5.2 EV-DNA Transfer and Uptake by Recipient Cells

While other EV cargo molecules such as RNA and proteins have been the focus of many functional studies, the role of EV-DNA in cell-to-cell communication has recently gained attention. Interest in this EV biomolecule is increasing as its diagnostic and functional potentials are being unravelled. It has already been demonstrated that EVs contain DNA and that this DNA can be transferred and internalised by recipient cells (Cai et al., 2013; Fischer et al., 2016; Thakur et al., 2014). While other working groups have used methods such as membrane permeable dyes or cloning DNA into a plasmid vector with a Venus-fluorescent protein for detecting EV-DNA in recipient cells, the method optimised here takes advantage of the cells natural EV production line, by directly incorporating EdU in to the cells gDNA before it is packaged in to EVs (Cai et al., 2013; Fischer et al., 2016). Use of the small-sized Click-iT kit Alexa Fluor Azide for the detection of DNA-incorporated EdU has the advantage that the DNA does not need to be denatured for it to reach the EdU, which is the case for other labelling techniques such as the secondary antibody in BrdU incorporation. As demonstrated here, it is very effective

for EV-DNA visualisation using confocal microscopy. Using this method, we have managed to verify previous reports of recipient cells uptaking EV-DNA and have been able to demonstrate that the EV-DNA is transported to the nucleus of the recipient cell.

Several of our confocal microscopy results indicate involvement of the endosomal pathway in the internalisation and transport of EV-DNA in recipient cells (Fig. 4.13/14). The association of EV-DNA with $Rab5^+$ and $Rab7^+$ endosomes provides evidence for endosomal pathway involvement. Rab5 is a GTPase which regulates endosome biogenesis and trafficking, and participates in the maturation of the early to the late endosome. This maturation results in a Rab conversion from the early endosomal Rab5 to the late endosomal Rab7 (Nagano et al., 2019). Our co-localisation finding is in line with a previous report that $CD9^+$ EV biomolecules were seen to be associated with a subdomain of $Rab7^+$ late endosomes and that small GTPase Rab7, along with VAP-A and ORP3, creates a complex (VOR) which is essential for transport of EV molecules to the nucleoplasm (Corbeil et al., 2020; Rappa et al., 2017; Santos et al., 2018). Any vesicles internalised by endocytosis will be enclosed in endosomes due to endosomal/lysosomal pathway activation (McKelvey et al., 2015). With this in mind, it is a little suspect that we did not observe co-localisation between the EV-DNA and lysosomal marker, Lamp1. Previous studies have shown some association of membrane-labelled EVs with lysosomes in recipient cells, but DNA cargo was not assessed (Eitan et al., 2015; Tian et al., 2010). Although it is sometimes possible for the endosome contents to be recycled back to the cell membrane or to escape in the trans-Golgi network (McKelvey et al., 2015), it would be highly unlikely that **all** of the internalised EV-DNA escapes the degradation pathway and is transported to the nucleus. Our Rab5 and Rab7 knockdown experiments appeared to show that EV-DNA was still being transferred and internalised despite reduced $Rab5^+$ or $Rab7^+$ endosome presence. These findings may support the idea that there is not just one method of EV uptake and transport, but several, with receptor-mediated endocytosis, micropinocytosis, direct fusion, lipid rafts and clathrin-coated pits having been previously indicated (Kalluri & LeBleu, 2020; Kamerkar et al., 2017; Tian et al., 2014). The efficiency of the knockdown could have also played a factor in the interpretation of these results, as evidently, a complete knockdown was not achieved. In future, it would be an option

to establish a cell line with a permanent Rab5 or Rab7 knockdown for further investigations, so that the recipient cells would not have to undergo knockdown for each experiment. Furthermore, it was also evident that not all the EV-DNA was associated with endosomes, as a lot of the observed EdU signals were not colocalised with Rab5 or Rab7. This again highlights that there must be more than one route of uptake and trafficking. It's also possible that the type of DNA can affect how it is trafficked. It has been demonstrated that gDNA and mitochondrial DNA (mtDNA) from donor cell EVs have different fates, whereby only gDNA, and not mtDNA, is transported to the recipient cell nucleus (Malkin & Bratman, 2020). Additionally, the association of the EV-DNA with microtubules observed in our results supports the previous reports that microtubules and filamentous actin are essential for the transport of vesicles containing internalised EVs or their cargo (McKelvey et al., 2015). In our experiments it was also observed that EV-DNA appeared to be interacting with the nuclear envelope due to colocalization with LaminB1 at several time points. This was to be expected following our observation that the EV-DNA is often localised in the recipient cell nucleus after 48 hours of education.

The cell lines used initially for the optimisation of this protocol were a mouse melanoma cell line, B16-F10, and a breast cancer cell line, MDA-MB-231. Besides the characteristics of B16-F10 cells (which multiply quickly and produce many EVs), these cell lines were chosen with the idea that it would be possible to detect the donor mouse EV-DNA in the human recipient cells which would allow us to confirm that the donor EV-DNA was really being internalised and translocating to the nucleus. This was confirmed by STR profiling of the DNA isolated from nuclear extracts of MDA-MB-231 cells that had been previously educated with B16-F10 EVs (Table 4.6). This result supports our confocal microscopy findings, and that of previous working groups, that the EV-DNA is transferred by EVs and that it is eventually transported to the nucleus of recipient cells (Corbeil et al., 2020; Rappa et al., 2017; Santos et al., 2018). One study by Fischer et al. (2016) also demonstrated that the EV-DNA was being integrated in to the recipient cell genome and could be transcribed. Although our further attempts to detect donor cell mutations in the recipient cell nuclei were not successful, there are several reasons why this could be the case, one being the small sample volume used for the PCR approaches. While developing the PEG/SEC isolation method, we observed it was possible to detect the

same AML mutations in the EV-DNA of OCI-AML3 and MV4-11 cell lines with GeneScan-based fragment length analysis, which were also used for the education of HeLa cells. Therefore, we can at least confirm that the EVs used in this assay contained the mutations. With the AS-RTPCR, despite using the same primers and protocol as previously published by Jarry et al. (2004), there was amplification present in samples when using the primers against the *BRAF* V600E mutation even in samples which should be negative for the mutation. Although the amplification always occurred later in negative samples, meaning a difference could still be observed between positive and negative samples, this assay is not reliable enough for mutational detection. It could be possible that the WT primers and MT primers are too similar as there is only one base-pair difference, which could have allowed for false amplification. Perhaps other detection methods should be considered in future such as digital droplet PCR or DNA barcoding, which allow higher sensitivity.

This EdU labelling method for confocal microscopy was also subsequently tested with other donor or recipient cell lines to confirm that it was applicable universally. With the idea that EV communication plays a role in tumour development as well as metastasis via preparation of the pre-metastatic niche by interaction with cells of the tumour niche (Peinado et al., 2012), B16-F10 cells were educated with their own EVs, and NIH/3T3 mouse fibroblast cells were cultured with B16-F10 EVs (also of murine origin). Some uptake was observed as presented here, however the recipient cells did not fare as well as the MDA-MB-231 cells during the preparation process of the slides for microscopy, with many cells being lost (Fig. 4.26). The protocol that was presented in this project for preparing cells for confocal microscopy is quite lengthy and requires a lot of manipulation of the microscope slides. The complete protocol can take 5-7 hours (depending on sample number or if additional antibody labelling and knockdowns are required) and preparation of just one microscopy experiment required an entire week from cell seeding through to end-point microscopy. With that in mind, I am sure that with further optimisation for other cell lines, it would also be possible to use this technique of EV-DNA visualisation with any cell type without major cell loss. One possible option would be coating the slides with Poly-L-lysine to improve cell attachment. Unfortunately, due to the cell loss in the other cell models in this project, judgement could not be made on whether uptake was similar to the previous MDA-MB-231 model. However another study showed that

in comparison to a number of donor cell-recipient cell combinations, B16-F10 cells appeared to internalise their own EVs in higher amounts than other EVs (Lara et al., 2020). Previous work of our group leader, Dr Thakur, supported the idea that cells that replicate and expand quickly, such as cancer cells, uptake more EVs and EV-DNA (data not shown). Treatment with aphidicolin also supported the fact that recipient cells must be actively replicating in order to internalise EVs (Fig. 4.20). This is an interesting find, as if EV-DNA is in some way contributing to cancer, metastasis or advancements of other diseases, we demonstrated here that its uptake can be halted, which could have positive connotations for disease therapeutics.

Although the method optimised here enabled us to effectively visualise EV-DNA in recipient cells and track its localisation at different time points, there was always variation in the amount of EV-DNA observed in the cells despite the same particle number being used for the education each time. Also, the same time points did not always look the same between different experiments, but this could be due to many factors, including the culturing conditions of donor and recipient cells such as pH, or stress inducing factors - all of which have been shown to effect EV production and uptake (Kalluri & LeBleu, 2020). In future, these factors should be monitored closely, in order to improve reproducibility. Another factor is that the unreliability of NTA as an EV characterisation method has been shown, a topic further discussed in section 5.4. This could mean that although the same particle number was used for education, this does not mean the same number of EVs were present. Furthermore, it is known that not all EVs contain DNA, with the mechanism of EV loading still being unclear (Becker et al., 2016; Thakur et al., 2014). The DNA being present in the nucleus of the cells after 48 hours was something that was very often observed, however, this was observed less often in the experiments performed later in the project, which could be due to the EdU becoming less effective over time, or due to the cells being passaged too often. As it was demonstrated in the aphidicolin tests that cells need to be actively replicating to uptake the EdU-EVs, the latter reasoning for reduction of uptake in later experiments could be valid. When the nucleus was seen to be emitting an EdU AF647 signal, in our confocal images it appeared as if the whole nucleus was simply a monotone red colour. Therefore, a colleague prepared samples for super resolution microscopy by Prof. Christoph Cremer, Mainz. In these initial test images, it was possible to see the individual EdU molecules within

the nucleus (data not shown), rather than the monotone red signal that we had seen in confocal. This highlights that super resolution microscopy could be a valid method to study EV-DNA uptake in more depth. Considering the points previously discussed, I feel the most effective way to monitor EV-DNA uptake and transport within the recipient cells would be to use live cell imaging. This technique has already been utilised to track EVs with membrane labels (Tian et al., 2010). This method would allow us to also follow the EV-DNA from the time point of internalisation, all the way to its destination of the nucleus. The only draw-back is that the EdU labelling cannot be used in live cell imaging due to the requirement of a fixation step for detection; however, many other DNA labels are available. Use of EVs with a GFP tag, such as the HEK-CD63-GFP used here, would be ideal for live cell imaging in combination with a DNA dye.

It can be said that the research presented here is very much just the beginning of this line of enquiry in to EV-DNA transfer with many questions remaining for future research. One of the biggest questions still left unanswered is whether this transferred EV-DNA has a function or effect when uptaken by recipient cells. This is a difficult line of investigation as it must be proven that any observed effects are directly related to the EV-DNA and not any other co-transferred cargo molecules. The introduction of any foreign DNA into a recipient cell normally brings about a cellular reaction. Some recent cancer model studies have identified that EV-DNA can have effects on cell function, including activation of pro-inflammatory- and pro-oncogenic signalling pathways (Malkin & Bratman, 2020)(Fig. 5.2). Although the research presented here cannot prove EV functionality in the recipient cells, the successful uptake of EV-DNA hints towards EV-DNA having a role in recipient cell gene expression. We successfully established and optimised a method of labelling and visualising EV-DNA, which is monumentally important. Here, we only touched upon the possible uptake methods and localisation within the recipient cells, however, the possible avenues for continuation of the ideas begun in this project are endless.

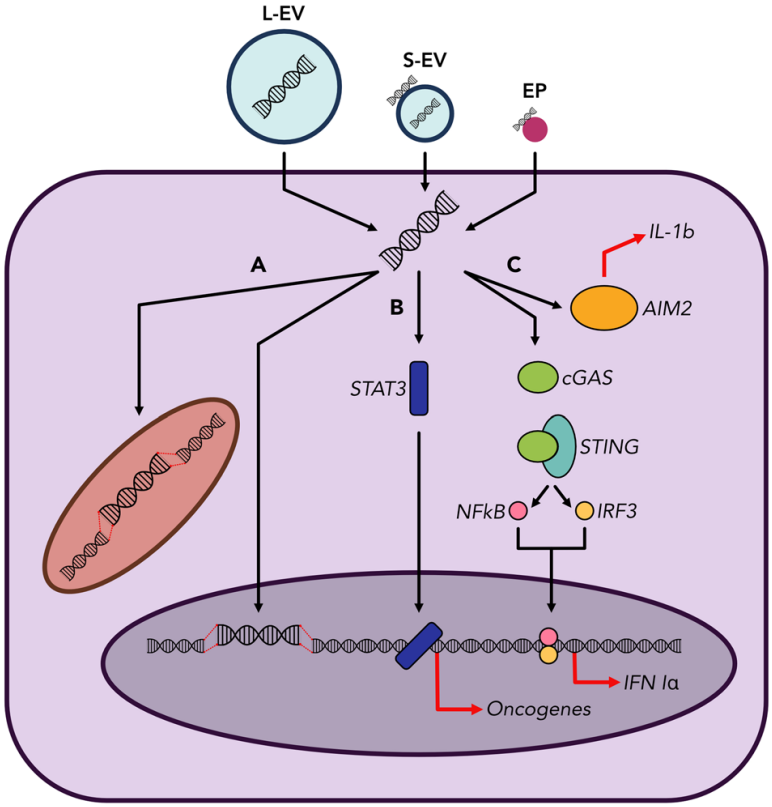

*Figure 5.2: EV-DNA as a Functional Mediator. EV-DNA is uptaken by the recipient cell where it mediates physiological effects. Route (**A**) demonstrates horizontal gene transfer, where the EV-DNA translocates to the cell nucleus or mitochondria, where it can be integrated into the host genome. If transcribed it could influence recipient cell function, and phenotypic changes. Route (**B**) demonstrates that EV-DNA activates oncogenic pathways causing the up-regulation of various intracellular signalling proteins causing translocation to the nucleus and over-expression of oncogenes. Route (**C**) demonstrates EV-DNA activating inflammatory pathways by triggering cytosolic DNA receptors, including AIM2 and cGAS, causing downstream release of Type I Interferons and interleukins. Image taken from Malkin and Bratman 2020.*

5.3 Optimisation of a PEG/SEC Isolation Method

Despite the growing number of EV isolation techniques, one of the most prominent problems in the EV field is the lack of a uniform isolation technique. If the future aim of using EVs in therapies or clinical settings is ever to be achieved, pure EV fractions free of contaminating biological molecules with biologically active EVs must firstly be obtainable. Cell lines are one of the most important tools in cancer and disease research as they enable primary investigations and establishment of protocols before the use of precious patient samples. A study in 2016 showed that 83% of 169 participants were using conditioned media as a starting material in their EV research (Gardiner et al., 2016). Relatively large volumes of conditioned media from cell lines can be processed for EV isolation using traditional ultracentrifugation, however, several disadvantages to this technique have become apparent. These disadvantages include damage to the vesicles due to high centrifugal forces, co-

isolation of high amounts of protein and lipoproteins, lengthy and laborious protocols, as well as issues concerning accessibility of ultracentrifuges to working groups due to their high price (Li et al., 2017).The volume of conditioned media that can be processed at one time is also limited to the number of spaces in the ultracentrifuge rotor. Therefore, in parallel to the other projects, we tried to optimise an alternative EV isolation method for large volumes of conditioned media which would bypass the need for an ultracentrifuge. This led to optimisation of the PEG/SEC isolation method presented here.

SEC is now a well-used method for the isolation of EVs (Gardiner et al., 2016; Hong et al., 2016; Lobb, Becker, Wen, et al., 2015). As the SEC process separates molecules based on their size due to the sample contents passing through a gel containing porous beads, it's thought of as a method that can produce more uniform EV fractions with less contaminating biomolecules (Hong et al., 2016). In the method presented here, we decided to adopt the 'mini-SEC' method previously published by Hong et al. (2016), in which samples were passed through a column packed with sepharose beads. Our first experiments were concerned with assessing the reproducibility of this isolation method using healthy donor plasma. The results presented here reflected and reinforced the previous findings of the 'mini-SEC' method (Hong et al., 2016), as the fourth fraction from mini-SEC isolation had a consistently higher number of particles and lower protein in comparison to the EV fraction isolated by UC (Table 4.7). One issue with this method, as with all SEC methods, is that there is a limit to the input volume. The method presented here allowed for addition of 1 mL of starting material - an issue when working with large starting volumes. Precipitation of EVs is a viable option to combat the problem of large starting volumes with agents such as polyethylene glycol (PEG), as presented here (Fig. 5.3). Originally used for capturing viruses, its properties have since been exploited for EV isolation (N. García-Romero et al., 2019; Rider et al., 2016; Weng et al., 2016). Although successful, the co-purification of other molecules lowering the purity of precipitated EV preparations has been mentioned in publications (Taylor & Shah, 2015). Our hypothesis was that combining this precipitation step with SEC would enable us to largely remove the previously documented co-purified molecules captured with PEG and give similar results as seen with plasma samples with SEC alone.

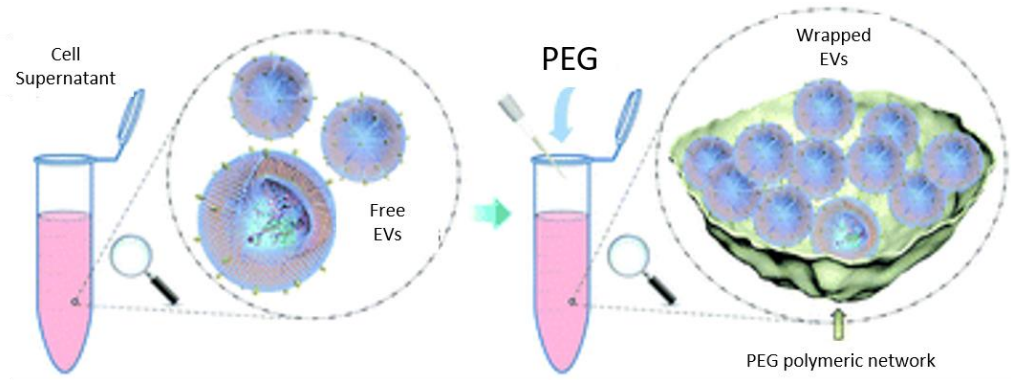

Figure 5.3: PEG Precipitation. EVs free in the cell supernatant are captured in net-like polymers, allowing precipitation of the EVs from large starting volumes. Image adapted from Weng et al., (2016).

As this mini-SEC method in combination with PEG (PEG/SEC) had not been previously established for cell line conditioned media, an optimal PEG/SEC EV fraction had to firstly be identified before comparison to the UC method could be performed. In the three cell lines presented here, from the NTA results it was clear that there was no overall PEG/SEC fraction that consistently yielded the highest number of particles, however the 3rd fraction never contained the highest number of particles. The 3rd PEG/SEC fraction consistently had the lowest protein content and the 6th fraction the highest, in all three cell lines; but despite its high purity the third fraction still contained visible protein aggregates when viewed with TEM (Fig. 4.31). For these reasons, it was decided that the 4th and 5th PEG/SEC fraction were more optimal than fractions 3 or 6 for further comparative analysis. Later data from a colleague subsequently further supported fraction 4 as the most optimal EV fraction (Appendix Fig. 10.1). When comparing the PEG/SEC fractions to the UC fractions, the results were not as clear-cut as had been previously seen in the SEC-only plasma experiments. There was variation in which method yielded the highest number of EVs and protein, depending on the cell line (Fig. 4.32).

It has previously been reported that less than 5% of EVs are recovered using UC methods (Baranyai et al., 2015), therefore, the higher number of EVs isolated by mini-SEC compared to UC in plasma samples showed an advantage of this method. The fact that this same method did not reflect this consistent trend in conditioned media of cell lines seems to point towards a problem in the PEG EV precipitation step. It is possible that PEG was not completely effective at capturing all EVs or had an effect on the downstream SEC application. If this is the case, using a different method to concentrate the conditioned media before the SEC isolation could improve the method. There are several other techniques and kits that have been

used by other working groups for EV precipitation or concentration (Karttunen et al., 2019). Other columns have also been tested for SEC isolation, some showing higher EV yields than the sepharose 2B columns used in this study, when working with plasma samples (Baranyai et al., 2015). Additionally, in order to increase the purity of EV preparations, some working groups use 'clean-up' kits (Gardiner et al., 2016). Some of these changes have been implemented in the ongoing investigation by a colleague in our working group in to an EV isolation technique that uses tangential flow filtration for the concentration of EVs, followed by SEC using an IZON column and further concentration with amnicon columns (TSC). Out of interest, I compared the B16-F10 EV fractions of PEG/SEC and TSC. Interestingly, this method showed higher percentage of CD9 and CD63 in TSC F2 in comparison to the other fractions, showing that the tetraspanin-containing EVs are being enriched in this method (Table 4.8). It also contained lower amounts of Apolipoprotein B, although the percentage was still high. Only the results of one cell line and one replicate were presented here, the method is still being optimised by a colleague and true effectiveness of this method remains to be shown; however, the first results are promising.

The morphology and integrity of EVs is an important factor to consider when biologically active EVs are required for the downstream applications following isolation. This is one of the downsides of traditional UC or any protocol that combines other isolation methods with UC, as the EV structure can become damaged in high centrifugal forces (Li et al., 2017). Hong et al. (2016) previously highlighted the ability of EVs to keep their biological activity after isolation using the mini-SEC method, which showed an advantage of this gentler isolation method. Although no functional comparison studies were made with the EVs isolated in this comparison study, all of the functional EV transfer experiments presented here were carried out using B16-F10 EVs from PEG/SEC fraction 4. This indicates that, despite lack of tetraspanin markers, there must be some form of biologically functioning EVs in these PEG/SEC F4 preparations which are also containing DNA. As our working group is interested in the use of nucleic acids (mainly dsDNA) from EVs as diagnostic and prognostic markers in cancer, the EVs of the comparison study were further evaluated for their RNA and dsDNA contents. It was shown that it was possible to isolate EV-dsDNA and RNA from the fourth and fifth PEG/SEC fractions and the UC fractions (Fig. 4.35). It was hypothesised that samples with the highest

number of EVs would also contain the highest dsDNA and RNA levels; however, this trend was not observed. This further supports the fact that dsDNA and RNA are not equally distributed between EVs and not all EVs contain dsDNA. Furthermore, the EVs from two cells lines, MV4-11 and OCI-AML, were isolated by both methods and analysed for the mutations FLT3/ITD and NPM1, respectively. Using both methods, it was possible to detect the mutations in both gDNA and EV-DNA showing that the new PEG/SEC method was just as capable as the UC method at providing useful mutational information with diagnostic and prognostic potential.

Of course there are several other isolation techniques available that have not been discussed here, such as microfluidic-based methods and sucrose cushion density gradient centrifugation, and a survey revealed that many groups are now using more than one isolation technique in their EV research (Gardiner et al., 2016). With so many isolation techniques available today with different advantages and disadvantages, it may be that the EV community will need to accept that there is no 'one size fits all method' when it comes to EV isolation. Instead, perhaps the isolation method must be selected depending upon factors such as starting material and downstream analyses. The technique presented here definitely poses a solution in cases where a large volume of starting material is to be processed and mutational analysis of EV nucleic acids is of interest. Additionally, the UC method also has the disadvantage of being a lengthy procedure, which requires access to an expensive piece of equipment, whereas SEC can be processed in a couple of hours - although it can also be costly due to the required materials. As it has been previously discussed that UC isolation has the potential to harm EVs due to high centrifugal forces (Hong et al., 2016; Lobb, Becker, Wen, et al., 2015), this PEG/SEC method of isolation could also prove to be advantageous to studies that require intact EVs for functional assays. However, the functional capability of EVs isolated in this manner and co-isolation of other molecules would firstly have to be rigorously evaluated, which is a line of investigation for future studies. If ever to be used in clinical settings, for instance as therapeutic agents in cancer patients, the whole composition of the EV fractions must be known; therefore, it is important to continue to further validate current EV isolation and characterisation techniques, which could help bring routine EV assays in to clinical and research laboratories in the future.

5.4 Exosomes, Microvesicles or Something Else Entirely?

While the EV research field is expanding rapidly, so are the regulations and recommended guidelines for EV isolation. This became very apparent during this doctoral thesis project, especially concerning EV characterisation. The variations in nomenclature and the emergence of several sub-groups of EVs with over lapping properties make it difficult for research groups to really identify what type of EVs they are working with. In recent years, it has also become apparent that EV fractions contain many lipoproteins which cannot be easily distinguished from EVs (Mørk et al., 2017). Although NTA has been largely used as a way to characterise EVs, it has become apparent that lipoproteins contribute to the particles tracked using NTA devices (Gardiner et al., 2016). Very low density lipoproteins (27-60 nm), intermediate density lipoproteins (23-27 nm), low density lipoproteins (18-23 nm) and chylomicrons (75-1200 nm) are all in the size range of EVs, whilst it's also possible for HDLs to form detectable aggregates (Mørk et al., 2017). Some of these lipoprotein particles expose ApoB (apolipoprotein B), high percentages of which were found to be present in B16-F10 fractions presented here. This lipoprotein co-isolation makes judgement of EV yield very difficult, especially in comparison studies like this one. Although it may be possible to remove lipoproteins from EV preparations before NTA, it has become apparent that some apolipoproteins can be bound to EVs; therefore, apolipoprotein depletion can also result in EV loss (Mørk et al., 2017).

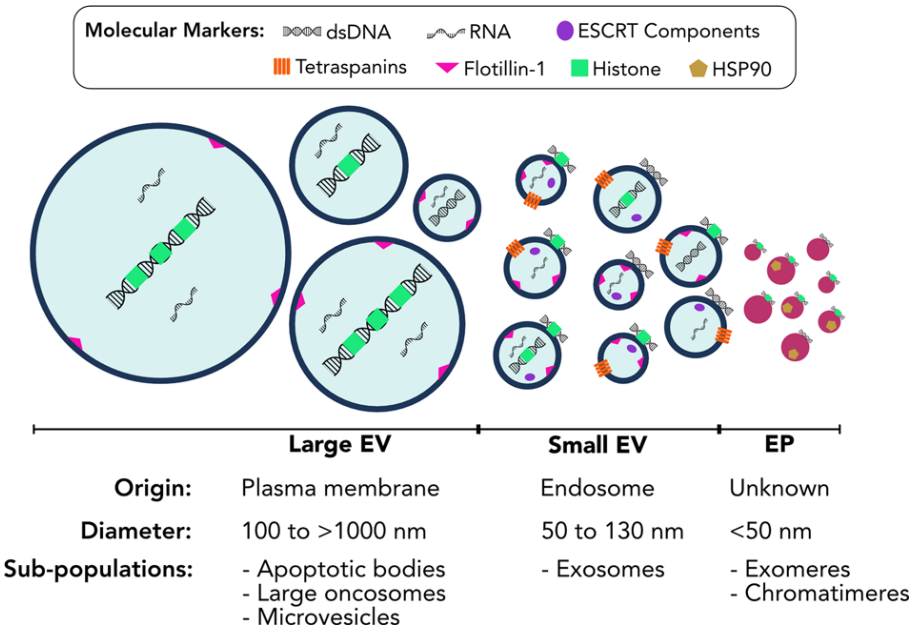

Figure 5.4: Overview of EV Sub-populations. Sub-populations of EVs depicted by their size, origin and EV cargo/markers. Image taken from Malkin & Bratman 2020.

It has also been established that nucleic acids, such as RNA species, can bind to lipoproteins and protein aggregates (Karttunen et al., 2019) which is a concerning issue for working groups that wish to assess EV nucleic acids. Recently, there has also been identification of a subgroup of extracellular particles (EP) which are protein-nucleic acid complexes (Malkin & Bratman, 2020), which further adds to the confusion (Fig 5.4). As all the EV subgroups appear to contain DNA as shown in the previous figure, DNA presence itself cannot be used to define which vesicles are in our preparations. One study tried to further define subgroups within the sEV subgroup based on density of the vesicles, and showed that more DNA was found in the high density EV group (Lázaro-Ibáñez et al., 2019). Other EV characterisation methods such as western blotting are very popular (Fig 5.5), but again there are disagreements on what proteins are true EV markers. The International Society for EVs (ISEV) currently states that both transmembrane or lipid bound extracellular proteins e.g. CD63, CD81 and CD9 should be present in western blotting, as well as cytosolic proteins e.g. syntenin and TSG101. Additionally intracellular proteins such as calnexin and histones would not be expected to be enriched in EVs (Lötvall et al., 2014). Considering that calnexin was seen in all preparations, and histones in one B16-F10 preparation, it would seem as though there is cell component contamination during the isolation procedure. There was also absence of tetraspanin markers CD63, CD81 and CD9, which some would argue must be present for true EV isolation. However, even early studies showed that not all EVs contain tetraspanins and that the cell of origin can influence which are present on EVs (Heijnen et al., 1999). Therefore, the absence or low levels of these markers does not necessarily mean that there are no EVs in the preparations, rather it could reflect that a non-tetraspanin-presenting subtype of EV is present. Furthermore, some claim the presence of histones in all EV subtypes, despite ISEVs position, as seen in Figure 5.4.

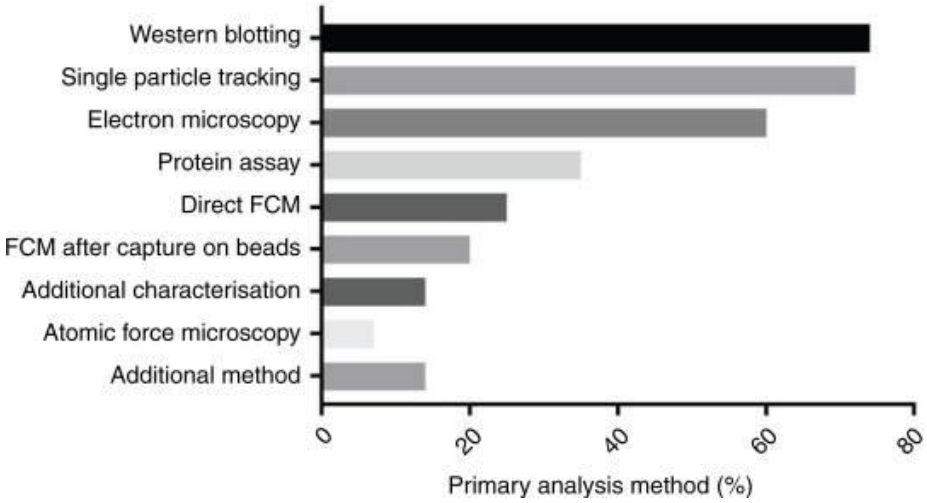

Figure 5.5: The Most Popular EV Characterisation Methods. Results of a 2016 survey showing the percentage of participants that use the mentioned EV characterisation methods. Image taken from Gardiner et al.2016.

FACS-based assays show great promise as a tool for EV characterisation. Originally, the small size of EVs meant that FACS was not an option, however, the development of bead capturing assays and flow cytometers with higher sensitivity has made this a valuable option for quantitative analysis (Gardiner et al., 2016). TEM in combination with EV-specific antibodies, or fluorescent tags could also help to further establish what sort of EV subpopulations are being observed during electron microscopy. The only drawback to these methods is again knowing which EV-specific markers are suitable for your isolated EV fractions.

With so many uncertainties, it has become difficult to navigate a path through the ever-changing landscape that is EV research. Hopefully, some of these issues become clearer over time as more data on EVs is collected. A sharing of findings, isolation methods and protocols should be encouraged by researchers in this field, so that EV-subtypes and cargo molecules can be better defined.

6. Conclusion

Here, we touched upon three aspects of EVs, namely their isolation, the biomarker potential of their nucleic acids and the functional uptake of EV-DNA to recipient cells. Relatively speaking, the EV field is still in its infancy; therefore, despite the recent increase in interest, there is still a lot to be learned about EVs, their cargo and their potential functions and uses. The data presented here lays a foundation for future projects that are based in one of these directions. While the results confirm some previous observations, they also highlight areas of potential future interest. Further research in to EVs and their cargo is of utmost importance, as only when their functional roles are fully understood can they be utilised in the fight against cancer and metastasis.

7. Abstract

Extracellular vesicles (EVs) are nanosized vesicles released by almost all cells. Interest in EVs has increased dramatically in recent years. Although several aspects of these vesicles such as composition, origin, purpose and potential uses have already been well evaluated, many possible avenues of research remain open. One aspect yet to be fully understood is the nucleic acids contained within EVs.

In this dissertation, we endeavoured to expand the current knowledge surrounding EV-DNA and EV-RNA by evaluating their potential diagnostic abilities in cancer models. As EVs can be isolated from body fluids and reflect their cell of origin, they are great candidates for liquid biopsies. Here, the ability to detect SMARCB1 mutations in EV-DNA of AT/RT cell lines and mouse plasma samples was investigated. Additionally, the ability to detect a FLI1 translocation in EV-RNA of a Ewing sarcoma cell line was demonstrated. Furthermore, EVs have important roles in cellular communication as well as tumour development and metastasis. Therefore, in the next step, the transfer of EV-DNA to recipient cells was investigated by establishing an EdU labelling method which allowed for the visualisation of EV-DNA with confocal microscopy. Here, the transfer and internalisation of EV-DNA by recipient cells was demonstrated. Additionally, the co-localisation of EV-DNA with donor cell components like $Rab5^+$ -and $Rab7^+$ endosomes as well as transfer of donor EV-DNA to the recipient cell nucleus were observed. In parallel to the aforementioned projects, the evaluation of an EV isolation method that combined two previously published methods of PEG precipitation and SEC was carried out, with hope of optimising a method that would circumvent the need for ultracentrifugation of our starting materials. Since the emergence of disadvantages of UC, several EV isolation methods have been developed - all with their own advantages and disadvantages. Here, EVs isolated by the PEG/SEC method were compared to EVs isolated using UC alone, and analysed for characteristics such as EV yield, EV fraction purity and nucleic acid content.

The work presented in this doctoral thesis has set the foundation for future research projects based in these areas and contributes to better understanding of EVs and their nucleic acid cargo.

8. Zusammenfassung

Extrazelluläre Vesikel (EVs) sind nanoskalige Vesikel, die von fast allen Zellen freigesetzt werden. Das Interesse an EVs hat in den letzten Jahren dramatisch zugenommen. Obwohl einige Aspekte dieser Vesikel wie Zusammensetzung, Herkunft, Zweck und mögliche Verwendungen bereits gut bewertet wurden, bleiben viele mögliche Forschungswege offen. Ein Aspekt, der noch vollständig verstanden werden muss, sind die in EVs enthaltenen Nukleinsäuren.

In dieser Dissertation haben wir uns bemüht, das aktuelle Wissen über EV-DNA und EV-RNA zu erweitern, indem wir ihre potenziellen diagnostischen Fähigkeiten in Krebsmodellen evaluierten. Da EVs aus Körperflüssigkeiten isoliert werden können und ihre Herkunftszelle widerspiegeln, sind sie hervorragende Kandidaten für flüssige Biopsien. Hier wurde die Fähigkeit zum Nachweis von SMARCB1-Mutationen in EV-DNA von AT/RT-Zelllinien und Mausplasmaproben untersucht. Zusätzlich wurde die Fähigkeit zum Nachweis einer FLI1-Translokation in EV-RNA einer Ewing-Sarkom-Zelllinie gezeigt. Darüber hinaus spielen EVs eine wichtige Rolle bei der zellulären Kommunikation sowie bei der Tumorentwicklung und Metastasierung. Deswegen, in dem nächsten Schritt, wurde der Transfer von EV-DNA auf Empfängerzellen untersucht, indem eine EdU-Markierungsmethode etabliert wurde, die die Visualisierung von EV-DNA mit konfokaler Mikroskopie ermöglichte. Hier wurden der Transfer und die Internalisierung von EV-DNA durch Empfängerzellen demonstriert. Zusätzlich wurde die Kolokalisation von EV-DNA mit Spenderzellkomponenten wie $Rab5^+$- und $Rab7^+$-Endosomen sowie die Übertragung von Donor-EV-DNA auf den Empfängerzellkern beobachtet. Parallel zu den oben genannten Projekten wurde die Evaluierung einer EV-Isolierungsmethode durchgeführt, die zwei zuvor veröffentlichte Methoden der PEG-Fällung und der SEC kombinierte, mit der Hoffnung, eine Methode zu optimieren, die die Notwendigkeit einer Ultrazentrifugation unserer Ausgangsmaterialien umgehen würde. Seit dem Auftreten von Nachteilen von UC wurden mehrere EV-Isolierungsmethoden entwickelt - alle mit ihren eigenen Vor- und Nachteilen. Hier wurden nach der PEG/SEC-Methode isolierte EVs mit EVs verglichen, die nur mit UC isoliert wurden, und auf Eigenschaften wie EV-Ausbeute, Reinheit der EV-Fraktion und Nukleinsäuregehalt analysiert.

Die in dieser Doktorarbeit vorgestellten Arbeiten haben die Grundlage für zukünftige Forschungsprojekte in diesen Bereichen gelegt und tragen zum besseren Verständnis von EVs und ihrer Nukleinsäurefracht bei.

9. References

Abels, E. R., & Breakefield, X. O. (2016). Introduction to Extracellular Vesicles: Biogenesis, RNA Cargo Selection, Content, Release, and Uptake. *Cellular and Molecular Neurobiology*, *36*(3), 301–312. https://doi.org/10.1007/s10571-016-0366-z

Alderton, G. K. (2012). Metastasis. Exosomes drive premetastatic niche formation. *Nature Reviews Cancer*, *12*(7), 447. https://doi.org/10.1038/nrc3304

Arneth, B. (2018). Update on the types and usage of liquid biopsies in the clinical setting: A systematic review. *BMC Cancer*, *18*(1). https://doi.org/10.1186/s12885-018-4433-3

Balaj, L., Lessard, R., Dai, L., Cho, Y. J., Pomeroy, S. L., Breakefield, X. O., & Skog, J. (2011). Tumour microvesicles contain retrotransposon elements and amplified oncogene sequences. *Nature Communications*, *2*(1). https://doi.org/10.1038/ncomms1180

Baranovskiy, A. G., Babayeva, N. D., Suwa, Y., Gu, J., Pavlov, Y. I., & Tahirov, T. H. (2014). Structural basis for inhibition of DNA replication by aphidicolin. *Nucleic Acids Research*. https://doi.org/10.1093/nar/gku1209

Baranyai, T., Herczeg, K., Onódi, Z., Voszka, I., Módos, K., Marton, N., Nagy, G., Mäger, I., Wood, M. J., El Andaloussi, S., Pálinkás, Z., Kumar, V., Nagy, P., Kittel, Á., Buzás, E. I., Ferdinandy, P., & Giricz, Z. (2015). Isolation of Exosomes from Blood Plasma: Qualitative and Quantitative Comparison of Ultracentrifugation and Size Exclusion Chromatography Methods. *PLOS ONE*, *10*(12), e0145686. https://doi.org/10.1371/journal.pone.0145686

Bebelman, M. P., Smit, M. J., Pegtel, D. M., & Baglio, S. R. (2018). Biogenesis and function of extracellular vesicles in cancer. *Pharmacology and Therapeutics*, *188*, 1–11. https://doi.org/10.1016/j.pharmthera.2018.02.013

Becker, A., Thakur, B. K., Weiss, J. M., Kim, H. S., Peinado, H., Lyden, D., Schiffelers, R. M., Wit, E. de, Berenguer, J., Ellenbroek, S. I., & al., et. (2016). Extracellular Vesicles in Cancer: Cell-to-Cell Mediators of Metastasis. *Cancer Cell*, *30*(6), 836–848. https://doi.org/10.1016/j.ccell.2016.10.009

Boire, A., Brandsma, D., Brastianos, P. K., Le Rhun, E., Ahluwalia, M., Junck, L., Glantz, M., Groves, M. D., Lee, E. Q., Lin, N., Raizer, J., Rudà, R., Weller, M., Van Den Bent, M. J., Vogelbaum, M. A., Chang, S., Wen, P. Y., & Soffietti, R. (2019). Liquid biopsy in central nervous system metastases: A RANO review and proposals for clinical applications. In *Neuro-Oncology* (Vol. 21, Issue 5, pp. 571–583). Oxford University Press. https://doi.org/10.1093/neuonc/noz012

Brennan, K., Martin, K., FitzGerald, S. P., O'Sullivan, J., Wu, Y., Blanco, A., Richardson, C., & Mc Gee, M. M. (2020). A comparison of methods for the isolation and separation of extracellular vesicles from protein and lipid particles in human serum. *Scientific Reports*, *10*(1), 1–13. https://doi.org/10.1038/s41598-020-57497-7

Bruno, S., Chiabotto, G., & Camussi, G. (2020). Extracellular vesicles: A therapeutic option for liver fibrosis. *International Journal of Molecular Sciences*, *21*(12), 1–18. https://doi.org/10.3390/ijms21124255

Cai, J., Han, Y., Ren, H., Chen, C., He, D., Zhou, L., Eisner, G. M., Asico, L. D., Jose, P. A., & Zeng, C. (2013). Extracellular vesicle-mediated transfer of donor genomic DNA to recipient cells is a novel mechanism for genetic influence between cells. *Journal of Molecular Cell Biology*, *5*(4), 227–238. https://doi.org/10.1093/jmcb/mjt011

Caspi, A., Yeger, O., Grosheva, I., Bershadsky, A. D., & Elbaum, M. (2001). A new dimension in retrograde flow: Centripetal movement of engulfed particles. *Biophysical Journal*,

81(4), 1990–2000. https://doi.org/10.1016/S0006-3495(01)75849-3

Chevillet, J. R., Kang, Q., Ruf, I. K., Briggs, H. A., Vojtech, L. N., Hughes, S. M., Cheng, H. H., Arroyo, J. D., Meredith, E. K., Gallichotte, E. N., Pogosova-Agadjanyan, E. L., Morrissey, C., Stirewalt, D. L., Hladik, F., Yu, E. Y., Higano, C. S., & Tewari, M. (2014). Quantitative and stoichiometric analysis of the microRNA content of exosomes. *Proceedings of the National Academy of Sciences of the United States of America*, *111*(41), 14888–14893. https://doi.org/10.1073/pnas.1408301111

Choi, D. S., Kim, D. K., Kim, Y. K., & Gho, Y. S. (2013). Proteomics, transcriptomics and lipidomics of exosomes and ectosomes. *Proteomics*, *13*(10–11), 1554–1571. https://doi.org/10.1002/pmic.201200329

Choi, D. S., Lee, J., Go, G., Kim, Y. K., & Gho, Y. S. (2013). Circulating extracellular vesicles in cancer diagnosis and monitoring: An appraisal of clinical potential. *Molecular Diagnosis and Therapy*, *17*(5), 265–271. https://doi.org/10.1007/s40291-013-0042-7

Ciardiello, C., Cavallini, L., Spinelli, C., Yang, J., Reis-Sobreiro, M., Candia, P. De, Minciacchi, V. R., & Di Vizio, D. (2016). Focus on extracellular vesicles: New frontiers of cell-to-cell communication in cancer. *International Journal of Molecular Sciences*, *17*(2), 1–17. https://doi.org/10.3390/ijms17020175

Cidre-Aranaz, F., & Alonso, J. (2015). EWS/FLI1 target genes and therapeutic opportunities in Ewing sarcoma. In *Frontiers in Oncology* (Vol. 5, Issue JUL). Frontiers Media S.A. https://doi.org/10.3389/fonc.2015.00162

Corbeil, D., Santos, M. F., Karbanová, J., Kurth, T., Rappa, G., & Lorico, A. (2020). Uptake and Fate of Extracellular Membrane Vesicles: Nucleoplasmic Reticulum-Associated Late Endosomes as a New Gate to Intercellular Communication. *Cells*, *9*(9). https://doi.org/10.3390/cells9091931

Dear, J. W., Street, J. M., & Bailey, M. A. (2013). Urinary exosomes: A reservoir for biomarker discovery and potential mediators of intrarenal signalling. *Proteomics*, *13*(10–11), 1572–1580. https://doi.org/10.1002/pmic.201200285

Dilsiz, N. (2020). Role of exosomes and exosomal microRNAs in cancer. *Future Science OA*, *6*(4). https://doi.org/10.2144/fsoa-2019-0116

Dykxhoorn, D. M., Palliser, D., & Lieberman, J. (2006). The silent treatment: SiRNAs as small molecule drugs. In *Gene Therapy* (Vol. 13, Issue 6, pp. 541–552). Nature Publishing Group. https://doi.org/10.1038/sj.gt.3302703

Eitan, E., Zhang, S., Witwer, K. W., & Mattson, M. P. (2015). Extracellular vesicle-depleted fetal bovine and human sera have reduced capacity to support cell growth. *Journal of Extracellular Vesicles*, *4*(2015), 1–10. https://doi.org/10.3402/jev.v4.26373

Fischer, S., Cornils, K., Speiseder, T., Badbaran, A., Reimer, R., Indenbirken, D., Grundhoff, A., Brunswig-Spickenheier, B., Alawi, M., & Lange, C. (2016). Indication of horizontal DNA gene transfer by extracellular vesicles. *PLoS ONE*, *11*(9), 1–22. https://doi.org/10.1371/journal.pone.0163665

Gámez-Valero, A., Monguió-Tortajada, M., Carreras-Planella, L., Franquesa, M., Beyer, K., & Borràs, F. E. (2016). Size-Exclusion Chromatography-based isolation minimally alters Extracellular Vesicles' characteristics compared to precipitating agents. *Scientific Reports*, *6*(June), 1–9. https://doi.org/10.1038/srep33641

García-Romero, N., Madurga, R., Rackov, G., Palacín-Aliana, I., Núñez-Torres, R., Asensi-Puig, A., Carrión-Navarro, J., Esteban-Rubio, S., Peinado, H., González-Neira, A., González-Rumayor, V., Belda-Iniesta, C., & Ayuso-Sacido, A. (2019). Polyethylene glycol improves current methods for circulating extracellular vesicle-derived DNA isolation. *Journal of*

Translational Medicine, *17*(1), 75. https://doi.org/10.1186/s12967-019-1825-3

García-Romero, Noemí, Carrión-Navarro, J., Esteban-Rubio, S., Lázaro-Ibáñez, E., Peris-Celda, M., Alonso, M. M., Guzmán-De-Villoria, J., Fernández-Carballal, C., de Mendivil, A. O., García-Duque, S., Escobedo-Lucea, C., Prat-Acín, R., Belda-Iniesta, C., & Ayuso-Sacido, A. (2017). DNA sequences within glioma-derived extracellular vesicles can cross the intact blood-brain barrier and be detected in peripheral blood of patients. *Oncotarget*, *8*(1), 1416–1428. https://doi.org/10.18632/oncotarget.13635

Gardiner, C., Vizio, D. Di, Sahoo, S., Théry, C., Witwer, K. W., Wauben, M., & Hill, A. F. (2016). Techniques used for the isolation and characterization of extracellular vesicles: Results of a worldwide survey. *Journal of Extracellular Vesicles*, *5*(1), 1–6. https://doi.org/10.3402/jev.v5.32945

Gould, S. J., & Raposo, G. (2013). As we wait: coping with an imperfect nomenclature for extracellular vesicles. *Journal of Extracellular Vesicles*. https://doi.org/10.3402/jev.v2i0.20389

Guescini, M., Genedani, S., Stocchi, V., & Agnati, L. F. (2010). Astrocytes and Glioblastoma cells release exosomes carrying mtDNA. *Journal of Neural Transmission*, *117*(1), 1–4. https://doi.org/10.1007/s00702-009-0288-8

Heijnen, H. F. G., Schiel, A. E., Fijnheer, R., Geuze, H. J., & Sixma, J. J. (1999). Activated platelets release two types of membrane vesicles: Microvesicles by surface shedding and exosomes derived from exocytosis of multivesicular bodies and α-granules. *Blood*. https://doi.org/10.1182/blood.v94.11.3791

Helwa, I., Cai, J., Drewry, M. D., Zimmerman, A., Dinkins, M. B., Khaled, M. L., Seremwe, M., Dismuke, W. M., Bieberich, E., Stamer, W. D., Hamrick, M. W., & Liu, Y. (2017). A comparative study of serum exosome isolation using differential ultracentrifugation and three commercial reagents. *PLoS ONE*, *12*(1), 1–22. https://doi.org/10.1371/journal.pone.0170628

Hessvik, N. P., & Llorente, A. (2018). Current knowledge on exosome biogenesis and release. *Cellular and Molecular Life Sciences*, *75*(2), 193–208. https://doi.org/10.1007/s00018-017-2595-9

Hong, C.-S., Funk, S., Muller, L., Boyiadzis, M., & Whiteside, T. L. (2016). Isolation of biologically active and morphologically intact exosomes from plasma of patients with cancer. *Journal of Extracellular Vesicles*, *5*(1), 29289. https://doi.org/10.3402/jev.v5.29289

Horibe, S., Tanahashi, T., Kawauchi, S., Murakami, Y., & Rikitake, Y. (2018). Mechanism of recipient cell-dependent differences in exosome uptake. *BMC Cancer*, *18*(1), 47. https://doi.org/10.1186/s12885-017-3958-1

Jarry, A., Masson, D., Cassagnau, E., Parois, S., Laboisse, C., & Denis, M. G. (2004). Real-time allele-specific amplification for sensitive detection of the BRAF mutation V600E. *Molecular and Cellular Probes*, *18*(5), 349–352. https://doi.org/10.1016/j.mcp.2004.05.004

Johann, P. D., Erkek, S., Zapatka, M., Kerl, K., Buchhalter, I., Hovestadt, V., Jones, D. T. W., Sturm, D., Hermann, C., Segura Wang, M., Korshunov, A., Rhyzova, M., Gröbner, S., Brabetz, S., Chavez, L., Bens, S., Gröschel, S., Kratochwil, F., Wittmann, A., … Kool, M. (2016). Atypical Teratoid/Rhabdoid Tumors Are Comprised of Three Epigenetic Subgroups with Distinct Enhancer Landscapes. *Cancer Cell*, *29*(3), 379–393. https://doi.org/10.1016/j.ccell.2016.02.001

Kahlert, C. (2014). Exosomes in Tumor Microenvironment Influence Cancer Progression and

Metastasis. *Journal of Molecular Medicine*, *91*(4), 431–437. https://doi.org/10.1007/s00109-013-1020-6.Exosomes

Kahlert, C., Melo, S. A., Protopopov, A., Tang, J., Seth, S., Koch, O., Zhang, J., Weitz, J., Chin, L., Futreal, A., & Kalluri, R. (2014). Identification of doublestranded genomic dna spanning all chromosomes with mutated KRAS and P53 DNA in the serum exosomes of patients with pancreatic cancer. *Journal of Biological Chemistry*, *289*(7), 3869–3875. https://doi.org/10.1074/jbc.C113.532267

Kalluri, R., & LeBleu, V. S. (2020). The biology, function, and biomedical applications of exosomes. *Science*, *367*(6478). https://doi.org/10.1126/science.aau6977

Kalra, H., Drummen, G. P. C., & Mathivanan, S. (2016). Focus on extracellular vesicles: Introducing the next small big thing. *International Journal of Molecular Sciences*, *17*(2). https://doi.org/10.3390/ijms17020170

Kamerkar, S., Lebleu, V. S., Sugimoto, H., Yang, S., Ruivo, C. F., Melo, S. A., Lee, J. J., & Kalluri, R. (2017). Exosomes facilitate therapeutic targeting of oncogenic KRAS in pancreatic cancer. *Nature*, *546*(7659), 498–503. https://doi.org/10.1038/nature22341

Karimi, N., Cvjetkovic, A., Jang, S. C., Crescitelli, R., Hosseinpour Feizi, M. A., Nieuwland, R., Lötvall, J., & Lässer, C. (2018). Detailed analysis of the plasma extracellular vesicle proteome after separation from lipoproteins. *Cellular and Molecular Life Sciences*, *75*(15), 2873–2886. https://doi.org/10.1007/s00018-018-2773-4

Karttunen, J., Heiskanen, M., Navarro-Ferrandis, V., Das Gupta, S., Lipponen, A., Puhakka, N., Rilla, K., Koistinen, A., & Pitkänen, A. (2019). Precipitation-based extracellular vesicle isolation from rat plasma co-precipitate vesicle-free microRNAs. *Journal of Extracellular Vesicles*, *8*(1). https://doi.org/10.1080/20013078.2018.1555410

Keerthikumar, S., Chisanga, D., Ariyaratne, D., Al Saffar, H., Anand, S., Zhao, K., Samuel, M., Pathan, M., Jois, M., Chilamkurti, N., Gangoda, L., & Mathivanan, S. (2016). ExoCarta: A Web-Based Compendium of Exosomal Cargo. *Journal of Molecular Biology*, *428*(4), 688–692. https://doi.org/10.1016/j.jmb.2015.09.019

Keller, S., Ridinger, J., Rupp, A.-K., Janssen, J. W., & Altevogt, P. (2011). Body fluid derived exosomes as a novel template for clinical diagnostics. *Journal of Translational Medicine*, *9*(1), 86. https://doi.org/10.1186/1479-5876-9-86

Koç, A., Wheeler, L. J., Mathews, C. K., & Merrill, G. F. (2004). Hydroxyurea Arrests DNA Replication by a Mechanism that Preserves Basal dNTP Pools. *Journal of Biological Chemistry*. https://doi.org/10.1074/jbc.M303952200

Kontopoulou, E., Strachan, S., Reinhardt, K., Kunz, F., Walter, C., Walkenfort, B., Jastrow, H., Hasenberg, M., Giebel, B., von Neuhoff, N., Reinhardt, D., & Thakur, B. K. (2020). Evaluation of dsDNA from extracellular vesicles (EVs) in pediatric AML diagnostics. *Annals of Hematology*, *99*(3), 459–475. https://doi.org/10.1007/s00277-019-03866-w

Kordelas, L., Rebmann, V., Ludwig, A. K., Radtke, S., Ruesing, J., Doeppner, T. R., Epple, M., Horn, P. A., Beelen, D. W., & Giebel, B. (2014). MSC-derived exosomes: A novel tool to treat therapy-refractory graft-versus-host disease. *Leukemia*, *28*(4), 970–973. https://doi.org/10.1038/leu.2014.41

Kunz, F., Kontopoulou, E., Reinhardt, K., Soldierer, M., Strachan, S., Reinhardt, D., & Thakur, B. K. (2019). Detection of AML-specific mutations in pediatric patient plasma using extracellular vesicle–derived RNA. *Annals of Hematology*, *98*(3), 595–603. https://doi.org/10.1007/s00277-019-03608-y

Lara, P., Palma-Florez, S., Salas-Huenuleo, E., Polakovicova, I., Guerrero, S., Lobos-Gonzalez, L., Campos, A., Muñoz, L., Jorquera-Cordero, C., Varas-Godoy, M., Cancino, J., Arias, E.,

Villegas, J., Cruz, L. J., Albericio, F., Araya, E., Corvalan, A. H., Quest, A. F. G., & Kogan, M. J. (2020). Gold nanoparticle based double-labeling of melanoma extracellular vesicles to determine the specificity of uptake by cells and preferential accumulation in small metastatic lung tumors. *Journal of Nanobiotechnology*, *18*(1), 1–17. https://doi.org/10.1186/s12951-020-0573-0

Lasda, E., & Parker, R. (2016). Circular RNAs co-precipitate with extracellular vesicles: A possible mechanism for circrna clearance. *PLoS ONE*, *11*(2), 1–11. https://doi.org/10.1371/journal.pone.0148407

Lässer, C., Seyed Alikhani, V., Ekström, K., Eldh, M., Torregrosa Paredes, P., Bossios, A., Sjöstrand, M., Gabrielsson, S., Lötvall, J., & Valadi, H. (2011). Human saliva, plasma and breast milk exosomes contain RNA: Uptake by macrophages. *Journal of Translational Medicine*, *9*(1), 9. https://doi.org/10.1186/1479-5876-9-9

Lázaro-Ibáñez, E., Lässer, C., Shelke, G. V., Crescitelli, R., Jang, S. C., Cvjetkovic, A., García-Rodríguez, A., & Lötvall, J. (2019). DNA analysis of low- and high-density fractions defines heterogeneous subpopulations of small extracellular vesicles based on their DNA cargo and topology. *Journal of Extracellular Vesicles*, *8*(1). https://doi.org/10.1080/20013078.2019.1656993

Lee, T. H., Chennakrishnaiah, S., Audemard, E., Montermini, L., Meehan, B., & Rak, J. (2014). Oncogenic ras-driven cancer cell vesiculation leads to emission of double-stranded DNA capable of interacting with target cells. *Biochemical and Biophysical Research Communications*, *451*(2), 295–301. https://doi.org/10.1016/j.bbrc.2014.07.109

Li, P., Kaslan, M., Lee, S. H., Yao, J., & Gao, Z. (2017). Progress in exosome isolation techniques. *Theranostics*, *7*(3), 789–804. https://doi.org/10.7150/thno.18133

Lobb, R. J., Becker, M., Wen, S. W., Wong, C. S. F., Wiegmans, A. P., Leimgruber, A., & Möller, A. (2015). Optimized exosome isolation protocol for cell culture supernatant and human plasma. *Journal of Extracellular Vesicles*, *4*(1), 1–11. https://doi.org/10.3402/jev.v4.27031

Lobb, R. J., Becker, M., Wen Wen, S., Wong, C. S. F., Wiegmans, A. P., Leimgruber, A., & Möller, A. (2015). Optimized exosome isolation protocol for cell culture supernatant and human plasma. *Journal of Extracellular Vesicles*, *4*(1), 27031. https://doi.org/10.3402/jev.v4.27031

Lötvall, J., Hill, A. F., Hochberg, F., Buzás, E. I., Di Vizio, D., Gardiner, C., Gho, Y. S., Kurochkin, I. V., Mathivanan, S., Quesenberry, P., Sahoo, S., Tahara, H., Wauben, M. H., Witwer, K. W., & Théry, C. (2014). Minimal experimental requirements for definition of extracellular vesicles and their functions: a position statement from the International Society for Extracellular Vesicles. *Journal of Extracellular Vesicles*, *3*(1), 26913. https://doi.org/10.3402/jev.v3.26913

Macías, M., Rebmann, V., Mateos, B., Varo, N., Perez-Gracia, J. L., Alegre, E., & González, Á. (2019). Comparison of six commercial serum exosome isolation methods suitable for clinical laboratories. Effect in cytokine analysis. *Clinical Chemistry and Laboratory Medicine (CCLM)*, *0*(0). https://doi.org/10.1515/cclm-2018-1297

Malkin, E. Z., & Bratman, S. V. (2020). Bioactive DNA from extracellular vesicles and particles. *Cell Death and Disease*, *11*(7). https://doi.org/10.1038/s41419-020-02803-4

Mathieu, M., Martin-Jaular, L., Lavieu, G., & Théry, C. (2019). Specificities of secretion and uptake of exosomes and other extracellular vesicles for cell-to-cell communication. *Nature Cell Biology*, *21*(1), 9–17. https://doi.org/10.1038/s41556-018-0250-9

McAndrews, K. M., & Kalluri, R. (2019). Mechanisms associated with biogenesis of exosomes

in cancer. *Molecular Cancer*, *18*(1), 1–11. https://doi.org/10.1186/s12943-019-0963-9

McKelvey, K. J., Powell, K. L., Ashton, A. W., Morris, J. M., & McCracken, S. A. (2015). Exosomes: Mechanisms of Uptake. *Journal of Circulating Biomarkers*, *4*, 1–9. https://doi.org/10.5772/61186

Melo, S. A., Sugimoto, H., O'Connell, J. T., Kato, N., Villanueva, A., Vidal, A., Qiu, L., Vitkin, E., Perelman, L. T., Melo, C. A., Lucci, A., Ivan, C., Calin, G. A., & Kalluri, R. (2014). Cancer Exosomes Perform Cell-Independent MicroRNA Biogenesis and Promote Tumorigenesis. *Cancer Cell*, *26*(5), 707–721. https://doi.org/10.1016/j.ccell.2014.09.005

Mørk, M., Handberga, A., Pedersen, S., Jørgensen, M. M., Bæk, R., Nielsen, M. K., & Kristensen, S. R. (2017). Prospects and limitations of antibody-mediated clearing of lipoproteins from blood plasma prior to nanoparticle tracking analysis of extracellular vesicles. *Journal of Extracellular Vesicles*, *6*(1). https://doi.org/10.1080/20013078.2017.1308779

Muller, L. (2020). Exosomes: nanodust? *Hno*, *68*, 56–59. https://doi.org/10.1007/s00106-019-00786-z

Murray, J. W., Bananis, E., & Wolkoff, A. W. (2000). Reconstitution of ATP-dependent movement of endocytic vesicles along microtubules in vitro: An oscillatory bidirectional process. *Molecular Biology of the Cell*, *11*(2), 419–433. https://doi.org/10.1091/mbc.11.2.419

Nagano, M., Toshima, J. Y., Elisabeth Siekhaus, D., & Toshima, J. (2019). Rab5-mediated endosome formation is regulated at the trans-Golgi network. *Communications Biology*, *2*(1), 1–12. https://doi.org/10.1038/s42003-019-0670-5

Németh, A., Orgovan, N., Sódar, B. W., Osteikoetxea, X., Pálóczi, K., Szabó-Taylor, K., Vukman, K. V., Kittel, Á., Turiák, L., Wiener, Z., Tóth, S., Drahos, L., Vékey, K., Horvath, R., & Buzás, E. I. (2017). Antibiotic-induced release of small extracellular vesicles (exosomes) with surface-associated DNA. *Scientific Reports*, *7*(1), 1–16. https://doi.org/10.1038/s41598-017-08392-1

Nguyen, B., Meehan, K., Pereira, M. R., Mirzai, B., Lim, S. H., Leslie, C., Clark, M., Sader, C., Friedland, P., Lindsay, A., Tang, C., Millward, M., Gray, E. S., & Lim, A. M. (2020). A comparative study of extracellular vesicle-associated and cell-free DNA and RNA for HPV detection in oropharyngeal squamous cell carcinoma. *Scientific Reports*, *10*(1), 1–10. https://doi.org/10.1038/s41598-020-63180-8

Parolini, I., Federici, C., Raggi, C., Lugini, L., Palleschi, S., De Milito, A., Coscia, C., Iessi, E., Logozzi, M., Molinari, A., Colone, M., Tatti, M., Sargiacomo, M., & Fais, S. (2009). Microenvironmental pH is a key factor for exosome traffic in tumor cells. *Journal of Biological Chemistry*, *284*(49), 34211–34222. https://doi.org/10.1074/jbc.M109.041152

Pathan, M., Fonseka, P., Chitti, S. V., Kang, T., Sanwlani, R., Van Deun, J., Hendrix, A., & Mathivanan, S. (2019). Vesiclepedia 2019: A compendium of RNA, proteins, lipids and metabolites in extracellular vesicles. *Nucleic Acids Research*, *47*(D1), D516–D519. https://doi.org/10.1093/nar/gky1029

Peinado, H., Alečković, M., Lavotshkin, S., Matei, I., Costa-Silva, B., Moreno-Bueno, G., Hergueta-Redondo, M., Williams, C., García-Santos, G., Ghajar, C. M., Nitadori-Hoshino, A., Hoffman, C., Badal, K., Garcia, B. A., Callahan, M. K., Yuan, J., Martins, V. R., Skog, J., Kaplan, R. N., … Lyden, D. (2012). Melanoma exosomes educate bone marrow progenitor cells toward a pro-metastatic phenotype through MET. *Nature Medicine*, *18*(6), 883–891. https://doi.org/10.1038/nm.2753

Potratz, J., Dirksen, U., Jürgens, H., & Craft, A. (2012). Ewing sarcoma: Clinical state-of-the-art. In *Pediatric Hematology and Oncology* (Vol. 29, Issue 1, pp. 1–11). Pediatr Hematol Oncol. https://doi.org/10.3109/08880018.2011.622034

Raeven, P., Zipperle, J., & Drechsler, S. (2018). Extracellular vesicles as markers and mediators in sepsis. *Theranostics*, *8*(12), 3348–3365. https://doi.org/10.7150/thno.23453

Raposo, G., & Stoorvogel, W. (2013). Extracellular vesicles: Exosomes, microvesicles, and friends. *The Journal of Cell Biology*, *200*(4), 373–383. https://doi.org/10.1083/jcb.201211138

Rappa, G., Santos, M. F., Green, T. M., Karbanová, J., Hassler, J., Bai, Y., Barsky, S. H., Corbeil, D., & Lorico, A. (2017). Nuclear transport of cancer extracellular vesicle-derived biomaterials through nuclear envelope invagination-associated late endosomes. *Oncotarget*, *8*(9), 14443–14461. https://doi.org/10.18632/oncotarget.14804

Ratajczak, J., Wysoczynski, M., Hayek, F., Janowska-Wieczorek, A., & Ratajczak, M. Z. (2006). Membrane-derived microvesicles: Important and underappreciated mediators of cell-to-cell communication. *Leukemia*, *20*(9), 1487–1495. https://doi.org/10.1038/sj.leu.2404296

Rider, M. A., Hurwitz, S. N., Meckes, D. G., & Jr. (2016). ExtraPEG: A Polyethylene Glycol-Based Method for Enrichment of Extracellular Vesicles. *Scientific Reports*, *6*, 23978. https://doi.org/10.1038/srep23978

Salguero-Aranda, C., Amaral, A. T., Olmedo-Pelayo, J., Diaz-Martin, J., & Álava, E. de. (2020). Breakthrough Technologies Reshape the Ewing Sarcoma Molecular Landscape. *Cells*, *9*(4), 804. https://doi.org/10.3390/cells9040804

Sansone, P., Savini, C., Kurelac, I., Chang, Q., Amato, L. B., Strillacci, A., Stepanova, A., Iommarini, L., Mastroleo, C., Daly, L., Galkin, A., Thakur, B. K., Soplop, N., Uryu, K., Hoshinob, A., Norton, L., Bonafé, M., Cricca, M., Gasparre, G., … Bromberg, J. (2017). Packaging and transfer of mitochondrial DNA via exosomes regulate escape from dormancy in hormonal therapy-resistant breast cancer. *Proceedings of the National Academy of Sciences of the United States of America*, *114*(43), E9066–E9075. https://doi.org/10.1073/pnas.1704862114

Santos, M. F., Rappa, G., Karbanová, J., Kurth, T., Corbeil, D., & Lorico, A. (2018). VAMP-associated protein-A and oxysterol-binding protein–related protein 3 promote the entry of late endosomes into the nucleoplasmic reticulum. *Journal of Biological Chemistry*, *293*(36), 13834–13848. https://doi.org/10.1074/jbc.RA118.003725

Schneegans, S., Lück, L., Besler, K., Bluhm, L., Stadler, J. C., Staub, J., Greinert, R., Volkmer, B., Kubista, M., Gebhardt, C., Sartori, A., Irwin, D., Serkkola, E., af Hällström, T., Lianidou, E., Sprenger-Haussels, M., Hussong, M., Mohr, P., Schneider, S. W., … Wikman, H. (2020). Pre-analytical factors affecting the establishment of a single tube assay for multiparameter liquid biopsy detection in melanoma patients. *Molecular Oncology*, 1–15. https://doi.org/10.1002/1878-0261.12669

Simons, M., & Raposo, G. (2009). Exosomes - vesicular carriers for intercellular communication. *Current Opinion in Cell Biology*, *21*(4), 575–581. https://doi.org/10.1016/j.ceb.2009.03.007

Sisquella, X., Ofir-Birin, Y., Pimentel, M. A., Cheng, L., Abou Karam, P., Sampaio, N. G., Penington, J. S., Connolly, D., Giladi, T., Scicluna, B. J., Sharples, R. A., Waltmann, A., Avni, D., Schwartz, E., Schofield, L., Porat, Z., Hansen, D. S., Papenfuss, A. T., Eriksson, E. M., … Regev-Rudzki, N. (2017). Malaria parasite DNA-harbouring vesicles activate

cytosolic immune sensors. *Nature Communications*, *8*(1). https://doi.org/10.1038/s41467-017-02083-1

Skog, J., Würdinger, T., van Rijn, S., Meijer, D. H., Gainche, L., Curry, W. T., Carter, B. S., Krichevsky, A. M., & Breakefield, X. O. (2008). Glioblastoma microvesicles transport RNA and proteins that promote tumour growth and provide diagnostic biomarkers. *Nature Cell Biology*, *10*(12), 1470–1476. https://doi.org/10.1038/ncb1800

Squadrito, M. L., Baer, C., Burdet, F., Maderna, C., Gilfillan, G. D., Lyle, R., Ibberson, M., & De Palma, M. (2014). Endogenous RNAs Modulate MicroRNA Sorting to Exosomes and Transfer to Acceptor Cells. *Cell Reports*, *8*(5), 1432–1446. https://doi.org/10.1016/j.celrep.2014.07.035

Street, J. M., Barran, P. E., Mackay, C. L., Weidt, S., Balmforth, C., Walsh, T. S., Chalmers, R. T. A., Webb, D. J., & Dear, J. W. (2012). Identification and proteomic profiling of exosomes in human cerebrospinal fluid. *Journal of Translational Medicine*, *10*(1), 5. https://doi.org/10.1186/1479-5876-10-5

Takahashi, A., Okada, R., Nagao, K., Kawamata, Y., Hanyu, A., Yoshimoto, S., Takasugi, M., Watanabe, S., Kanemaki, M. T., Obuse, C., & Hara, E. (2017). Exosomes maintain cellular homeostasis by excreting harmful DNA from cells. *Nature Communications*, *8*(May), 1–14. https://doi.org/10.1038/ncomms15287

Taverna, S., Giallombardo, M., Gil-Bazo, I., Carreca, A. P., Castiglia, M., Chacártegui, J., Araujo, A., Alessandro, R., Pauwels, P., Peeters, M., & Rolfo, C. (2016). Exosomes isolation and characterization in serum is feasible in non-small cell lung cancer patients: Critical analysis of evidence and potential role in clinical practice. *Oncotarget*, *7*(19), 28748–28760. https://doi.org/10.18632/oncotarget.7638

Taylor, D. D., & Shah, S. (2015). Methods of isolating extracellular vesicles impact down-stream analyses of their cargoes. *Methods*, *87*, 3–10. https://doi.org/10.1016/j.ymeth.2015.02.019

Thakur, B. K., Zhang, H., Becker, A., Matei, I., Huang, Y., Costa-Silva, B., Zheng, Y., Hoshino, A., Brazier, H., Xiang, J., Williams, C., Rodriguez-Barrueco, R., Silva, J. M., Zhang, W., Hearn, S., Elemento, O., Paknejad, N., Manova-Todorova, K., Welte, K., … Lyden, D. (2014). Double-stranded DNA in exosomes: A novel biomarker in cancer detection. *Cell Research*, *24*(6), 766–769. https://doi.org/10.1038/cr.2014.44

Théry, C. (2011). Exosomes: Secreted vesicles and intercellular communications. *F1000 Biology Reports*, *3*(1), 1–8. https://doi.org/10.3410/B3-15

Tian, T., Wang, Y., Wang, H., Zhu, Z., & Xiao, Z. (2010). Visualizing of the cellular uptake and intracellular trafficking of exosomes by live-cell microscopy. *Journal of Cellular Biochemistry*, *111*(2), 488–496. https://doi.org/10.1002/jcb.22733

Tian, T., Zhu, Y. L., Zhou, Y. Y., Liang, G. F., Wang, Y. Y., Hu, F. H., & Xiao, Z. D. (2014). Exosome uptake through clathrin-mediated endocytosis and macropinocytosis and mediating miR-21 delivery. *Journal of Biological Chemistry*, *289*(32), 22258–22267. https://doi.org/10.1074/jbc.M114.588046

Valadi, H., Ekström, K., Bossios, A., Sjöstrand, M., Lee, J. J., & Lötvall, J. O. (2007). Exosome-mediated transfer of mRNAs and microRNAs is a novel mechanism of genetic exchange between cells. *Nature Cell Biology*, *9*(6), 654–659. https://doi.org/10.1038/ncb1596

Van Balkom, B. W. M., Eisele, A. S., Michiel Pegtel, D., Bervoets, S., & Verhaar, M. C. (2015). Quantitative and qualitative analysis of small RNAs in human endothelial cells and exosomes provides insights into localized RNA processing, degradation and sorting. *Journal of Extracellular Vesicles*, *4*(2015), 1–14. https://doi.org/10.3402/jev.v4.26760

Van Niel, G., D'Angelo, G., & Raposo, G. (2018). Shedding light on the cell biology of extracellular vesicles. In *Nature Reviews Molecular Cell Biology* (Vol. 19, Issue 4, pp. 213–228). Nature Publishing Group. https://doi.org/10.1038/nrm.2017.125

Villata, S., Canta, M., & Cauda, V. (2020). Evs and bioengineering: From cellular products to engineered nanomachines. In *International Journal of Molecular Sciences* (Vol. 21, Issue 17, pp. 1–32). MDPI AG. https://doi.org/10.3390/ijms21176048

Wagstaff, K. M., Sivakumaran, H., Heaton, S. M., Harrich, D., & Jans, D. A. (2012). Ivermectin is a specific inhibitor of importin α/β-mediated nuclear import able to inhibit replication of HIV-1 and dengue virus. *Biochemical Journal*, *443*(3), 851–856. https://doi.org/10.1042/BJ20120150

Waldenström, A., Gennebäck, N., Hellman, U., & Ronquist, G. (2012). Cardiomyocyte Microvesicles Contain DNA/RNA and Convey Biological Messages to Target Cells. *PLoS ONE*, *7*(4), e34653. https://doi.org/10.1371/journal.pone.0034653

Weng, Y., Sui, Z., Shan, Y., Hu, Y., Chen, Y., Zhang, L., & Zhang, Y. (2016). Effective isolation of exosomes with polyethylene glycol from cell culture supernatant for in-depth proteome profiling. *Analyst*, *141*(15), 4640–4646. https://doi.org/10.1039/c6an00892e

Willms, E., Cabañas, C., Mäger, I., Wood, M. J. A., & Vader, P. (2018). Extracellular vesicle heterogeneity: Subpopulations, isolation techniques, and diverse functions in cancer progression. *Frontiers in Immunology*, *9*(APR). https://doi.org/10.3389/fimmu.2018.00738

Wilson, B. G., & Roberts, C. W. M. (2011). SWI/SNF nucleosome remodellers and cancer. *Nature Reviews Cancer*, *11*(7), 481–492. https://doi.org/10.1038/nrc3068

Zhang, G., Zhang, Y., Zhang, C., Wang, Y., Ma, G., Nie, K., Xie, H., Liu, J., & Wang, L. (2015). Diffusion Kurtosis Imaging of Substantia Nigra Is a Sensitive Method for Early Diagnosis and Disease Evaluation in Parkinson's Disease. *Parkinson's Disease*, *2015*, 207624. https://doi.org/10.1155/2015/207624

Zhang, J., Li, S., Li, L., Li, M., Guo, C., Yao, J., & Mi, S. (2015). Exosome and exosomal microRNA: Trafficking, sorting, and function. *Genomics, Proteomics and Bioinformatics*, *13*(1), 17–24. https://doi.org/10.1016/j.gpb.2015.02.001

Zhao, Hong, Halicka, H. D., Li, J., Biela, E., Berniak, K., Dobrucki, J., & Darzynkiewicz, Z. (2013). DNA damage signaling, impairment of cell cycle progression, and apoptosis triggered by 5-ethynyl-2'-deoxyuridine incorporated into DNA. *Cytometry Part A*, *83*(11), 979–988. https://doi.org/10.1002/cyto.a.22396

Zhao, Hongyun, Yang, L., Baddour, J., Achreja, A., Bernard, V., Moss, T., Marini, J. C., Tudawe, T., Seviour, E. G., San Lucas, F. A., Alvarez, H., Gupta, S., Maiti, S. N., Cooper, L., Peehl, D., Ram, P. T., Maitra, A., & Nagrath, D. (2016). Tumor microenvironment derived exosomes pleiotropically modulate cancer cell metabolism. *ELife*, *5*(FEBRUARY2016). https://doi.org/10.7554/eLife.10250

Zhu, Q., Heon, M., Zhao, Z., & He, M. (2018). Microfluidic engineering of exosomes: Editing cellular messages for precision therapeutics. *Lab on a Chip*, *18*(12), 1690–1703. https://doi.org/10.1039/c8lc00246k

10. Appendix

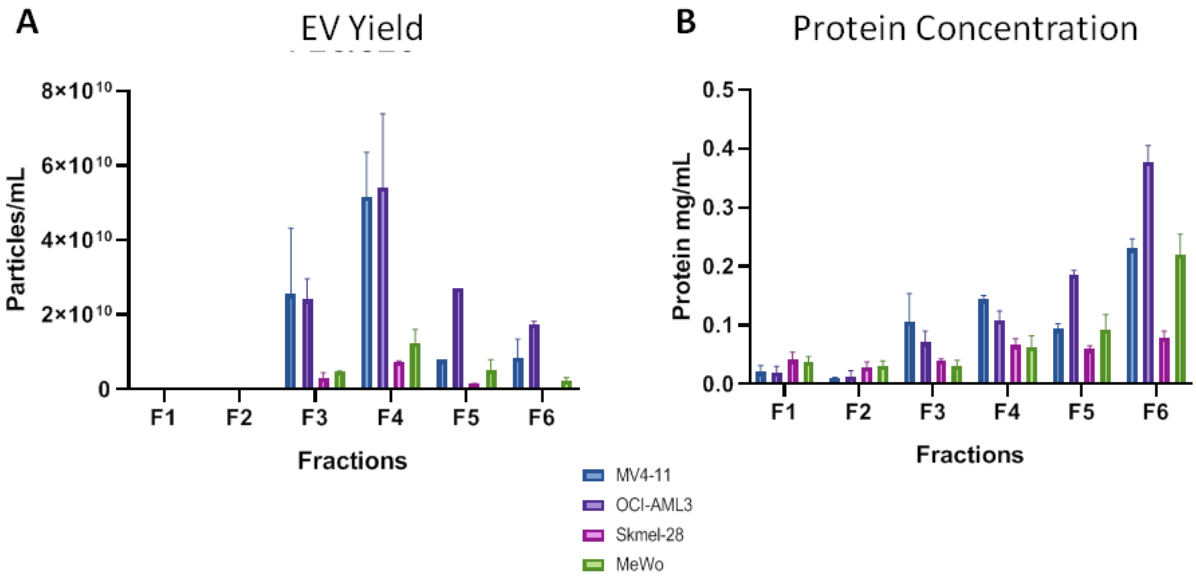

Figure 10.1: Comparison of PEG/SEC Fraction Characteristics. Six PEG/SEC EV fractions from four cell lines were analysed using NTA and BCA assay. Characterisation was performed by a colleague after a period of optimisation of the PEG/SEC isolation method.

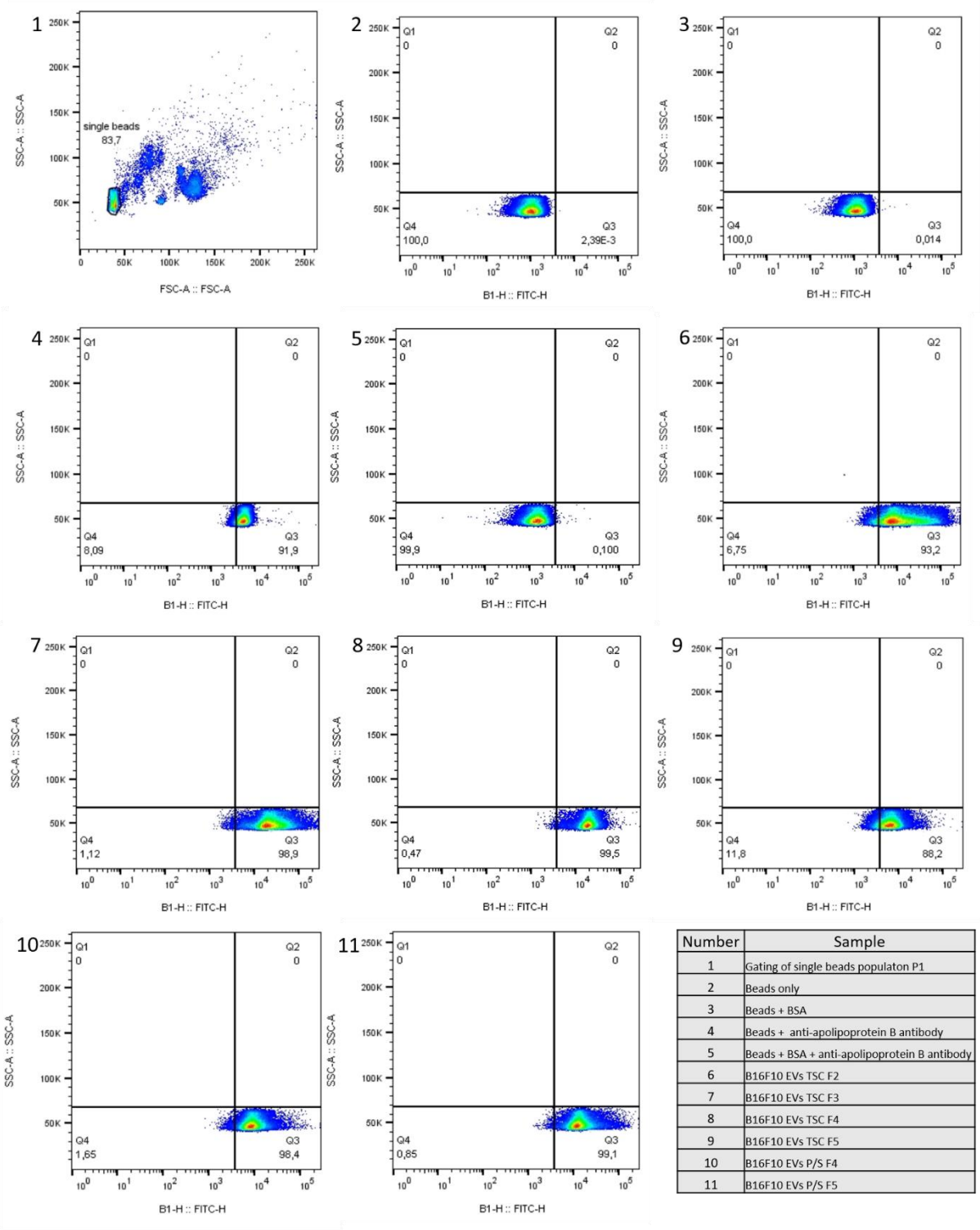

Number	Sample
1	Gating of single beads populaton P1
2	Beads only
3	Beads + BSA
4	Beads + anti-apolipoprotein B antibody
5	Beads + BSA + anti-apolipoprotein B antibody
6	B16F10 EVs TSC F2
7	B16F10 EVs TSC F3
8	B16F10 EVs TSC F4
9	B16F10 EVs TSC F5
10	B16F10 EVs P/S F4
11	B16F10 EVs P/S F5

Figure 10.2: Gating of Bead-based FACS data. For detection of Apolipoprotein in EV fractions, EVs were bound to beads and labelled with anti-APOB antibodies. Single beads population was selected for analysis (1+2); Beads plus antibodies control was used as a positive control for the antibody (4); Beads plus BSA plus antibody was used to set the gates for all samples as to reduce false positive signal of antibodies binding to the beads even after BSA blocking (5). The same gating strategy was used for CD9 and CD63 detection assays. Analysis performed using FlowJo software.

11. Acknowledgements

Firstly, I would like to thank my supervisor Dr. Basant Kumar Thakur for giving me the opportunity to work on this project, and for his knowledge and guidance. I would also like to thank Prof. Dr. Dirk Reinhardt, director of the children's hospital, University Clinic Duisburg-Essen, for his time and support throughout this project.

I would also like to thank all of our collaborators for providing cell lines, plasma samples, protocols or allowing access to their instruments, without whom this research would not have been possible. In particular, thank you to all members of the IMCES facility of the University Hospital Essen for assistance with all TEM and confocal microscopy approaches. Furthermore, I would like to thank my all of my past and present colleagues, in particular Maren Soldierer, and Evangelia Kontopoulou, for their support, guidance and team-work throughout this project, and for providing a great working atmosphere

Finally, I would like to thank my partner Jens, my family and my close friends for their endless support throughout this project. Their words of encouragement and unwavering belief in my abilities have helped me more than words can say. Moreover, a special mention for my son, Ryan, whose presence has reminded me every day what I am working for.

12. Curriculum Vitae

13. Eidesstattliche Erklärungen

Erklärung:

Hiermit erkläre ich, gem. § 7Abs. (2) d) + f) der Promotionsordnung der Fakultät für Biologie zur Erlangung des Dr. rer. nat., dass ich die vorliegende Dissertation selbständig verfasst und mich keiner anderen als der angegebenen Hilfsmittel bedient, bei der Abfassung der Dissertation nur die angegeben Hilfsmittel benutzt und alle wörtlich oder inhaltlich übernommenen Stellen als solche gekennzeichnet habe.

Essen, den_____ _____

Unterschrift der Doktoradin

Erklärung:

Hiermit erkläre ich, gem. § 7Abs. (2) e) + g) der Promotionsordnung der Fakultät für Biologie zur Erlangung des Dr. rer. nat., dass ich keine anderen Promotionen bzw. Promotionsversuche in der Vergangenheit durchgeführt habe und dass diese Arbeit von keiner anderen Fakultät/Fachbereich abgelehnt worden ist.

Essen, den_____ _____

Unterschrift der Doktoradin

Erklärung:

Hiermit erkläre ich, gem. § 6 Abs. (2) g) der Promotionsordnung der Fakultät für Biologie zur Erlangung der Dr. rer. nat., dass ich das Arbeitsgebiet, dem das Thema „Investigating the biomarker potential of extracellular vesicle nucleic acids in cancer, and the role of extracellular vesicle DNA in cell-to-cell communication“ zuzuordnen ist, in Forschung und Lehre vertrete und den Antrag von Sarah Strachan befürworte und die Betreuung auch im Falle eines Weggangs, wenn nicht wichtige Gründe dem entgegenstehen, weiterführen werde.

Essen, den _____	_____	_____
	Name des wissenschaftl. Betreuers/Mitglieds der Universität Duisburg-Essen	Unterschrift des wissenschaftl. Betreuers/Mitglieds der Universität Duisburg-Essen